Copyright

by

Dmitri A. Kraptchetov

2008

The Dissertation Committee for Dmitri A. Kraptchetov Certifies that this is the approved version of the following dissertation:

CONJUGATED DITHIOLS AS MODEL SYSTEMS FOR MOLECULAR ELECTRONICS: ASSEMBLY, STRUCTURE, AND ELECTRICAL RESPONSE

Committee:

Yueh-Lin Loo, Supervisor

Isaac Sanchez, Supervisor

Ananth Dodabalapur

Gyeong Hwang

Chris Mack

Charles Mullins

CONJUGATED DITHIOLS AS MODEL SYSTEMS FOR MOLECULAR ELECTRONICS: ASSEMBLY, STRUCTURE, AND ELECTRICAL RESPONSE

by

Dmitri A. Kraptchetov, B.S.

Dissertation

Presented to the Faculty of the Graduate School of

The University of Texas at Austin

in Partial Fulfillment

of the Requirements

for the Degree of

Doctor of Philosophy

The University of Texas at Austin

May, 2008

Dedication

To my family.

Acknowledgements

I am grateful to the many people that helped me during the course of my Ph.D. program. First, I would like to thank my advisor, Professor Yueh-Lin Loo, for her support and advice throughout the course of my studies. Her continuous guidance was invaluable in helping me navigate through the multiple challenges of graduate research. I would like to thank the members (former and current) of the Loo group: Drs. Kimberly Dickey and Kwang Seok Lee for thoughtful scientific discussions, their help and advice with equipment training and the many details of experimentation; Tracy Bucholz and Kyle Guice for insightful discussions of the many aspects of my work and the editorial feedback during my dissertation writing process; Reken Patel for his help and advice with microscopy; Joung Eun Yoo and Jacob Tarver for being inspiring colleagues.

I would like to acknowledge our many collaborators: Drs. Hong Ma and Alex K. Y. Jen for providing the dithiols used in my studies, Dr. Daniel A. Fischer for his help and advice with NEXAFS spectroscopy studies, Dr. Yangming Sun for his help and guidance with XPS studies. I am also grateful to late Prof. Michael White who donated the FTIR spectrometer used for my IR studies. I thank Dr. Ken Shih and Alexander Khajetoorians for their willingness to explore and help with preliminary STM attempts, Drs. Brian Korgel and Grant Willson for allowing me to use their facilities for my experiments, Alec Nepomnyashchii for his help with mercury probe preparation. Special thanks to Dr. Victor Pryamitsyn for being an insightful mentor and a constant source of scientific advice.

I thank Drs. Ananth Dodabalapur, Charles Mullins, Chris Mack, and Gyeong Hwang for providing feedback for my research as my doctorate committee members.

I am forever grateful to my family in Russia whose unconditional love and support have always helped me persevere through my studies in the United States.

Finally, I acknowledge the following funding agencies: the Camille and Henry Dreyfus New Faculty Award, the National Science Foundation (DMR – 0314707), Ricoh Innovations, and the Keck Foundation.

CONJUGATED DITHIOLS AS MODEL SYSTEMS FOR MOLECULAR ELECTRONICS: ASSEMBLY, STRUCTURE, AND ELECTRICAL RESPONSE

Publication No._____________

Dmitri A. Kraptchetov, Ph.D.
The University of Texas at Austin, 2008

Supervisors: Yueh-Lin Loo and Isaac C. Sanchez

Molecular assemblies are promising candidates for nano-scale electronics due to their chemical and structural versatility. The successful fabrication of assembly-based nano-scale electronics, where molecular assemblies comprise the electrically-active components, requires the ability to reliably form molecular assemblies and the ability to 'wire' them into electrical junctions. This dissertation focuses on the processing-structure relationships of model conjugated dithiols, the formation of electrical junctions with these molecular assemblies, and the characterization of these junctions.

Biphenyldithiol (BPDT), terphenyldithiol (TPDT), and quaterphenyldithiol (QPDT) are assembled in solution from their thioacetyl precursors which are converted *in-situ* to thiolates using NH_4OH. We elucidated how the type of substrate, the solvent quality, and the concentrations of NH_4OH and the thioacetyl precursors affect the final structures of these assemblies. BPDT molecular assemblies are disordered on both gold (Au) and gallium arsenide (GaAs) at all conditions explored. TPDT and QPDT adopt the

most upright molecular orientations on both Au and GaAs when the assembly is carried out from EtOH-rich solutions at low NH_4OH and high precursor concentrations. At these conditions, the assembly formation process is dominated by the adsorption of thioacetyl-terminated molecules. When the assembly is carried with high NH_4OH and low precursor concentrations, adsorption is dominated by thiolates; TPDT and QPDT are disordered on Au and GaAs. None of the molecules adsorb significantly on GaAs from THF.

The presence of S-Au bonds at the molecular assembly – top Au contact interface was directly probed by x-ray photoelectron spectroscopy. Depositing Au electrodes on QPDT assemblies by nTP in dichloroethane results in the reproducible formation of S-Au bonds at the molecule-Au interface.

Finally, we measured the electrical response of the model conjugated molecular assemblies on GaAs through direct contact with galinstan. The current densities scale inversely with the tunneling distance, which is determined by factors including the length of the conjugated molecule and the molecular orientation of the assembly. We also examined the electrical response of GaAs—QPDT—Au junctions in which the Au electrodes were transferred using an elastomeric stamps. The electrical characteristics of these junctions were independent of orientation of the molecules and the presence of S-Au bonds at the charge transfer interface. Hydrocarbon contamination on the Au electrodes left by the elastomeric stamp during transfer masked any electrical response from QPDT. It is therefore crucial to ensure the pristine quality of the electrical contact in order to reliably measure the electrical response of the molecular assembly.

The fabrication and testing of assembly-based electrical junctions is challenging in terms of both controlling the assembly structures and measuring their electrical response. Careful attention must therefore be paid to each aspect of molecular assembly-based junction formation and characterization.

Table of Contents

List of Tables

List of Figures

List of Illustrations

Chapter 1: Introduction

MOTIVATION

Molecular assemblies are lateral arrays of molecules that spontaneously adsorb on a substrate via solution or vapor deposition. The individual molecules which compose the molecular assembly typically contain a head group, a backbone (spacer), and an end group[1], as illustrated in Figure 1.1. The head group is a functional group that facilitates the attachment of the molecule to the substrate. The backbone generally points away from the substrate and terminates with the end group. The end group thus normally determines the surface properties of the molecular assembly, while the backbone governs the way in which the molecules organize within the molecular assembly. The molecular orientation within the molecular assembly is determined by an interplay of molecule-substrate and intermolecular (Van der Waals)[1] interactions. Molecular assemblies can be highly ordered; such assemblies are commonly referred to as self-assembled monolayers (SAMs). Molecular assemblies can also incorporate a wide variety of backbone and terminal chemical functionalities.

Due to the variety of structural and chemical characteristics molecular assemblies have to offer, they have been looked at for a number of potential applications. For instance, the dense packing often exhibited by molecules with alkyl backbones makes these assemblies effective barriers against oxidation[2,3] and biofilm formation[4,5] on metal and semiconductor surfaces. Due to their chemical stability, alkyl-based molecular assemblies can also act as effective etch resists in lithographic patterning applications.[6,7] Additionally, molecular assemblies can be used to tailor surface tribological properties.[8,9] By tailoring the end group functionality and the length of the alkyl backbone, precise control over frictional properties can be achieved in micro-electronic mechanical systems (MEMS)[10,11] applications. Further, molecular assemblies can be used as model surfaces for understanding interfacial phenomena, such as adhesion and surface properties of polymer films[1] and of assembly-passivated nanowires.[12]

The recent interest in molecular assemblies has been also instigated by the promise of nano-scale electronics,[13] where individual molecules or molecular assemblies comprise the electrically-active components. To explore the electrical characteristics of individual molecules and to enable the fabrication of functional molecular-scale devices, the molecules must be in intimate electrical contact with at least two electrodes.[14] By exploiting the proper head group functionality, molecules can be covalently attached to an electrode, frequently the substrate. A separate technique, however, is necessary to place the second, or top, electrode in contact with the molecules. Generally, there are two approaches to 'wiring' the molecules to the second electrode. One involves making electrical contact to the molecules directly with the metal of interest (so no top electrode). An example of this approach is the hanging-drop mercury (Hg) electrode. The hanging-drop Hg electrode[15,16] setup involves making direct macroscopic contact to a molecular assembly surface using a drop of Hg, as schematically illustrated in Figure 1.2. The second approach to 'wire' the molecules involves first depositing a top electrode (usually gold, Au) and then making electrical contact to the Au electrode. The Au electrode can be first defined on a sacrificial substrate and then transferred onto the molecular assembly. Nano-transfer printing (nTP) is one such example.[17] Originally developed by Loo and co-workers using 1,8-octanedithiol assemblies on gallium arsenide (GaAs),[17] nTP is schematically illustrated in Figure 1.3. This procedure involves a molecular assembly of dithiols adsorbed on a substrate, resulting in the chemical attachment of molecules to the substrate via one of the thiol groups. Separately, an elastomeric poly(dimethylsiloxane)

(PDMS) stamp is fabricated by casting and curing against a silicon master. A 5-20 nm metal layer, most commonly Au, is evaporated on stamp surface, and the stamp is brought into contact with the dithiol assembly on the substrate. The intimate contact between the stamp and the substrate allows the free thiol end groups to covalently bond to the metal that is on the stamp surface.[18] When the stamp is removed, the metal is transferred and remains on the dithiol assembly surface due to covalent bonding with the free thiol groups. Junctions of n^+GaAs—1,8-octanedithiol—Au were fabricated by nTP in this fashion. Electrical studies indicate that the current densities of these junctions scale with the Au contact area; this technique is deemed a reliable process for depositing the top Au electrodes.[19]

The goal of our research was to fabricate and characterize molecular assembly-based junctions with model electrically-active molecules. In this work, we focused on molecules containing simple aromaticity, or n-phenyldithiols ($n = 2 – 4$), illustrated in Figure 1.4. In contrast to simple alkyl systems, biphenyldithiol (BPDT), terphenyldithiol (TPDT), and quaterphenyldithiol (QPDT) are more similar to the electronically-complex systems of interest to the molecular electronics community. They are potentially capable of charge transport due to backbone conjugation. Additionally, these conjugated molecules have thiol end groups so they can bind on both ends. Similar to 1,8-octanedithiol employed for the development of nTP by Loo et. al.,[17,19-21] n-phenyldithiols can therefore be covalently constrained between two electrodes. Covalent molecule-electrode attachment is expected to facilitate reliable electrical contact, a necessary prerequisite to fabricating functional devices.[14,22]

In the course of our research, we addressed the major aspects of forming the molecular assembly-based junctions from the bottom up, including aspects of molecule adsorption on substrates, making electrical contact to these molecular assemblies, and measuring charge transport across them. The first part of our work focused on elucidating how processing conditions influence the way n-phenyldithiols organize on common substrates, such as Au and GaAs. Specifically, we examined how the choice of the assembly solvent and concentrations of precursors affect the final structures of the molecular assemblies. The molecular assemblies were characterized by synchrotron-based near-edge x-ray absorption fine structure spectroscopy (NEXAFS), Fourier-transform infrared spectroscopy (FTIR), and spectroscopic ellipsometry. The combination of these analytical techniques provided information about the relative surface coverage, molecular orientation, and surface termination of the molecular assemblies.

With a better understanding of the processing-structure relationships that govern the molecular assemblies of model conjugated dithiols on Au and GaAs, the second part of this work focused on depositing Au electrodes on the conjugated dithiol assembly surfaces using nTP. Specifically, we pursued the fabrication of two-terminal GaAs—dithiol—Au junctions, akin to those demonstrated by Loo et. al.[17,19-21] for 1,8-octanedithiol assemblies. Following the deposition of the top Au electrodes by nTP, we carried out spectroscopic characterization of both the dithiol-GaAs (bottom) and the dithiol-Au (top) interfaces using x-ray photoelectron spectroscopy (XPS).

Finally, with the elucidation of both the assembly structure and the nature of molecule-electrode contact, we used galinstan as the soft contact material for electrical characterization. Galinstan is a liquid metal alloy consisting of gallium, indium, and tin, and is an alternative to mercury in the hanging-drop mercury setup.[23] First, we measured the electrical response of BPDT, TPDT, and QPDT molecular assemblies by making direct electrical contact to the molecular assembly surfaces using galinstan. Second, GaAs—dithiol—Au junctions prepared via nTP were examined using the same galinstan setup.

We selected Au and GaAs, substrates already common in the field of thiol assembly,[1,24-26] for our studies. GaAs exhibits a roughness rms of ≈0.3 nm after native oxide removal. Au exhibits a roughness rms of ≈1.3 nm when prepared using conventional evaporation techniques.[27] Figure 1.5 contains atomic force microscopy (AFM) images obtained on a GaAs substrate after the removal of its native oxide and a silicon substrate covered with freshly-evaporated Au, respectively. We focused on GaAs as the substrate for our spectroscopic studies because the S-GaAs bonds are energetically different from the S-Au bonds.[1,28] We were thus able to distinguish the covalent bonds at the bottom electrode-molecule and at the molecule-top electrode interfaces. We selected GaAs as the substrate for our electrical studies because GaAs does not cold-weld with Au.[29] Specifically, when two Au surfaces are brought into contact, they tend to form metallic bonds at the interface.[29] The possibility of such metallic bond formation would increase the tendency for electrical shorts if Au were used as both the top and bottom electrodes. Since GaAs does not bond with Au, the use of GaAs, instead of Au, as the bottom substrate eliminates the possibility of accidental electrical shorts in GaAs—dithiol—Au junctions.

BACKGROUND

Molecule adsorption

The adsorption of alkylthiols on coinage metal and semiconductor surfaces has been characterized extensively.[1] The thiol groups are particularly effective at bonding to coinage metals[1,30-36] and Hg[37] via covalent S-metal bonds. For example, alkylthiols adsorb on Au via covalent S-Au bonds of ≈1.3 eV.[1,28] Alkylthiols have also been reported to adsorb on GaAs,[1,3,7,32] although via a weaker semi-ionic interaction of ≈0.81 eV.[28] Molecular assemblies consisting of alkylthiols with longer backbones generally exhibit preferentially upright molecular orientation due to increased intermolecular interactions.[30-32] The details of molecular orientation can be further affected by a variety of processing conditions, including the types of substrate,[38] the solvent quality,[39] the molecule concentration in solution,[25,39,40] the temperature at which assembly takes place,[41] and post-assembly cleaning protocols.[42]

In contrast to alkylthiols, the assembly of conjugated molecules is far more complicated. Recent structural studies have demonstrate the assembly of simple n-phenyl,[27,43,44] oligo(phenylene ethynylene),[45] and a number of yet-more-complex porphyrin-[46] and rotaxane-based[47] conjugated systems. Like alkylthiols, conjugated thiols with longer conjugated backbones tend to adsorb in a preferentially upright fashion due to increased intermolecular interactions.[48-51] The procedures employed for forming conjugated thiol assemblies tend to be more involved than those used for alkylthiol assemblies. For example, conjugated dithiols are usually assembled from their acetyl-protected precursors because aromatic thiols are prone to oxidation[52] and dimerization.[53] The structures of the acetyl-protected precursors of the molecules used in our study are shown in Figure 1.6. The acetyl-protecting groups are normally cleaved *in-situ* using a deprotecting agent (commonly, NH_4OH[54]) to facilitate molecular assembly. To this end, the details of the deprotection procedure have also been reported to affect the final assembly structure.[44,45,55] The studies addressing the assembly of conjugated dithiols are limited and have focused exclusively on metal substrates.[27,56-58] Additionally, the details of molecular orientation and the factors that govern the organization of conjugated dithiols on either Au or GaAs have not been systematically investigated. We were therefore interested in understanding the factors that govern the adsorption and molecular orientation of conjugated dithiols on both Au and GaAs. Additionally, electrical studies of conjugated systems that have been reported thus far do not provide any information about the molecular orientation of the investigated molecular assemblies.[22,59] We therefore sought to understand the interplay between the molecular orientation of the model conjugated molecular assemblies with their electrical properties.

Characterization of electrical junctions

The idea of molecular electronics is more than three decades old.[13] The practical conception of molecular electronics in its current meaning is commonly credited to Aviram and Ratner who, in 1974, proposed, and supported with semi-quantitative calculations a method for making a rectifier based on a single molecule.[13] In fact, the first electrical measurements on molecular assemblies of simple molecules were performed in 1971, where Mann and Kuhn measured tunneling characteristics of alkyl-based fatty acid salts using an Al substrate and Hg to form the top metal contact.[60] To-date, the extensive research efforts in this field resulted in a number of elegant techniques of making electrical contact to both molecular assemblies[61] and single molecules.[61,62] Measuring the electrical characteristics of molecular junctions, however, remains challenging due to the inherent resolution and signal-to-noise limitations of these measurements.[14,61] Specifically, the measured electrical response of molecular assembly junctions is influenced by the details of the how the molecules are contacted. For example, the resistance measured for 1-dodecanethiol assemblies on Au by Akkerman et.al.[61] using conductive polymer top contacts ($5x10^7$ MΩ/molecule) is significantly higher than that measured by Engelkes et.al.[63] using conductive atomic force microscopy (10^6 MΩ/molecule). The resistance measured for these assemblies by Milani et.al.[64] using PmPV polymer electrodes is higher yet ($5x10^{11}$ MΩ/molecule). Similarly, the resistance measured for 1-octanethiol assemblies on Au by using conductive polymer top contacts[61]

($2x10^6$ MΩ/molecule) is significantly higher than that measured using evaporated Au contacts[61,65] ($2x10^4$ MΩ/molecule). The resistance measured for these assemblies using conductive atomic force microscopy[62] is higher yet (10^{11} MΩ/molecule). These variations in the measured electrical response are believed to stem from differences in the details of molecular organization on the surface,[66] as well as the quality of the molecule-electrode contact.[14] For instance, the current densities of both alkylthiols and conjugated thiols have been reported to increase as the molecular assemblies adopt a less upright molecular orientation.[16,66] This phenomenon has been attributed to the fact that less ordered molecular assemblies result in shorter tunneling distances.[16,66] We were therefore interested in examining how the molecular orientation of our model conjugated molecular assemblies affected the measured current densities.

In addition to the details of molecular orientation, electrical conduction through molecules is believed to be affected by the molecule-electrode contact.[14] For example, Cui et. al.[62] reported that the Au—1,8-octanedithiol—Au junctions were at least four orders of magnitude more conductive than the Au—1-octanethiol—Au junctions. The higher conductance of the dithiol junctions, relative to that of the monothiol junctions, was attributed to covalent S-Au interactions at both of the S-Au interfaces for dithiol and at only one S-Au interface for monothiol assemblies.[62] In the case of substrate—molecule—metal junctions, there are few methods to evaluate the molecule-metal interface.[67-71] The fact that this interface is buried under the top metal electrode presents clear challenges for direct spectroscopic analysis, so the nature of the molecule-metal contact is often evaluated indirectly.[59,72] In the case of GaAs—dithiol—Au junctions, the ‘Scotch tape test’[19] has been a dominant, albeit indirect, method used to speculate the nature of the top dithiol-Au interface. In this test, Scotch tape is attached to the deposited top Au electrode and then pulled off. One surmises the presence of covalent S-Au bonds at the dithiol-Au interface if the Au electrode remains on the assembly surface after the Scotch tape is pulled off. The potential of the nature of the top dithiol-Au interface to affect electrical conduction through our GaAs—n-phenyldithiol—Au junctions coupled with the lack of direct methods of examination of this interface prompted our effort in developing a direct spectroscopic method to address these issues.

THESIS OVERVIEW

Chapter 2 describes the synthesis of the acetyl-protected precursors of BPDT, TPDT, and QPDT used for forming the molecular assemblies in our work. This Chapter also describes the experimental techniques employed in our studies and introduces the associated data analysis protocols. The off-normal s-polarized transmission IR approach we developed and the grazing-angle x-ray photoelectron spectroscopy method we employed for probing the structures of our molecular assemblies on GaAs and their interfaces with Au deposited via nTP, respectively, are also detailed in this Chapter. Finally, the approach of using galinstan as the soft electrode material for electrical measurements is described.

Chapters 3 and 4 elucidate the impacts of processing conditions on the final structure of the molecular assemblies of conjugated dithiols. Specifically, Chapter 3 details the effect of solvent quality on the final structures of BPDT, TPDT, and QPDT assembled on Au and GaAs surfaces. Chapter 4 examines the effects of the deprotecting agent (NH_4OH) and acetyl-protected precursor concentrations on the final structure of molecular assemblies of the conjugated dithiols. The combined understanding of processing-structure relationships developed in Chapters 3 and 4 gave us the ability to assemble BPDT, TPDT, and QPDT with control and formed the basis of the junction work reported in Chapters 5 and 6.

Chapter 5 examines the nature of S-GaAs and S-Au interactions at the dithiol-GaAs and dithiol-Au interfaces in GaAs—dithiol—Au junctions. Specifically, we deposited very thin Au by nTP to simulate the Au electrodes (generally much thicker in the GaAs—dithiol—Au junctions). We then employed XPS to demonstrate that depositing Au by nTP in solvent (dichloroethane) results in more reliable S-Au bond formation than doing so at ambient conditions. The thickness of the Au was chosen such that we could obtain XPS signal through the printed layer.

Chapter 6 details our attempts to make reproducible electrical contact to the molecular assemblies. We extended the hanging-drop mercury approach (Figure 1.2) by using galinstan as the soft electrode. This allowed us to directly measure electrical conduction of and charge transport through GaAs—dithiol—Au junctions fabricated by nTP.

Finally, Chapter 7 summarizes the major achievements of our research effort and presents suggestions for future work.

FIGURES

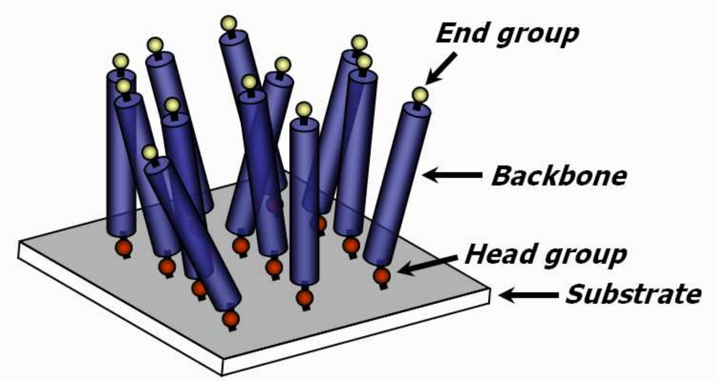

Figure 1.1. Schematic representation of a molecular assembly formed on a substrate. The head group, the backbone, and the end group of the constituent molecule are identified.

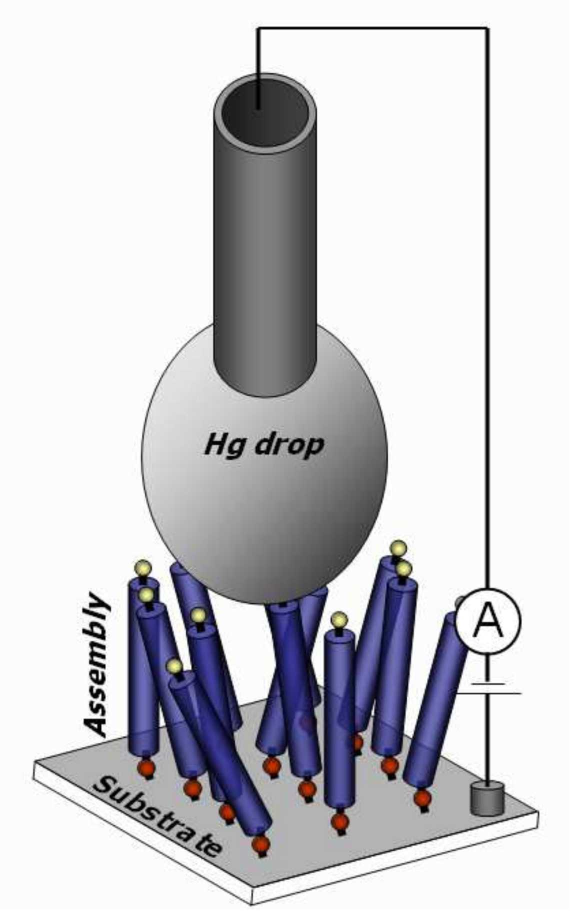

Figure 1.2. Schematic representation of the hanging-drop mercury electrode setup.

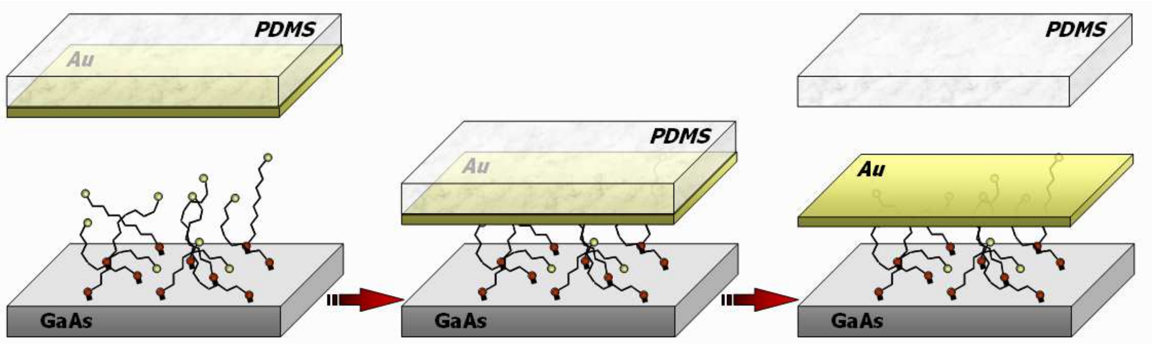

Figure 1.3. Schematic of Au transfer onto an 1,8-octanedithiol molecular assembly by nano-transfer printing.

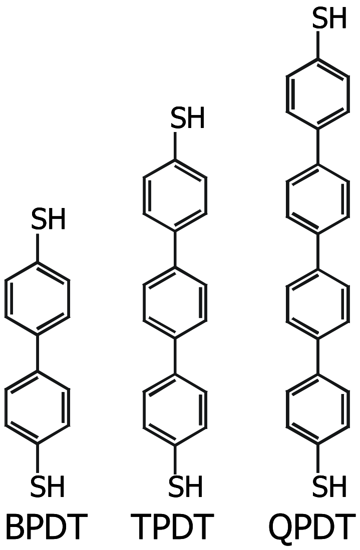

Figure 1.4. Chemical structures of biphenyldithiol (BPDT), terphenyldithiol (TPDT), and quaterphenyldithiol (QPDT) used in this work.

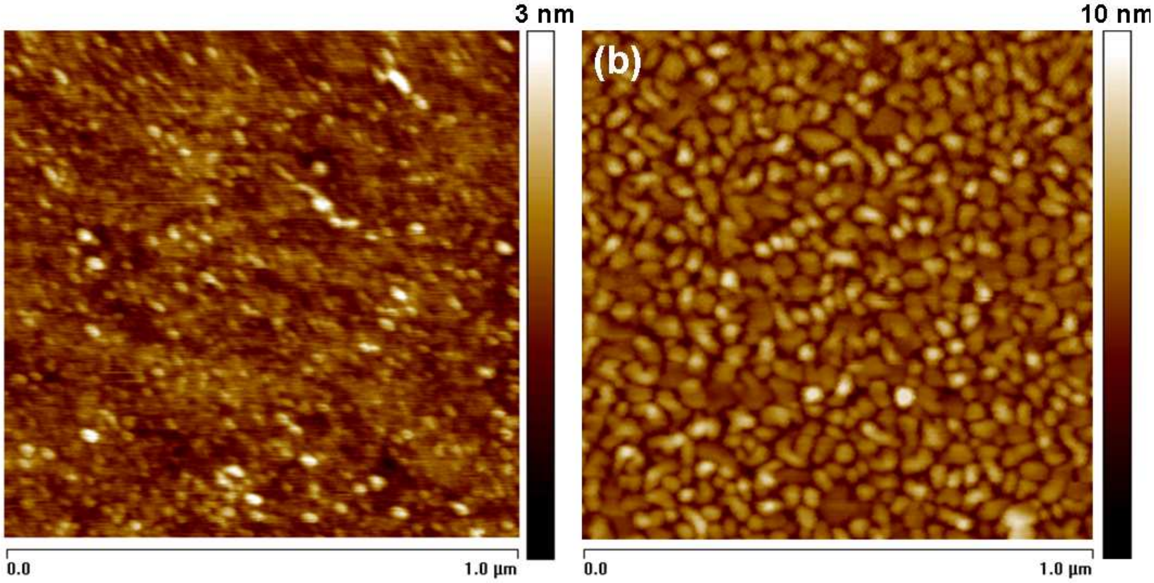

Figure 1.5. Atomic force microscopy topographical images of (a) etched GaAs substrate (rms roughness of ≈ 0.3 nm) and (b) a Si substrate with 100 nm thick Au (rms roughness of ≈ 1.3 nm).

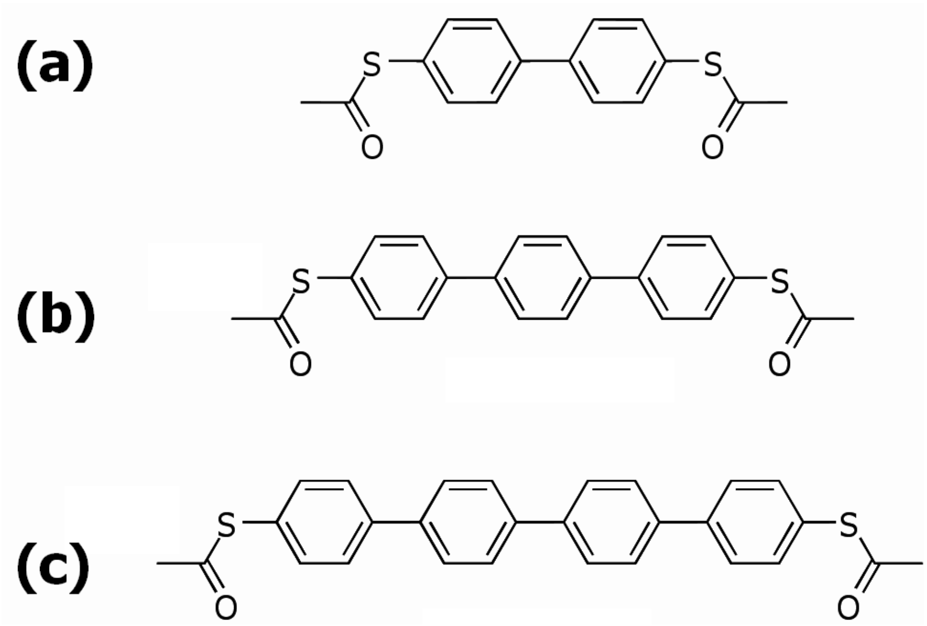

Figure 1.6. Chemical structures of the acetyl-protected precursors of (a) BPDT, (b) TPDT, and (c) QPDT. These acetyl-protected precursors were used to form molecular assemblies of BPDT, TPDT, and QPDT in this work.

REFERENCES

1. Ulman, A. *Chemical Reviews* **1996,** *96*, 1533.
2. Lim, H.; Carraro, C.; Maboudian, R.; Pruessner, M. W.; Ghodssi, R. *Langmuir* **2004,** *20*, 743.
3. Baum, T.; Ye, S.; Uosaki, K. *Langmuir* **1999,** *15*, 8577.
4. Cox, J. D.; Curry, M. S.; Skirboll, S. K.; Gourley, P. L.; Sasaki, D. Y. *Biomaterials* **2001,** *23*, 929.
5. Ostuni, E.; Chapman, R. G.; Liang, M. N.; Meluleni, G.; Pier, G.; Ingber, D. E.; Whitesides, G. M. *Langmuir* **2001,** *17*, 6336.
6. Sung, I.-H.; Kim, D.-E. *Applied Surface Science* **2005,** *239*, 209.
7. Tiberio, R. C.; Craighead, H. G.; Lercel, M.; Lau, T.; Sheen, C. W.; Allara, D. L. *Applied Physics Letters* **1993,** *62*, 476.
8. Ahn, H.-S.; Cuong, P. D.; Park, S.; Kim, Y.-W.; Lim, J.-C. *Wear* **2003,** *255*, 819.
9. Perry, S. S.; Lee, S.; Shon, Y.-S.; Colorado, R., Jr.; Lee, T. R. *Tribology Letters* **2001,** *10*, 81.
10. Maboudian, R.; Carraro, C. *Annual Review of Physical Chemistry* **2004,** *55*, 35.
11. Maboudian, R.; Carraro, C. *Journal of Adhesion Science and Technology* **2003,** *17*, 583.
12. Hang, Q.; Wang, F.; Carpenter, P. D.; Zemlyanov, D.; Zakharov, D.; Stach, E. A.; Buhro, W. E.; Janes, D. B. *Nano Letters* **2008,** *8*, 49.
13. Aviram, A.; Ratner, M. A. *Chemical Physics Letters* **1974,** *29*, 277.
14. Hipps, K. W. *Science* **2001,** *294*, 536.
15. Nesher, G.; Shpaisman, H.; Cahen, D. *Journal of the American Chemical Society* **2007,** *129*, 734.
16. Nesher, G.; Vilan, A.; Cohen, H.; Cahen, D.; Amy, F.; Chan, C.; Hwang, J.; Kahn, A. *Journal of Physical Chemistry B* **2006,** *110*, 14363.
17. Loo, Y.-L.; Willett, R. L.; Baldwin, K. W.; Rogers, J. A. *Applied Physics Letters* **2002,** *81*, 562.

18. Hsu, J. W. P.; Loo, Y. L.; Lang, D. V.; Rogers, J. A. *Journal of Vacuum Science & Technology B* **2003,** *21*, 1928.

19. Loo, Y.-L.; Lang, D. V.; Rogers, J. A.; Hsu, J. W. P. *Nano Letters* **2003,** *3*, 913.

20. Loo, Y.-L.; Hsu, J. W. P.; Willett, R. L.; Baldwin, K. W.; West, K. W.; Rogers, J. A. *Journal of Vacuum Science & Technology B* **2002,** *20*, 2853.

21. Loo, Y.-L.; Willett, R. L.; Baldwin, K. W.; Rogers, J. A. *Journal of the American Chemical Society* **2002,** *124*, 7654.

22. Kushmerick, J. G. *Materials Today* **2005,** *8*, 26.

23. Smith Linda, S. *Journal of Gerontological Nursing* **2003,** *29*, 26.

24. Krapchetov, D. A.; Ma, H.; Jen, A. K. Y.; Fischer, D. A.; Loo, Y.-L. *Langmuir* **2005,** *21*, 5887.

25. Jun, Y.; Zhu, X. Y.; Hsu, J. W. P. *Langmuir* **2006,** *22*, 3627.

26. Nicoara, N.; Cerrillo, I.; Xueming, D.; Garcia, J. M.; Garcia, B.; Gomez-Navarro, C.; Mendez, J.; Baro, A. M. *Nanotechnology* **2002,** *13*, 352.

27. de Boer, B.; Meng, H.; Perepichka, D. F.; Zheng, J.; Frank, M. M.; Chabal, Y. J.; Bao, Z. *Langmuir* **2003,** *19*, 4272.

28. Camillone, N.; Khan, K. A.; Osgood, R. M. *Surface Science* **2000,** *453*, 83.

29. Kim, C.; Burrows, P. E.; Forrest, S. R. *Science* **2000,** *288*, 831.

30. Dubois, L. H.; Nuzzo, R. G. *Annual Review of Physical Chemistry* **1992,** *43*, 437.

31. Dubois, L. H.; Zegarski, B. R.; Nuzzo, R. G. *Journal of Chemical Physics* **1993,** *98*, 678.

32. Ye, S.; Li, G.; Noda, H.; Uosaki, K.; Osawa, M. *Surface Science* **2003,** *529*, 163.

33. Karpovich, D. S.; Blanchard, G. J. *Langmuir* **1994,** *10*, 3315.

34. Fischer, D.; Marti, A.; Hahner, G. *Journal of Vacuum Science & Technology A* **1997,** *15*, 2173.

35. Laibinis, P. E.; Whitesides, G. M.; Allara, D. L.; Tao, Y. T.; Parikh, A. N.; Nuzzo, R. G. *Journal of the American Chemical Society* **1991,** *113*, 7152.

36. Kondoh, H.; Nambu, A.; Ehara, Y.; Matsui, F.; Yokoyama, T.; Ohta, T. *Journal of Physical Chemistry B* **2004,** *108*, 12946.

37. Tamam, L.; Kraack, H.; Sloutskin, E.; Ocko, B. M.; Pershan, P. S.; Ulman, A.; Deutsch, M. *Journal of Physical Chemistry B* **2005,** *109*, 12534.

38. McGuiness, C. L.; Shaporenko, A.; Mars, C. K.; Uppili, S.; Zharnikov, M.; Allara, D. L. *Journal of the American Chemical Society* **2006,** *128*, 5231.

39. Dannenberger, O.; Buck, M.; Grunze, M. *Journal of Physical Chemistry B* **1999,** *103*, 2202.

40. Bain, C. D.; Troughton, E. B.; Tao, Y. T.; Evall, J.; Whitesides, G. M.; Nuzzo, R. G. *Journal of the American Chemical Society* **1989,** *111*, 321.

41. Asadi, K.; Gholamrezaie, F.; Smits, E. C. P.; Blom, P. W. M.; de Boer, B. *Journal of Materials Chemistry* **2007,** *17*, 1947.

42. Castner, D. G.; Hinds, K.; Grainger, D. W. *Langmuir* **1996,** *12*, 5083.

43. Shaporenko, A.; Adlkofer, K.; Johansson, L. S. O.; Ulman, A.; Grunze, M.; Tanaka, M.; Zharnikov, M. *Journal of Physical Chemistry B* **2004,** *108*, 17964.

44. Shaporenko, A.; Elbing, M.; Blaszczyk, A.; Von Haenisch, C.; Mayor, M.; Zharnikov, M. *Journal of Physical Chemistry B* **2006,** *110*, 4307.

45. Cai, L.; Yao, Y.; Yang, J.; Price, D. W., Jr.; Tour, J. M. *Chemistry of Materials* **2002,** *14*, 2905.

46. Hutchison, J. E.; Postlethwaite, T. A.; Murray, R. W. *Langmuir* **1993,** *9*, 3277.

47. Collier, C. P.; Wong, E. W.; Belohradsky, M.; Raymo, F. M.; Stoddart, J. F.; Kuekes, P. J.; Williams, R. S.; Heath, J. R. *Science* **1999,** *285*, 391.

48. Kang, J. F.; Ulman, A.; Liao, S.; Jordan, R.; Yang, G.; Liu, G.-Y. *Langmuir* **2001,** *17*, 95.

49. Zharnikov, M.; Grunze, M. *Journal of Physics: Condensed Matter* **2001,** *13*, 11333.

50. Frey, S.; Stadler, V.; Heister, K.; Eck, W.; Zharnikov, M.; Grunze, M.; Zeysing, B.; Terfort, A. *Langmuir* **2001,** *17*, 2408.

51. Himmel, H.-J.; Terfort, A.; Woell, C. *Journal of the American Chemical Society* **1998,** *120*, 12069.

52. Tour, J. M.; Jones, L.; Pearson, D. L.; Lamba, J. J. S.; Burgin, T. P.; Whitesides, G. M.; Allara, D. L.; Parikh, A. N.; Atre, S. *Journal of the American Chemical Society* **1995,** *117*, 9529.

53. Weckenmann, U.; Mittler, S.; Naumann, K.; Fischer, R. A. *Langmuir* **2002,** *18*, 5479.

54. Tour, J. M.; II, L. J.; Pearson, D. L.; Lamba, J. J. S.; Burgin, T. P.; Whitesides, G. M.; Allara, D. L.; Parikh, A. N.; Atre, S. V. *Journal of American Chemical Society* **1995,** *117*, 9529.

55. Krapchetov, D. A.; Ma, H.; Jen, A. K. Y.; Fischer, D. A.; Loo, Y.-L. *Langmuir* **2008,** *24*, 851.

56. Azzam, W.; Wehner, B. I.; Fischer, R. A.; Terfort, A.; Woell, C. *Langmuir* **2002,** *18*, 7766.

57. Jiang, W.; Zhitenev, N.; Bao, Z.; Meng, H.; Abusch-Magder, D.; Tennant, D.; Garfunkel, E. *Langmuir* **2005,** *21*, 8751.

58. de Boer, B.; Frank, M. M.; Chabal, Y. J.; Jiang, W.; Garfunkel, E.; Bao, Z. *Langmuir* **2004,** *20*, 1539.

59. Kushmerick, J. G.; Holt, D. B.; Yang, J. C.; Naciri, J.; Moore, M. H.; Shashidhar, R. *Physical Review Letters* **2002,** *89*, 086802/1.

60. Mann, B.; Kuhn, H. *Journal of Applied Physics* **1971,** *42*, 4398.

61. Akkerman Hylke, B.; Naber Ronald, C. G.; Jongbloed, B.; van Hal Paul, A.; Blom Paul, W. M.; de Leeuw Dago, M.; de Boer, B. *Proceedings of the National Academy of Sciences of the United States of America* **2007,** *104*, 11161.

62. Cui, X. D.; Primak, A.; Zarate, X.; Tomfohr, J.; Sankey, O. F.; Moore, A. L.; Moore, T. A.; Gust, D.; Harris, G.; Lindsay, S. M. *Science* **2001,** *294*, 571.

63. Engelkes, V. B.; Beebe, J. M.; Frisbie, C. D. *Journal of the American Chemical Society* **2004,** *126*, 14287.

64. Milani, F.; Grave, C.; Ferri, V.; Samori, P.; Rampi, M. A. *ChemPhysChem* **2007,** *8*, 515.

65. Kim, T.-W.; Wang, G.; Lee, H.; Lee, T. *Nanotechnology* **2007,** *18*, 315204/1.

66. Ishida, T.; Mizutani, W.; Liang, T.-T.; Azehara, H.; Miyake, K.; Sasaki, S.; Tokumoto, H. *Annals of the New York Academy of Sciences* **2003,** *1006*, 164.

67. Lummerstorfer, T.; Sohar, C.; Friedbacher, G.; Hoffmann, H. *Langmuir* **2006,** *22*, 18.

68. Richter, C. A.; Hacker, C. A.; Richter, L. J. *Journal of Physical Chemistry B* **2005,** *109*, 21836.

69. Haick, H.; Ghabboun, J.; Niitsoo, O.; Cohen, H.; Cahen, D.; Vilan, A.; Hwang, J.; Wan, A.; Amy, F.; Kahn, A. *Journal of Physical Chemistry B* **2005,** *109*, 9622.

70. Walker, A. V.; Tighe, T. B.; Cabarcos, O. M.; Reinard, M. D.; Haynie, B. C.; Uppili, S.; Winograd, N.; Allara, D. L. *Journal of the American Chemical Society* **2004,** *126*, 3954.

71. Qu, D.; Uosaki, K. *Journal of Physical Chemistry B* **2006,** *110*, 17570.

72. Salomon, A.; Boecking, T.; Gooding, J. J.; Cahen, D. *Nano Letters* **2006,** *6*, 2873.

Chapter 2: Experimental Techniques

This Chapter provides an overview of the synthetic, experimental, and analytical details of our work. This Chapter begins with a description of the synthesis of the acetyl-protected precursors of biphenyldithiol (BPDT), terphenyldithiol (TPDT), and quaterphenyldithiol (QPDT). The formation of molecular assemblies with these precursors is then detailed. Following is the description of nanotransfer printing (nTP),[1-4] a technique that is used for transferring Au onto the surfaces of the molecular assemblies. Finally, the various analytical techniques employed to characterize the molecular assemblies are described. Associated data analysis approaches are also described.

SYNTHESIS OF DITHIOLS

The molecules used during this study were provided through a collaboration with Dr. Hong Ma and Prof. Alex K.Y. Jen in the Materials Science and Engineering Department, at the University of Washington in Seattle. Chemicals were purchased from Aldrich and used as-received unless otherwise stated. Tetrahydrofuran (THF) that was used during the synthesis of the model conjugated compounds was distilled under nitrogen from sodium using benzophenone as an indicator. Methylene chloride was distilled over P_2O_5. ^1H NMR spectra (200 MHz) were acquired on a Bruker-200 FT NMR spectrometer. ESI-MS spectra were collected on a Bruker Daltonics Esquire Ion Trap Mass Spectrometer.

Compound 1. The acetyl-protected precursor of BPDT. This molecule (Compound **1**, Scheme 2.1) was synthesized using the following sequence. To a solution of 4,4’-dibromobiphenyl (3.12 g, 10.0 mmol) in dry THF (100 mL), *tert*-butyllithium

(25.9 mL, 1.7 M in pentane) was added dropwise at -78 ^oC under a nitrogen atmosphere. The solution was stirred at -78 ^oC for 2 h, followed by the addition of sulfur powder (0.90 g, 28.0 mmol). The reaction mixture was then stirred at –78 ^oC for 1 h, warmed to 0 ^oC, and stirred again for an additional 1.5 h. The reaction mixture was then cooled to –78 ^oC, followed by a dropwise addition of acetyl chloride (2.0 mL, 2.20 g, 28.0 mmol). The resulting reaction mixture was slowly warmed to room temperature and stirred overnight. The reaction was quenched with water, and THF was evaporated *in vacuo*. The residue was extracted with methylene chloride. The combined methylene chloride layers were washed with water, dried with Na_2SO_4, and concentrated. The crude product was then purified over a silica gel column with hexane/methylene chloride (1:1 to 1:2) as the eluent, yielding a white solid (0.44 g, 15%). ^1H NMR (200 MHz, $CDCl_3$): δ 7.63 (4H, d, J = 8.1 Hz), 7.49 (4H, d, J = 8.1 Hz), 2.45 (6H). ESI-MS (m/z): Calcd. 302.0; Found 302.1.

Compound 2. The methylated intermediate (Compound **2**, Scheme 2.1) that is subsequently used for TPDT (Compound **3**) synthesis was prepared using the following steps. A Grignard solution was prepared by the dropwise addition of a solution of 1-bromo-4-methylthiobenzene (10.56 g, 52.0 mmol) in dry THF (20 mL) to magnesium (1.33 g, 54.6 mmol) in dry THF (40 mL) under nitrogen. The combined solution was refluxed for 3.5 h at 65°C. The resulting Grignard solution was then cooled to room temperature and transferred to a suspension of 1,4-dibromobenzene (4.72 g, 20.0 mmol) and $Ni(dppp)Cl_2$ (0.11 g, 0.2 mmol) in dry THF (100 mL) at 0 ^oC under nitrogen. The mixture was further stirred for 24 h under reflux, cooled, and poured into 1 N HCl solution (200 mL). The precipitate was filtered, washed with water, hexane, and methylene chloride, and dried overnight at 40 ^oC under vacuum to yield a light-yellow solid (5.90 g, 92%). ^{1}H NMR (200 MHz, $CDCl_3$): δ 7.65 (s, 4H), 7.55 (d, *J* = 8.0 Hz, 4H), 7.32 (d, *J* = 8.0 Hz, 4H), 2.55 (s, 6H). ESI-MS (*m*/*z*): Calcd. 322.1; Found 322.0.

Compound 3. TPDT. To a solution of **2** (Scheme 2.1) (1.00 g, 3.1 mmol) in anhydrous dimethylformamide (DMF, 25 mL), sodium *tert*-butylthiolate (1.04 g, 9.3 mmol) was added. The reaction mixture was stirred vigorously and refluxed for 6 h under nitrogen at 153°C.[5,6] The solution was cooled to room temperature and was poured into a 10% HCl solution (65 mL). The resulting precipitate was filtered off, washed with water and cold ethanol, and dried overnight at 40 ^{o}C under vacuum to yield a pale white solid (0.86 g, 95%). ^{1}H NMR (200 MHz, $CDCl_3$): δ 7.62 (s, 4H), 7.51 (d, *J* = 8.2 Hz, 4H), 7.36 (d, *J* = 8.2 Hz, 4H), 3.51 (s, 2H). ESI-MS (*m*/*z*): Calcd. 294.1; Found 294.0.

Compound 4. Acetyl-protected precursor of TPDT. Due to the reported tendency for dithiols to oxidize,[7] the thiol end groups were converted to thiolacetyl end groups per details below. The thioacetyl end groups were then converted back to thiolates during molecular assembly formation (see details in Molecular Assembly Formation below). To convert the thiols into thioacetyl groups, triethylamine (0.30 g, 3.0 mmol) followed by acetyl chloride (0.24 g, 3.0 mmol)[8,9] were added dropwise to a solution of Compound **3** (TPDT, Scheme 2.1) (0.40 g, 1.4 mmol) in dry methylene chloride (20 mL) under nitrogen. The mixture was then stirred for 24 h at room temperature, poured into water, and extracted with methylene chloride. The combined methylene chloride layers were washed with water, dried with Na_2SO_4, and concentrated. The crude product was purified over silica gel column chromatography with hexane/methylene chloride (1:1) to methylene chloride as the eluent, yielding a light-yellow solid (0.39 g, 75%). ^{1}H NMR (200 MHz, $CDCl_3$): δ 7.65-7.75 (m, 8H), 7.50 (d, *J* = 7.8 Hz, 4H), 2.46 (s, 6H). ESI-MS (*m*/*z*): Calcd. 378.1; Found 378.1.

Compound 5. Acetyl-protected precursor of QPDT. The acetyl-terminated QPDT precursor (Compound **5**, Scheme 2.1) was synthesized with 4,4'-dibromobiphenyl as the starting material and using the same three-step procedure that was used to synthesize Compound **4** (Scheme 2.1). A slightly yellow solid was obtained. ^{1}H NMR (200 MHz, $CDCl_3$): δ 7.65-7.75 (m, 12H), 7.51 (d, J = 8.0 Hz, 4H), 2.47 (s, 6H). ESI-MS (m/z): Calcd. 454.1; Found 454.0.

MOLECULAR ASSEMBLY FORMATION

SureSeal^{TM}-grade solvents from Aldrich were used as-received to assemble the molecules on Au and GaAs. Polycrystalline Au substrates were prepared by evaporating 5 nm of Ti followed by 25 nm of Au on polished silicon test wafers (Wacker) in an evaporation chamber with a base pressure of $\approx 1\times10^{-7}$ Torr. These substrates were immediately transferred into a glove box (MBraun, <0.1 ppm O_2, <0.1 ppm H_2O) for immersion in the assembly solutions. Single-side-polished n+ Si-doped ($0.8\text{-}1\text{x}10^{18}$ cm^{-3}) GaAs (100) from AXT was used for near-edge x-ray absorption fine structure (NEXAFS) spectroscopy, x-ray photoelectron spectroscopy (XPS), and current-voltage (I-V) characterization; double-side-polished undoped (100) GaAs from AXT was used for transmission Fourier transform infrared (FTIR) spectroscopy.

The general steps of molecular assembly formation on Au and/or GaAs substrates are illustrated in Figure 2.1. The assembly sequence consists of dissolving the acetyl-terminated precursors in a solvent (EtOH, THF, or a combination of the two) at prescribed concentrations, followed by the addition of NH_4OH to convert the thioacetyl end groups to thiolates. As illustrated in Scheme 2.2, the addition of NH_4OH results in the deprotection of the acetyl-protected precursors by cleaving the acetyl protecting groups. The substrates are then immersed for approximately 18-24 hours before they are retrieved, sonication and/or rinsed with EtOH and dried with a stream of nitrogen. During this process, the solvent quality, concentrations of NH_4OH and acetyl-protected precursors, temperature at which the assembly takes place, and post-assembly cleaning procedures can significantly affect the final structure of the resulting molecular assemblies. In the subsequent chapters, we outline how careful control of these variables allowed us to achieve high surface coverage molecular assemblies that are preferentially upright.

For studies aimed at examining the impact of solvent quality on the final structure of the model conjugated dithiol assemblies (Chapter 3), the native oxide layer on GaAs was removed by etching the substrates in concentrated hydrochloric acid (HCl) for 1 minute, followed by rinsing with deionized water and drying with a stream of nitrogen.[10] For all other studies, the native oxide layer on GaAs was removed by etching the substrates in concentrated HCl for 30 seconds and then in concentrated NH_4OH for 30 seconds;[11,12] this procedure was repeated once again before the substrates were rinsed with EtOH and dried with a stream of nitrogen following the first three etches. After the fourth and last etch in NH_4OH, the substrates were rinsed with deionized water and dried with a stream of nitrogen. The more tedious HCl/NH_4OH etching procedure was adopted later in this project because it was reported to yield cleaner GaAs surfaces compared to the former etching procedure with HCl alone.[12] The etched substrates were immediately transferred into the glove box for immersion in the assembly solutions.

In studying how the solvent quality impacts the final structure of the molecular assemblies (Chapter 3), we prepared the assembly solutions by dissolving acetyl-protected precursors of BPDT, TPDT or QPDT precursors at 80 μM in either EtOH, THF, or in cosolvents of EtOH and THF. Throughout this Dissertation, we describe the assembly solvent in terms of EtOH fraction in the solvent, or EF. EF = 1 indicates that neat EtOH was used to assemble the molecules, while EF = 0 indicates that neat THF was used. Accordingly, EF = 0.5 indicates a 50/50 (v/v) EtOH/THF cosolvent mixture. NH_4OH at 25 μL per 5 mL of assembly solution was then added to facilitate the conversion of thioacetyl end groups to thiolates ($S^-NH_4^+$).[7] After the addition of NH_4OH, the solutions were agitated for 1 minute and left for an hour before freshly-evaporated Au or freshly-etched GaAs substrates were immersed. The substrates remained immersed for 24 hours before they were removed and copiously rinsed with EtOH and dried in a stream of nitrogen. The post-assembly protocol of rinsing with EtOH and drying with a stream of nitrogen is used for all studies unless otherwise noted. Due to the low solubility of acetyl-protected precursor of QPDT in EtOH, we were not able to assemble QPDT from pure EtOH. We therefore assembled QPDT from solutions ranging from pure THF to a cosolvent with EF = 0.9. The complete range of EtOH/THF solution compositions was explored for TPDT. BPDT was only assembled from solutions with neat EtOH and THF.

In studies examining the concentration effects of NH_4OH and acetyl-protected precursor on the final structure of the molecular assemblies (Chapter 4), TPDT solutions were prepared by dissolving the acetyl-protected TPDT precursor (at 250 μM for NH_4OH concentration studies; at a range of 50 – 500 μM for precursor concentration studies) in either EtOH or THF. QPDT solutions were prepared by dissolving the acetyl-protected precursor of QPDT (at 50 μM for NH_4OH concentration studies; at a range of 50 – 250 μM for precursor concentration studies) in a cosolvent with EF = 0.75. NH_4OH at 1, 10, 30, or 160 mM was then added to the solutions (no NH_4OH was added for select samples, as noted in Chapter 4). After the addition of NH_4OH, the solutions were left for an hour before freshly-evaporated Au or freshly-etched GaAs substrates were immersed for 18 - 24 hours. TPDT assemblies were carried out at 55°C; QPDT assemblies were carried out at room temperature for NH_4OH concentration studies and at 55°C for experiments to examine the effect of varying precursor concentration on the structure of the final assembly. The increased temperature was selected to aid the dissolution of the acetyl-protected precursors in EtOH at the elevated concentrations. The Au and GaAs samples, upon removal from the assembly solution, were rinsed thoroughly with EtOH, sonicated in a 2 mM solution of tri-*n*-butylphosphine (TBP) in EtOH for 15 minutes, and left immersing in the same TBP solution for 40 minutes to remove any disulfides that may have formed during the assembly.[13] After TBP treatment, the samples were thoroughly rinsed with EtOH and dried in a stream of nitrogen.

For experiments examining how QPDT assembly surfaces interact with printed Au (Chapter 5) and for the electrical studies of QPDT molecular assemblies (Chapter 6), QPDT solutions were prepared by dissolving the acetyl-protected QPDT precursor in a cosolvent with EF = 0.75 at 50 μM. For the same electrical studies, BPDT and TPDT solutions were prepared by dissolving the corresponding acetyl-protected precursor at 250 μM in EtOH. NH_4OH, was added at 1 mM (BPDT and TPDT) and 10 mM (QPDT) before freshly-etched GaAs substrates were submerged for assembly 1 hour later. No NH_4OH was added for select samples, as noted in Chapter 6. The assembly of BPDT and TPDT was carried out at 55°C; QPDT assembly was carried out at room temperature.

1,8-octanedithiol (99%; Acros Organics) was dissolved in EtOH as-received at 5 mM, immediately followed by substrate immersion. The assembly on Au and GaAs was carried out for 18-24 hours at ambient conditions. The samples were copiously rinsed with EtOH and dried in a stream of nitrogen. 1-hexadecanethiol (92%; Aldrich) molecular assemblies on GaAs were formed in the same fashion.

NANO-TRANSFER PRINTING (nTP)

We employed nano-transfer printing (nTP), originally developed by Loo and co-workers[4] to transfer Au contacts, to make electrical contact to our model conjugated assemblies on GaAs (Chapter 6). In this procedure, illustrated above in Figure 1.3, a dithiol assembly is formed on a substrate, resulting in the covalent attachment between one of the thiol groups and the substrate. Separately, an elastomeric poly(dimethylsiloxane) (PDMS) stamp – commonly used in soft lithography[14] – is fabricated by casting and curing the prepolymer against a silicon master (flat or patterned by conventional photolithography).[14-16] Metal (Au in our case) is evaporated on the raised and recessed regions of the elastomeric stamp, and the stamp is brought into contact with the dithiol-treated substrate. Due to the intimate contact between the stamp and the assembly surface, the free thiol end groups can bond to the metal that is on the stamp surface without external pressure.[17] Gently peeling the stamp away results in the transfer of the metal from the raised regions of the stamp to the molecular assembly surface. Currently, the deposition of Au and Cu on 1,8-octanedithiol molecular assemblies on GaAs via nTP has been successfully demonstrated.[2,18]

Silicon masters,[1,15,16] with recessed circular features having diameters ranging from 100 to 2000 μm, were fabricated by conventional photolithography. Prior to casting PDMS, the master treated with (tridecafluoro-1,1,2,2-tetrahydroctyl) trichlorosilane[14] (Gelest) to render the silicon surface non-stick. The treatment was carried out by first cleaning the silicon masters in a UV/Ozone chamber for 10 minutes, followed by placing them over trichlorosilane vapors for 30 minutes under house vacuum.

PDMS stamps were made with Dow Corning Sylgard 184 PDMS formulation. Sylgard 184 consists of a PDMS prepolymer and a crosslinker. We mixed the prepolymer and crosslinker in a ratio of 10:1 (w:w) and allowed the mixture to degas.[18] PDMS stamps were then fabricated by casting and curing the PDMS prepolymer mixture against a silicon master. The cure condition was 70°C for 2 hrs. The cured PDMS was then peeled from the master. The PDMS stamp takes on the negative image of the silicon master so we end up with posts of varying diameter in PDMS.

For the x-ray photoelectron spectroscopy studies (Chapter 5), the PDMS stamps were leached prior to nTP. This procedure was adopted based on the discovery by Felmet et.al.[18] that the Au surface in contact with the PDMS stamps during nTP is normally contaminated by residual oligomers transferred from the stamp. The residual oligomer contamination can be reduced by leaching the elastomeric stamps in boiling toluene for 2-3 days and drying them in the oven overnight prior to nTP.[18] We carried out leaching in toluene at constant reflux (110°C) for 48 hours.[18] Following the removal from toluene, the stamps were dried of residual toluene in air at ambient conditions overnight, then in a vacuum oven at 50°C overnight. While leaching with toluene produces cleaner elastomeric stamps, we found these stamps to be less flexible and more 'sticky' toward the evaporated Au.

In addition to conventional nTP, we developed and employed 'wet' nTP where the Au pattern was transferred from the PDMS stamp onto the molecular assembly surface in a solvent. Here, the wetting of the substrate surface by the Au film on the PDMS stamp is governed by the surface tension, λ, of the solvent.[19] Specifically, in order for the Au film to wet a substrate, the solvent must be excluded from the Au-substrate interface. Vilan and Cahen[20] have argued that the solvent surface tension must typically exceed 25 mJ m^{-2} for a Au leaf to float on the solvent surface. Additionally, Shimizu et. al.[19] have pointed out the importance of using a high surface tension solvent to ensure its exclusion from the Au-substrate interface during printing. Indeed, we could not induce wetting of the Au on the PDMS stamp to the molecular assembly surfaces in EtOH, a solvent with low surface tension (λ = 23 mJ m^{-2})[21]. From a range of solvents with surface tension above 25 mJ m^{-2} (anisole, λ = 35 mJ m^{-2}; benzene, λ = 28 mJ m^{-2}; chloroform, λ = 27 mJ m^{-2}; cyclopentanone, λ = 33 mJ m^{-2}; dichloroethane, λ = 39 mJ m^{-2})[21], we found dichloroethane (DCE) to result in the most controlled and reproducible wetting while minimizing stamp distortion. We have thus selected DCE for our 'wet' nTP experiments.

NEAR-EDGE X-RAY ABSORPTION FINE STRUCTURE (NEXAFS) SPECTROSCOPY

NEXAFS spectroscopy uses polarized synchrotron x-rays to excite core electrons into unoccupied antibonding states. We monitor the subsequent relaxation of these electrons in order to obtain chemical and structural information about our molecular assemblies. The NEXAFS spectra reflect the element's characteristic transitions and, accordingly, the elemental bonding environments.[22] Due to the strong directional character of molecular orbitals and the high degree of polarization of incident x-rays, NEXAFS resonance intensities are proportional to the dot product of the electric field vector, ***E***, and the transitional dipole moment. Hence, if the molecules within the molecular assembly are preferentially oriented, the integrated intensities of their characteristic resonances will depend strongly on the x-ray incident angle. NEXAFS is therefore an ideal technique of probing the ensemble-average orientation[22] of molecular assemblies adsorbed on substrates. In addition, NEXAFS provides relative surface coverage information.

NEXAFS spectroscopy experiments were carried out at the NIST/Dow soft x-ray materials characterization facility located at beamline U7A at the National Synchrotron Light Source at Brookhaven National Laboratories.[23] The partial electron yield (PEY)

NEXAFS spectra were obtained at the C K-edge using a retarding entrance grid bias of -150V for enhanced surface sensitivity.[24] Linearly polarized synchrotron soft x-rays with a polarization factor, P, of ≈ 85% were used.[25] For studies examining the effect of solvent quality on the final structure of the molecular assemblies (Chapter 3), we used a scan step of 0.1 eV in the region of interest (280-310 eV) and a scan step of 0.2 eV at the pre- (270-280 eV) and post-edge (310-320 eV) regions.[10] For all other experiments, we scanned in increments of 0.1 eV in the region of interest (280-300 eV) and in increments of 0.5 eV at the pre- (250-280 eV) and post-edge (300-330 eV) regions.[11] All NEXAFS spectra were collected in high vacuum of $\approx 1\times10^{-8}$ torr at ambient temperature. Raw NEXAFS spectra were normalized by the corresponding incident beam intensity, I_o, obtained concomitantly on a freshly-coated Au grid located upstream from the sample chamber. This normalization accounts for any incident beam intensity fluctuations and monochromator absorption features.[26] For studies examining the effect of solvent quality on the final structure of the molecular assemblies (Chapter 3), we corrected the background curvature in the spectra of assemblies on Au by dividing each sample spectrum by a third-order polynomial fit to the spectrum of bare Au.[27]

To evaluate the normalized surface coverage in molecular assemblies on Au and GaAs, polarization-independent spectra were acquired at an x-ray incident angles (the angle between the incidence beam and the substrate plane) of 50 or 55°. Both of these angles are near 51°, commonly referred to as the 'magic angle'.[22] At the 'magic angle', the spectra are independent of the details of molecular orientation and can therefore be compared directly across various samples.[22] A sample pre-edge normalized C 1s NEXAFS spectrum of TPDT assembled on Au is shown in Figure 2.2. Clearly visible are the prominent resonance at 285 eV attributed to the $C1s \rightarrow \pi^*_{C=C}$ transition[22] of the TPDT backbone and the broad resonances at 293 and 303 eV associated with the C1s →

σ_1* and σ_2* transitions.[22] To quantify the relative surface coverage, we employed the ratio of the integrated intensity of the π* resonance at 285 eV and the magnitude of the carbon-edge jump[10] (labeled ‘jump’ in Figure 2.2). Since the peak at 285 eV emanates exclusively from the π* transition of phenyl backbones of the molecules and the magnitude of the edge jump reflects the total carbon content on the surface, this ratio accurately represents the relative surface coverage in our samples. This ratio is referred to as π*/jump from this point forward.

Angle-dependent NEXAFS data were obtained by varying the x-ray incident angle between 20° (grazing) and 75° (near-normal). A sample set of pre- and post-edge normalized NEXAFS spectra of TPDT assembled on Au acquired at varying x-ray incident angles is shown in Figure 2.3. The ensemble-average orientation of the molecules with respect to the substrate surface can be quantified by examining the details of angular dependence of the π* resonance intensity in these spectra. Specifically, the resonance intensities in this sample set of spectra vary with the x-ray incident angle: the π* resonance intensifies while the σ* resonances subside when the incident angle is increased from 20° to 75°. This phenomenon, where the π* resonance intensifies at the expense of the σ* resonances, is an indication that the assemblies are preferentially oriented.[28] The presence of preferential orientation is further corroborated by the difference spectra presented in the lower portion the plot. We obtained the difference spectra by subtracting the NEXAFS spectra acquired at 20° from the NEXAFS spectra obtained at other x-ray incident angles, i.e., $I(\theta) - I(20°)$. As such, the difference spectra emphasize the angle-dependent resonances originating from features that are preferentially oriented. The ensemble-average orientation of the assemblies can be qualitatively deduced from the way in which the orbitals interact with the electric field vector, ***E***, of the incident x-rays. Specifically, only orbitals with components collinear with the electric field vector of the incident polarized x-rays can absorb energy.[22] The spectral intensity of a given resonance therefore depends on the extent of collinearity of the molecular orbital with the electric field vector of incident x-rays. Considering that the electric field vector, ***E***, is normal to the x-ray incidence,[22,27] we can qualitatively deduce its interactions with the molecular orbitals by examining the NEXAFS spectra at varying x-ray incident angles. For instance, the spectrum acquired at 75° in Figure 2.3 exhibits the highest intensity of the π* resonance (285 eV) and the weakest intensity minimal intensities of the σ* resonances (293 and 303 eV). At 20°, the spectrum is reversed, with the π* resonance (285 eV) exhibiting the weakest intensity and the σ* resonances (293 and 303 eV) exhibiting the highest intensity. According to the dipole selection rule outlined above, these trends indicate that the π* orbitals of the molecular backbones are nearly collinear with ***E*** (hence maximal intensity), while the σ* planes are nearly perpendicular to ***E*** (hence minimal intensity) in this configuration. In contrast, at grazing x-ray incidence of 20°, the π* orbitals must be oriented nearly perpendicular to ***E*** (hence minimal intensity of the π* resonance in this configuration), while the σ* planes must be nearly collinear with ***E***. Considering that the π* orbitals are normal to the long molecular backbone axis, while the σ* planes are parallel to it, it follows from the intensity trends in Figure 2.3 that the molecules must be oriented with their backbone axes preferentially upright on the substrate surface.[28]

The ensemble-average molecular orientation can be quantified by a dichroic ratio (DR):[29]

$$DR = \frac{I(75^{o}) - I(20^{o})}{I(75^{o}) + I(20^{o})} \qquad \text{Equation (2.1)}$$

where $I(\theta)$ represents the integrated π* intensity obtained at an x-ray incident angle of θ with respect to the substrate surface. DR quantifies the level of anisotropy of the molecular assembly. According to the NEXAFS dipole selection rules,[10,29] DR > 0 indicates a preferentially upright ensemble-average molecular orientation, while DR < 0 indicates that the molecules are preferentially 'lying down'. Accordingly, DR ≈ 0 indicates the absence of any preferential orientation, i.e., the assembly is disordered.

We can also quantify the ensemble-average molecular orientation in a more rigorous fashion by using the building block (BB) model,[30,31] which allows us to estimate the ensemble-average molecular backbone tilt angle relative to the substrate normal. To apply this model, the difference spectra are first fitted with a series of Gaussian functions in order to determine the positions and the peak widths of the angle-dependent features.[30] The resulting peak parameters, along with a C1s → continuum transition edge, are then used to fit the spectrum obtained at the 'magic angle'.[30] The difference between the fit and the NEXAFS spectrum at its 'magic angle' is then subtracted from all the other spectra in the set to isolate the angle-dependent features. Finally, the intensities that result from this subtraction are fitted again by floating the intensities of the previously specified Gaussian functions to obtain the integrated peak intensities.[30] We selected the π* resonance at 285 eV – the most intense spectral feature – for quantitative analysis of the ensemble-average molecular backbone tilt. The π* resonance integrated intensity, I_v, that originates from the corresponding vector orbital, assuming a three-fold substrate symmetry, can be described by:[22]

$$I_v(\alpha,\theta) = A\{\tfrac{1}{3}P[1+\tfrac{1}{2}(3\cos^2\theta-1)(3\cos^2\alpha-1)]+\tfrac{1}{2}(1-P)\sin^2\alpha\} \qquad \text{Equation (2.2)}$$

where A is a proportionality constant; P is the x-ray polarization factor (≈85% in our set-up); θ is the x-ray incident angle; and α is the angle between the orbital vector and the substrate normal. Figure 2.4 presents a schematic of an adsorbed molecule, and it illustrates the different angles involved in this analysis. From a geometrical standpoint:

$$\cos^2 \alpha = \cos^2 \varphi \sin^2 \rho \qquad \text{Equation (2.3)}$$

Equation (2.3) can be equivalently expressed as:

$$\sin^2 \alpha = 1 - \cos^2 \varphi \sin^2 \rho \qquad \text{Equation (2.4)}$$

where ρ is the tilt angle of the molecular backbone axis away from the substrate normal (see Figure 2.4); φ is the ring-plane twist angle, defined as the angle between the π transition dipole moment vector of the phenyl rings and the plane spanned by the molecular backbone axis and the substrate normal. The average molecular tilt angle is estimated by fitting the π* integrated resonance intensity as a function of x-ray incident angle to Equation (2.2).[22,30] During the fitting process, A and ρ are floating parameters. We assumed $\varphi = 32^{o}$ and a planar backbone (i.e., successive phenyl rings are coplanar) in our analysis for TPDT and QPDT molecular assemblies (BPDT assemblies are disordered at all the conditions we explored).[32-35] An example outcome of this fitting procedure is shown in Figure 2.5, where we plotted the integrated π* intensities extracted from the spectra in Figure 2.3 (black squares), along with their theoretical fits to Equation (2.2), as a function of x-ray incident angle. The best fit (solid line) and the corresponding backbone tilt angle, ρ, are highlighted. The dotted lines are graphical representations of Equation (2.2) at other specified backbone tilt angles and are provided for reference. In this example, our analysis indicates that TPDT on Au adopts an ensemble-average backbone tilt of 32±3°. The uncertainty of the calculated backbone tilt angles is estimated to be ±3°, based on experimental uncertainties and the uncertainty associated with the assumed twist angle and phenyl backbone planarity.[36-38]

As evident from the fits (dotted and solid lines) shown in Figure 2.5, the rigorous NEXAFS analysis based on the BB model does not distinguish between an assembly that is disordered and an assembly with an ensemble-average backbone tilt of 43° away from the substrate normal. In both of these cases, the integrated π^* intensities do not depend on the x-ray incident angle.[10] This limitation is a result of the assumption of 3-fold substrate symmetry, where the orbital tilt, α, and the incident angle, θ, are mathematically equivalent in Equation (2.2). There thus exists a 'magic orientation' at $\alpha = 55°$ where the NEXAFS resonance intensities do not depend on x-ray incident angle. Because we assumed a molecular backbone twist of $\varphi = 32°$ in our analysis, this magic orientation occurs when the molecular backbone tilt happens to be 43°.

FOURIER TRANSFORM INFRARED (FTIR) SPECTROSCOPY

We used a dry-air purged Nicolet Magna-IR 860 spectrometer equipped with a liquid nitrogen cooled MCT detector for both reflection measurements on Au and transmission measurements on GaAs. All IR spectra are reported in absorbance units, A, where $A = -\log R/R_0$, R is the reflectivity of the IR beam, and R_0 is the reflectivity of a reference sample. Assemblies on Au were characterized by reflection-absorption infrared spectroscopy (RAIRS) and assemblies on GaAs were characterized by transmission IR spectroscopy. All RAIRS spectra were recorded for 1000 scans at a resolution of 2 cm^{-1}. We used a spectrum of hexadecanethiol assembled on Au[39] for background correction.

Ideally, the background spectrum should be acquired from a clean Au substrate.[40] Preparing a pristine Au surface, however, is very difficult due to ambient hydrocarbon adsorption on the surface. We therefore used hexadecanethiol assembled on Au as background. The resonances associated with hexadecanethiol[41] assembled on Au found at 1262, 1383 and 1468 cm^{-1} are weak, and do not interfere with the resonances associated with n-phenyldithiol assemblies. With this background correction procedure, the hexadecanethiol resonances appear as dips (or negative intensities) in the RAIRS spectra of n-phenyldithiol assemblies on Au. We used a commercial VeeMax II variable-angle accessory using p-polarized light with the grazing incident angle fixed at 79° relative to the substrate normal for all RAIRS experiments.

A sample RAIRS spectrum of QPDT assembled on Au is shown in Figure 2.6a. Prominent resonances originating from the phenyl backbone of QPDT include the in-plane, *ip*, (1475 cm^{-1} and 1001 cm^{-1}) and out-of-plane, *op*, (807 cm^{-1}) phenyl ring vibrational modes.[9] Additionally, Figure 2.6a reveals features associated with the acetyl protecting group: the peaks at 1706 and 1353 cm^{-1} are assigned to C=O and CH_3 (CH_3-CO) vibrations[9,42] of the thioacetyl functionality, respectively. Besides chemical identification, we can assess the molecular orientation of the QPDT assembly on the substrate by examining the intensities of the *ip* and *op* resonances.[9,41] In RAIRS, the electric field component that is parallel to the substrate is screened by the electronic polarization of Au.[9] The observed spectral intensity therefore depends solely on the magnitude of the projected transitional dipole moment onto the substrate normal. As such, only bonds vibrating along the substrate normal will be detected. We can therefore qualitatively assess the orientation of the molecular assembly by comparing its spectrum with that obtained from a powder sample.[43] As illustrated in the model on the right in Figure 2.6, the phenyl ring *ip* bands at 1475 and 1001 cm^{-1} exhibit a dipole moment in the direction parallel to the phenyl backbone plane, while the *op* mode near 807 cm^{-1} vibrates in the direction normal to the phenyl backbone plane. The reference spectrum – shown in Figure 2.6b – is obtained from the powder of the QPDT acetyl-protected precursor dispersed in KBr (1:150 mg). To examine the ensemble-average molecular orientation of the QPDT assembly on Au (Figure 2.6a), we calculated the orientation ratio, OR_r, defined for RAIRS experiments as:

$$OR_r = \frac{(ip/op)_{assembly}}{(ip/op)_{powder}} \qquad \text{Equation (2.5)}$$

where $(ip/op)_{\text{assembly}}$ and $(ip/op)_{\text{powder}}$ are the *ip*/*op* ratios for an assembly on Au and the corresponding powder, respectively. OR_r therefore compares the molecular orientation of the molecular assembly to that of the powder. Considering the RAIRS dipole selection rule mentioned above, $OR_r > 1$ suggests that the molecular assembly is preferentially upright while $OR_r < 1$ suggests that the molecules are ‘lying down’. Correspondingly, $OR_r \approx 1$ indicates that the molecular assembly is disordered. The OR_r extracted from the spectrum in Figure 2.6a is ≈15, suggesting that QPDT is preferentially upright on Au.

Because GaAs is transparent to IR,[44] we carried out FTIR studies of GaAs samples in transmission mode. Transmission IR data were acquired at a resolution of 2 cm^{-1} for 1000 scans. S-polarized light at an incident angle $\theta = 30°$ relative to the substrate normal was used.[43] This configuration was achieved experimentally by twisting the sample so that the substrate normal is $\theta = 30°$ away from the incident irradiation. For all transmission IR studies, sulfur-passivated GaAs was used for background correction.[43] Sulfur-passivated GaAs was prepared by first etching the substrates in concentrated hydrochloric acid for 1 minute, rinsing in deionized water, and then immediately immersing the etched substrates in a solution of ammonium sulfide in water (20% v/v, Aldrich) for 10 minutes.[45] This procedure results in a stable overlayer of sulfur that resists surface oxidation and hydrocarbon adsorption.[45] The background-corrected spectra were smoothed using conventional 12-point Fast Fourier Transform (FFT) smoothing[46] in Origin 6.1 commercial software to remove periodic interference[44,47] (see Figure 2.7a and b for representative spectra before and after smoothing). A multi-point baseline correction was applied in GRAMS/AI commercial software to all transmission IR spectra.

For our transmission IR experiments, we used s-polarized, rather than p-polarized, light to examine the molecular orientation of the assemblies because s-polarized light is selective for components of the dipole moment that are parallel to the substrate regardless of the incident angle of irradiation.[43] As a result, an unambiguous selection rule for the phenyl backbone with respect to the substrate exists. In contrast, p-polarized light results in sensitivity to a combination of dipole moments depending on the incident angle of the irradiation; the determination of orientation from IR spectra obtained using p-polarized light is therefore challenging and requires rigorous spectral simulations.[48]

As an example, consider an assembly of QPDT on GaAs with the dipole moment directions of the molecule illustrated on the right in Figure 2.7. The two major features providing insight into the molecular orientation are the *ip* ring vibration (1475 cm^{-1}), with a dipole moment directed along the molecular axis, and the *op* ring vibration (807 cm^{-1}), with a dipole moment directed perpendicular to the molecular axis and out of the phenyl ring plane. That aromatic molecules obey a unique dipole selection rule in transmission IR experiments using s-polarized light is best illustrated in Figure 2.8. A molecular assembly with an azimuthally-average backbone tilt, ρ, away from the substrate normal can be represented by an orientation cone. This orientation cone is characterized by a dipole moment coordinate system with the *z* axis oriented along the cone symmetry axis. The electric field vectors for s- and p-polarized light are also illustrated in Figure 2.8. For an n-phenyldithiol assembly on GaAs whose substrate normal is parallel to the IR incidence (as sketched in Figure 2.8b), the *ip* vibration of the n-phenyl backbone (1475 cm^{-1}) is characterized by a dipole moment directed along the *z* axis, while the *op* vibration (807 cm^{-1}) is characterized by dipole moments directed along the *x* or *y* axes. In order for a specific vibrational mode to absorb energy, the dipole moment of that particular bond must be collinear with the electric field vector of the incident polarized light. The comparison of Figures 2.8b and c reveals that the *op* vibration (dipole moment along *y*) is collinear with the electric field vector of s-polarized light regardless of θ. The *op* vibration therefore absorbs s-polarized light with a constant sampling cross-section. As a result, the intensity of the *op* vibration is constant regardless of θ. Accordingly, the intensity of the *ip* vibration is also independent of θ when s-polarized light is used. It follows that an examination of the *op/ip* ratio – which does not depend on θ when s-polarized light is used – should serve as an indication of the average orientation of the molecular assembly. To illustrate this concept, representative transmission IR spectra of a QPDT assembly on GaAs[43] acquired with s-polarized light at θ = 25°, 45°, and 65° are presented in Figure 2.9. A comparison of these spectra reveals *ip* and *op* intensities that are each in itself independent of θ. The *op*/*ip* ratio is thus constant with θ when s-polarized light is used. We can therefore directly infer the average orientation of the molecular assembly from spectra obtained using s-polarized light. We empirically found θ = 30° to be the optimal angle for transmission IR experiments using s-polarized light as the optimal position of the specimen depends on a balance between increasing interference at lower θ and decreasing substrate transmissivity at higher θ. Specifically, the periodic interference fringes resulting from back-reflection of the double-side polished GaAs wafer are maximized at lower θ.[44] At higher θ, however, the transmissivity of the GaAs substrate and, therefore, the amount of intensity transmitted through the substrate decrease.[44]

To examine the orientation of assemblies on GaAs, we employed a transmission IR orientation ratio, OR_t:

$$OR_t = \frac{(op\,/\,ip)_{assembly}}{(op\,/\,ip)_{powder}} \qquad \text{Equation (2.6)}$$

where $(op/ip)_{\text{assembly}}$ and $(op/ip)_{\text{powder}}$ are the *op*/*ip* ratios for the conjugated molecular assembly on GaAs and those obtained from the spectrum of the corresponding powder, respectively. Compared to OR_r employed for RAIRS, which uses *ip/op* intensity ratios, OR_t employed for transmission IR uses the reciprocal, i.e., *op/ip* intensity ratios. This distinction results from the fact that the selection rules for transmission IR (selectivity to dipole moment components parallel to substrate) is orthogonal to those for RAIRS (selectivity to dipole moment components normal to substrate).[44] $OR_t > 1$ therefore indicates a preferentially upright assembly and $OR_t < 1$ indicates that the molecules are preferentially 'lying down'. Accordingly, $OR_t \approx 1$ indicates that the molecular assembly does not exhibit any preferential orientation. The OR_t extracted from the spectra in Figure 2.9 is ≈4, suggesting that the QPDT assembly on GaAs adopts a preferentially upright orientation.

Transmission IR experiments using p-polarized light, however, are dramatically different. When $\theta = 0°$ (Figure 2.8b), the *op* vibration (dipole moment along *x*) presents the largest sampling cross-section for p-polarized light. This sampling cross-section, however, decreases as the sample is twisted away from the incident irradiation (increasing θ). When $\theta \rightarrow 90°$ (Figure 2.8c), the *ip* vibration (dipole moment along *z*) presents the largest sampling cross-section for p-polarized light. This cross-section in turn decreases with decreasing θ. Consequently, *op*/*ip* from experiments using *p*-polarized light does not only reflect the molecular orientation, but also changes in the sampling cross-sections of the two dipole moments. Figure 2.10 contains transmission IR spectra of the same QPDT assembly[43] acquired with p-polarized light at $\theta = 25°$, 45°, and 65°. The *ip* peak grows while the *op* peak diminishes with increasing θ. The *op*/*ip* ratio varies dramatically with θ when p-polarized light is used. In contrast to experiments using s-polarized light, orientation analysis using p-polarized light would require rigorous spectral simulations to decouple the orientation contributions from changes in the sampling cross-sections.[43] Although an unambiguous selection rule for aromatic molecules exists for experiments with s-polarized light, this is not the case for molecules with alkyl backbones. Orientation analysis of molecular assemblies with alkyl backbones is therefore challenging in either s- or p- polarization.[44]

UV-VIS-NIR

A Varian Cary 500 UV-Vis-NIR spectrophotometer and Starna Cells Q6 quartz UV-Vis cuvettes with a path length of 1 mm were used to examine the deprotection reaction of TPDT in solution, illustrated in Scheme 2.2 (details in Chapter 4). All spectra were collected at 1 nm resolution and a scan rate of 600 nm/min. Baseline correction was carried out using the spectra of neat solvents. To quantify the fraction of thioacetyl-terminated TPDT that is converted to thiolates, we normalized the integrated intensity of the thiolate absorption band (345 and 312 nm in EtOH and THF, respectively) by the sum of the integrated intensities of the thiolate and the thioacetyl (298 and 301 nm in EtOH and THF, respectively) absorption bands. Integrated intensities of thioacetyl- and thiolate- absorption bands were obtained by fitting each band with a Gaussian function. The peak widths and positions were obtained from fits of spectra of acetyl-protected precursors and solutions in which the deprotection reaction (Scheme 2.2) was complete.

ELLIPSOMETRY

The thickness of molecular assemblies on Au and GaAs was measured with a spectroscopic ellipsometer (J.A. Woollam Co.). Measurements were carried out between 285-500 nm at incidence angles of 60, 65, and 70^o with respect to the substrate normal. The data were fitted using Wvase32 software using the conventional 2-layer model consisting of a substrate and a top organic layer.[49-51] Optical constants for bare Au substrates were obtained from the same batches of freshly-evaporated Au on which the molecules were assembled. Optical constants for GaAs were obtained from substrates etched identically to those used for assembly and subsequently passivated with ammonium sulfide.[43] Refractive index values of $n = 1.55$[9] and $n = 1.45$[50] were assumed for the analysis of n-phenyl- and alkyl-based assemblies, respectively. We used the Cauchy model for the top organic layer with $A = n$, $B = 0.01$, and $C = 0$.[50]

X-RAY PHOTOELECTRON SPECTROSCOPY (XPS)

We performed XPS measurements on two types of samples – (1) molecular assemblies on Au and GaAs and (2) the same molecular assemblies on GaAs after ≈15Å of Au was deposited on the assembly surface using nTP. XPS experiments were carried out using either a Physical Electronics ESCA 5700 or a Kratos Axis Ultra DLD spectrophotometer equipped with a monochromatic Al Kα X-ray source (1486.6 eV), a hemispherical electron analyzer, and a low energy electron flood gun. All spectra were collected in ultra high vacuum at a base pressure of ≈2x10^{-9} Torr at ambient temperature. All elemental spectra were acquired at a photoelectron take off angle of 75° with respect to substrate normal; analyzer pass energy of 20 eV; resolution of 0.1 eV; sweep time of 1000 ms/eV. The S 2p elemental spectra were collected with 10 energy sweeps and fitted with symmetric Voigt functions and linear backgrounds.[52] The individual S 2p doublets were resolved with peaks with an S $2p_{3/2,1/2}$ branching ratio of 2[53-56] and separation of 1.18 eV.[57] During data fitting, the full width at half maximum (FWHM) of the peaks and the peak positions were held constant with the peak intensity being the only floating parameter. Peaks with FWHM of 0.95 and 1.05 eV were used to fit the S 2p spectra of 1,8-octanedithiol and QPDT, respectively. S 2p doublets attributed to S-Au bonds, S-GaAs bonds, and unbound thiol/thiolate/thioacetyl groups are located at ≈162, ≈162.8, and ≈164 eV, respectively. The spectra of C 1s, Au 4f, and Cl 2p were acquired with 1 energy sweep; Ga 2p spectra were acquired with 5 energy sweeps. All elemental spectra besides S 2p were corrected using Shirley background.[52,58,59]

SCANNING ELECTRON MICROSCOPY (SEM)

We used a LEO 1530 SEM with low operating voltage capabilities and an in-lens annular detector to image the Au that had been printed onto the molecular assembly surfaces by nTP. SEM images were acquired at 6-8kV with working distances of 5-6 mm.

ATOMIC FORCE MICROSCOPY (AFM)

The morphologies of the substrates and that of the Au that had been printed onto molecular assembly surfaces by nTP were characterized using a Digital Instruments Dimension 3100 AFM in tapping mode. We employed silicon tips with a resonant frequency of 300 kHz, a spring constant of 40 N/m, and a tip radius of <10 nm, obtained from NanoDevices. The r.m.s roughness was quantified using NanoScope software ver.6.12r1. A typical scan window was 1 μm^2.

CURRENT-VOLTAGE (I-V) CHARACTERIZATION

An Agilent 4156C Precision Semiconductor Parameter Analyzer was used to make all electrical measurements. For current-voltage characterization of GaAs—molecule—electrode junctions, 2 types of probes were used: a common tungsten probe and a hanging-drop galinstan electrode which was constructed in-house. The needle-like tungsten probe (available from Probing Solutions Inc.) was grounded to the GaAs substrate through a scribed indium contact. The hanging-drop galinstan electrode was used to contact either the molecular assembly surface or the printed top Au contact, depending on experiment. Galinstan (can be acquired from www.scitoycatalog.com) hanging drops were dispensed from a standard plastic 1 mL syringe through a 250 μm goniometer needle (Hamilton). The needle was permanently attached to a stainless steel wire using silver paint (high-purity, SPI). The stainless steel wire was clipped into the parameter analyzer probe, providing electrical contact between the dispensed hanging galinstan drop and the parameter analyzer while preventing any damage to the needle. The cross-sections of the galinstan drop contacts were imaged using a video camera, which allowed for measuring the contact area. Figure 2.11 shows examples of galinstan contacts on a GaAs-molecule-Au junction and directly on the molecular assembly. Because galinstan is prone to surface oxidation in air,[60] all I-V characterization was carried out under nitrogen purge. We applied a -0.5 V to 0.5 V bias to the hanging-drop galinstan electrode in 0.1 V increments.

OPTICAL MICROSCOPY

An Eclipse ME 600L Nikon Metallurgical Microscope equipped with episcopic differential interference contrast (DIC) and a Nomarski prism was used to image the top Au contacts deposited by nTP. All images were collected at ambient conditions with a digital camera (Nikon DXM 1200).

FIGURES

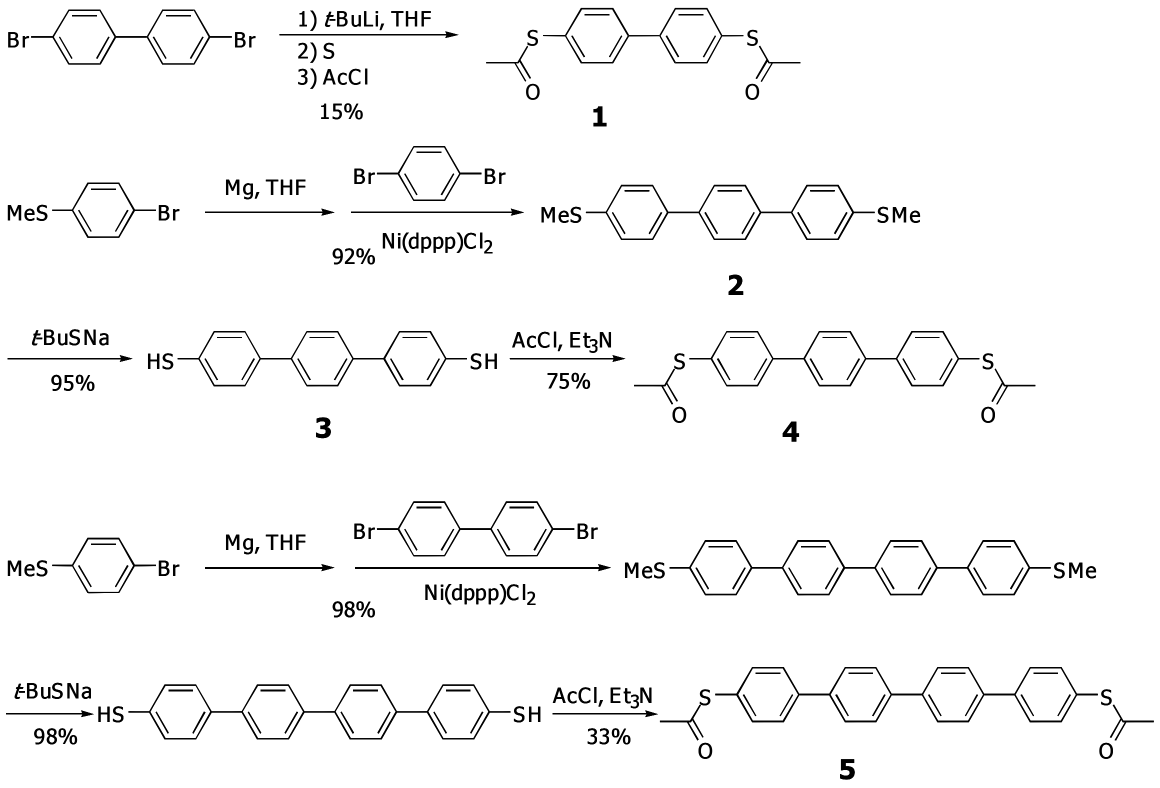

Scheme 2.1. Synthesis schemes for the acetyl-protected precursors of biphenyldithiol (BPDT), terphenyldithiol (TPDT) and quaterphenyldithiol (QPDT).

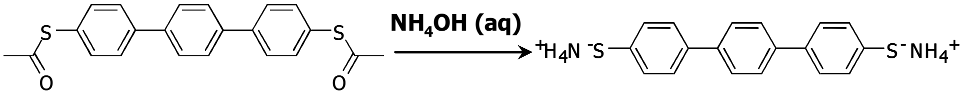

Scheme 2.2. The conversion of thioacetyl end groups to thiolates with the addition of NH_4OH.

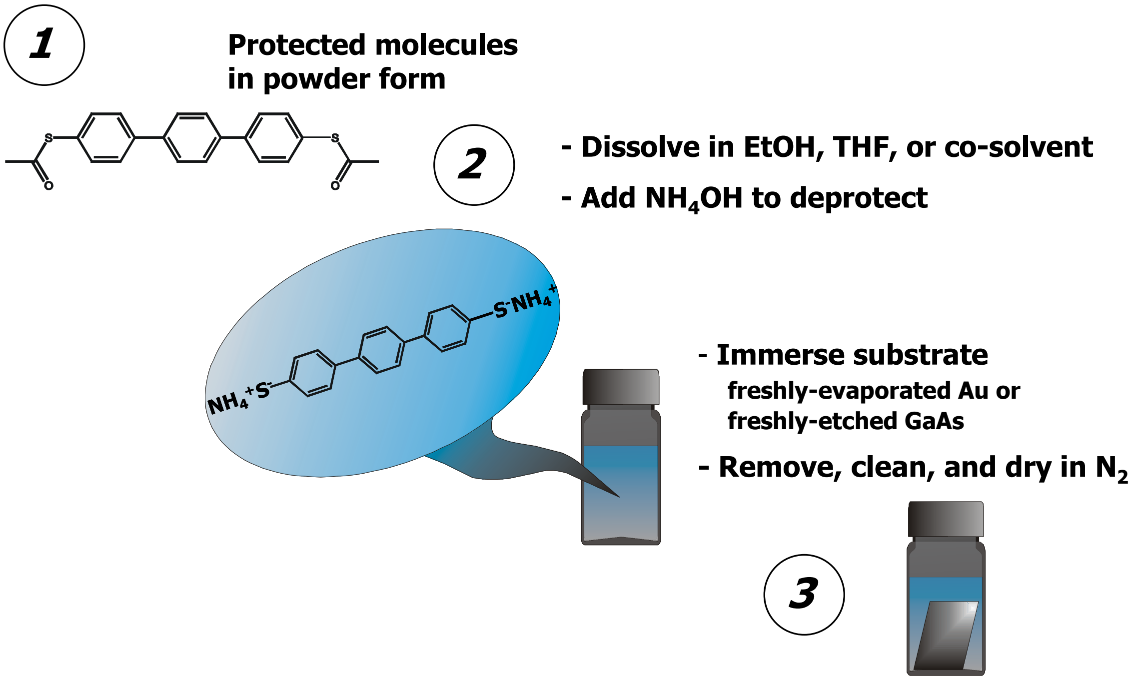

Figure 2.1. Schematic of the assembly procedure with the major steps consecutively numbered.

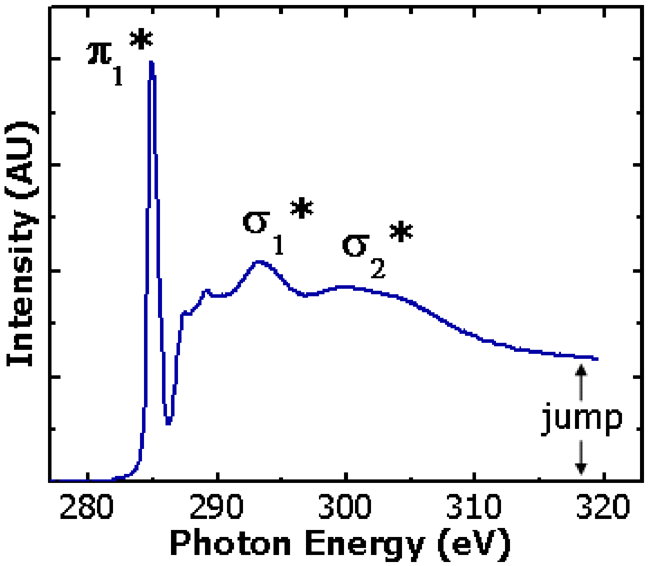

Figure 2.2. A sample pre-edge normalized C 1s NEXAFS spectrum of TPDT assembled on Au. The major spectral features are identified.

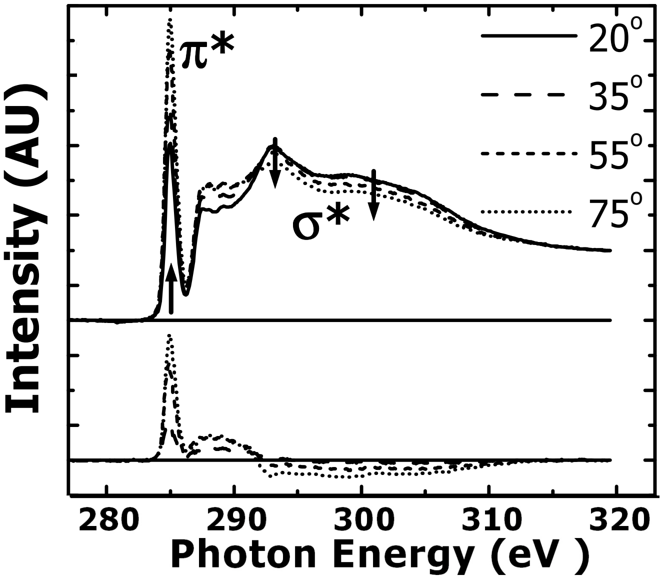

Figure 2.3. A sample set of angle-dependent, pre- and post-edge normalized C 1s NEXAFS spectra of TPDT assembled on Au acquired at the specified x-ray incident angles. The difference spectra (bottom portion of the plot) emphasize the angle-dependent spectral features, and are offset along the y-axis from the NEXAFS data for clarity.

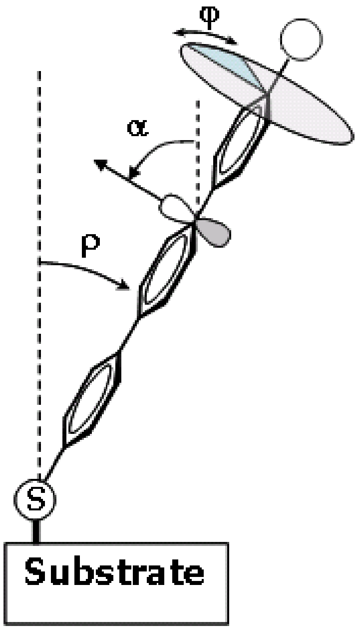

Figure 2.4. Schematic of a TPDT molecule adsorbed on a substrate. The angles used in our NEXAFS orientation analysis based on the BB model[30] are identified.

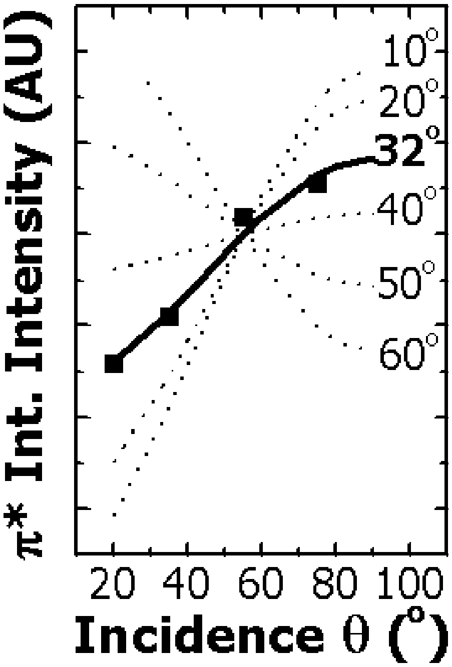

Figure 2.5. The π* integrated intensities derived from the spectra in Figure 2.4 as a function of x-ray incident angle and the corresponding theoretical fits (dotted lines) to Equation (2.2). The best fit (solid line) and the resulting backbone tilt angle are highlighted.

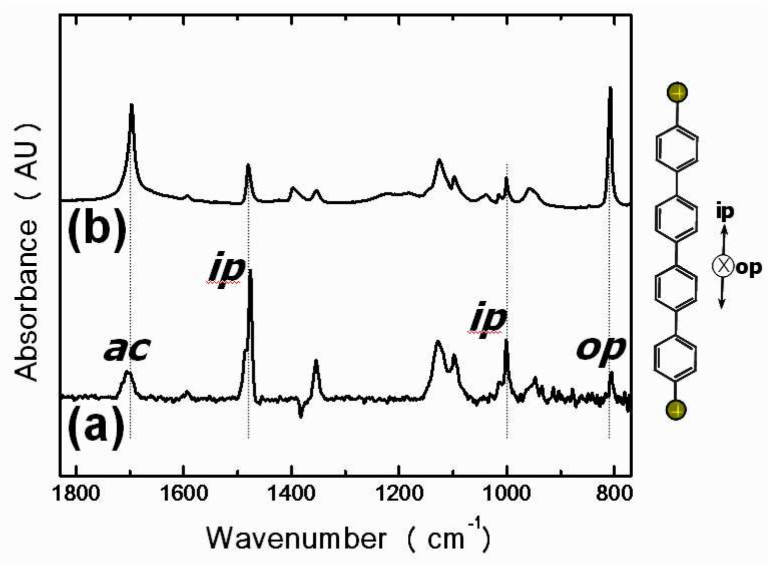

Figure 2.6. (a) RAIRS spectrum of QPDT on Au; (b) transmission IR spectrum of the acetyl-protected QPDT precursor powder dispersed in KBr. The major in-plane (*ip*), out-of-plane (*op*), and acetyl (*ac*) vibrations are labeled. The directions of phenyl backbone vibrations are illustrated in the cartoon on the right. The dips visible in (a) at 1383 and 1468 cm^{-1} are due to background correction with the spectrum of 1-hexadecanethiol molecular assembly on Au.

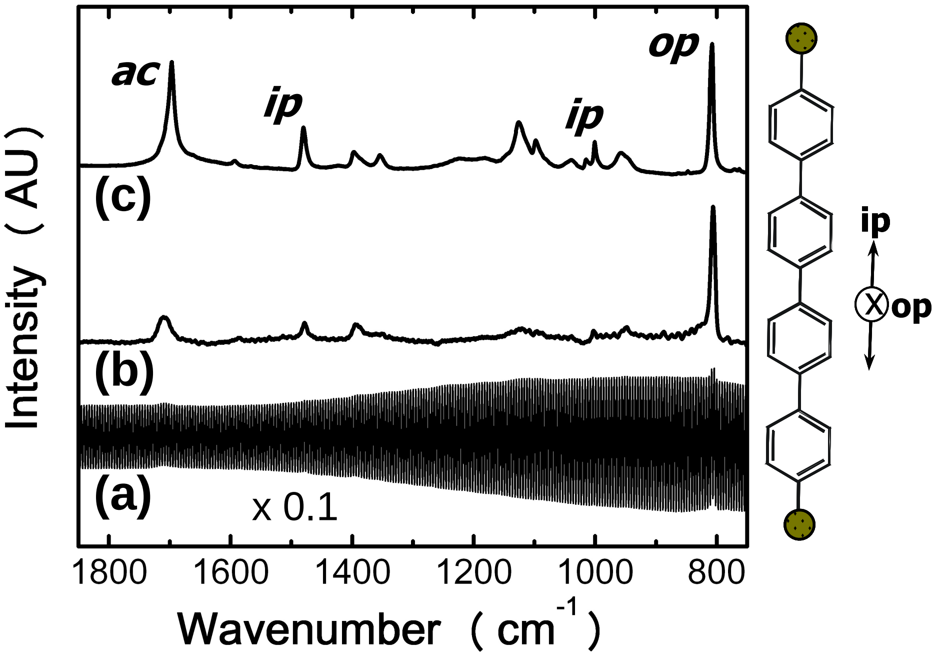

Figure 2.7. Background-corrected transmission IR spectra of a QPDT assembly on GaAs acquired at $\theta = 30°$ with s- polarized light (a) before and (b) after smoothing. (c) Transmission IR spectrum of the acetyl-protected QPDT precursor dispersed in KBr. The major in-plane (*ip*), out-of-plane (*op*), and acetyl (*ac*) vibrations are labeled. The directions of phenyl backbone vibrations are illustrated in the cartoon on the right.

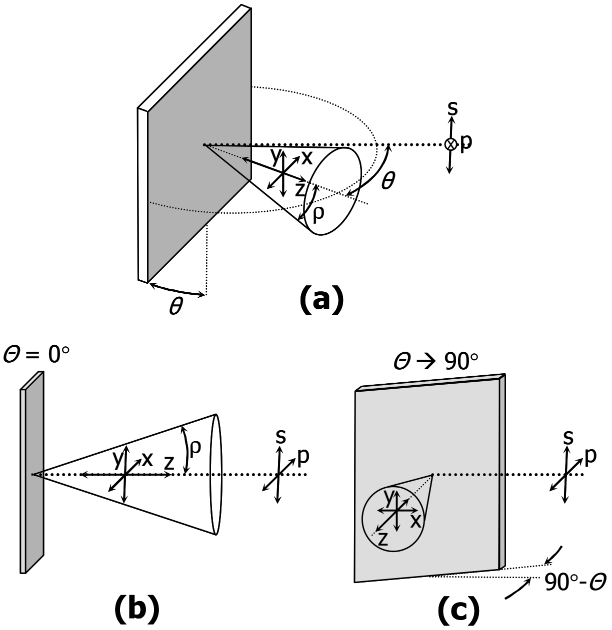

Figure 2.8. (a) Schematic of the transmission IR setup with the substrate twisted θ relative to the incident irradiation. The orientation cone of a molecule tilted ρ away from the substrate normal and the corresponding dipole coordinate system are included; (b) the experimental setup when $\theta = 0°$; (c) the experimental setup as $\theta \rightarrow 90°$.

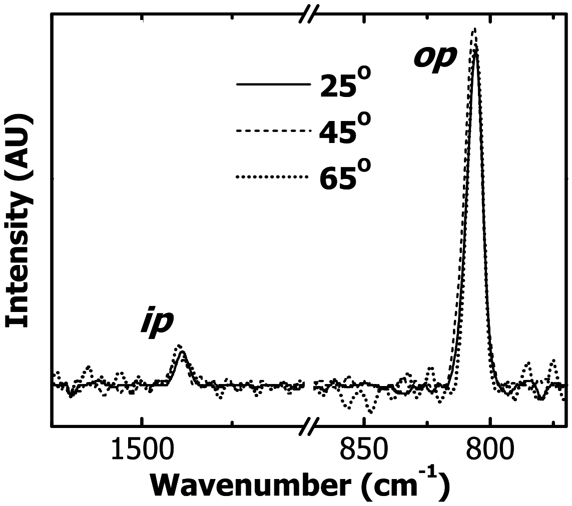

Figure 2.9. Transmission IR spectra of a QPDT assembly on GaAs acquired at varying incident angles, θ, using s-polarized light.

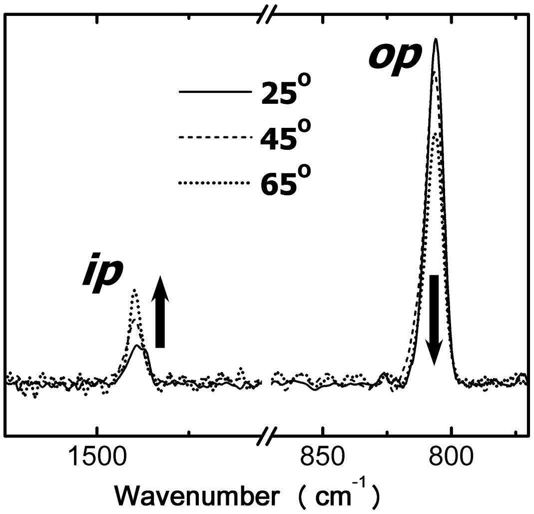

Figure 2.10. Transmission IR spectra of a QPDT assembly on GaAs acquired at varying incident angles, θ, using p-polarized light.

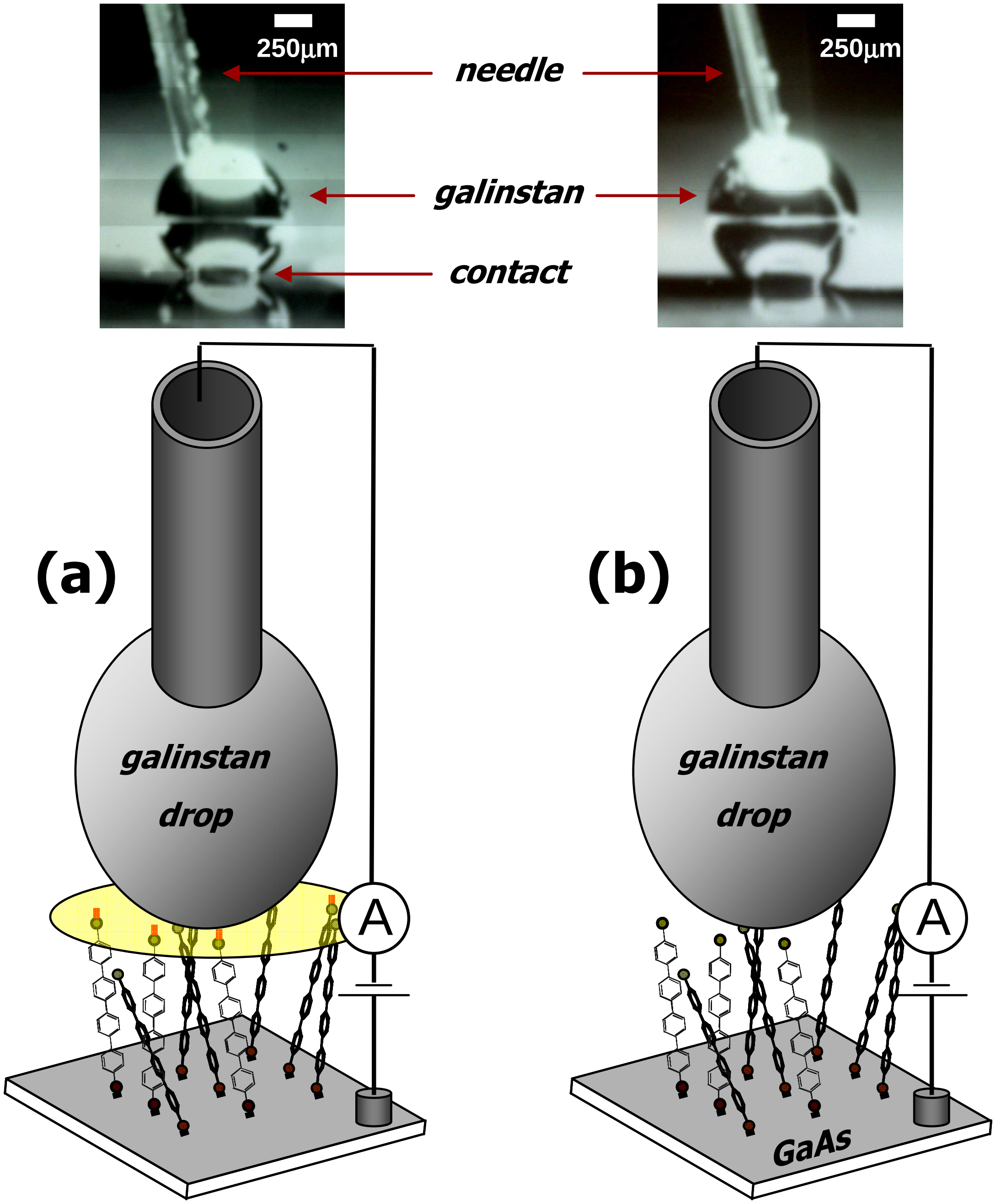

Figure 2.11. Schematic of the hanging-drop galinstan probe making electrical contact to (a) GaAs—molecule—Au and (b) the molecular assembly directly. Representative photographs of the galinstan drop in contact with the surface of interest are included.

REFERENCES

1. Loo, Y.-L.; Hsu, J. W. P.; Willett, R. L.; Baldwin, K. W.; West, K. W.; Rogers, J. A. *Journal of Vacuum Science & Technology B* **2002,** *20*, 2853.

2. Loo, Y.-L.; Lang, D. V.; Rogers, J. A.; Hsu, J. W. P. *Nano Letters* **2003,** *3*, 913.

3. Loo, Y.-L.; Willett, R. L.; Baldwin, K. W.; Rogers, J. A. *Journal of the American Chemical Society* **2002,** *124*, 7654.

4. Loo, Y.-L.; Willett, R. L.; Baldwin, K. W.; Rogers, J. A. *Applied Physics Letters* **2002,** *81*, 562.

5. Pinchart, A.; Dallaire, C.; Van Bierbeek, A.; Gingras, M. *Tetrahedron Letters* **1999,** *40*, 5479.

6. Kang, J. F.; Ulman, A.; Liao, S.; Jordan, R.; Yang, G.; Liu, G.-Y. *Langmuir* **2001,** *17*, 95.

7. Tour, J. M.; Jones, L.; Pearson, D. L.; Lamba, J. J. S.; Burgin, T. P.; Whitesides, G. M.; Allara, D. L.; Parikh, A. N.; Atre, S. *Journal of the American Chemical Society* **1995,** *117*, 9529.

8. Pearson, D. L.; Tour, J. M. *Journal of Organic Chemistry* **1997,** *62*, 1376.

9. de Boer, B.; Meng, H.; Perepichka, D. F.; Zheng, J.; Frank, M. M.; Chabal, Y. J.; Bao, Z. *Langmuir* **2003,** *19*, 4272.

10. Krapchetov, D. A.; Ma, H.; Jen, A. K. Y.; Fischer, D. A.; Loo, Y.-L. *Langmuir* **2005,** *21*, 5887.

11. Krapchetov, D. A.; Ma, H.; Jen, A. K. Y.; Fischer, D. A.; Loo, Y.-L. *Langmuir* **2008,** *24*, 851.

12. Jun, Y.; Zhu, X. Y.; Hsu, J. W. P. *Langmuir* **2006,** *22*, 3627.

13. Weckenmann, U.; Mittler, S.; Naumann, K.; Fischer, R. A. *Langmuir* **2002,** *18*, 5479.

14. Xia, Y.; Whitesides, G. M. *Angewandte Chemie* **1998,** *37*, 550.

15. Kumar, A.; Whitesides, G. M. *Applied Physics Letters* **1993,** *63*, 2002.

16. Xia, Y.; Rogers, J. A.; Paul, K. E.; Whitesides, G. M. *Chemical Reviews* **1999,** *99*, 1823.

17. Hsu, J. W. P.; Loo, Y. L.; Lang, D. V.; Rogers, J. A. *Journal of Vacuum Science & Technology B* **2003,** *21*, 1928.

18. Felmet, K.; Loo, Y.-L.; Sun, Y. *Applied Physics Letters* **2004,** *85*, 3316.

19. Shimizu, K. T.; Fabbri, J. D.; Jelincic, J. J.; Melosh, N. A. *Advanced Materials* **2006,** *18*, 1499.

20. Vilan, A.; Cahen, D. *Advanced Functional Materials* **2002,** *12*, 795.

21. Lide, D. R., *CRC Handbook of Chemistry and Physics*. CRC Press: Boca Raton, FL, 1994.

22. Stohr, J.; Outka, D. A. *Physical Review B* **1987,** *36*, 7891.

23. Detailed information on the NIST/Dow Soft X-Ray Materials Characterization Facility at NSLS BNL see: http://www.nsls.bnl.gov/newsroom/publications/newsletters/1996/96-nov.pdf

24. Genzer, J.; Kramer, E. J.; Fischer, D. A. *Journal of Applied Physics* **2002,** *92*, 7070.

25. Genzer, J.; Sivaniah, E.; Kramer, E. J.; Wang, J.; Koerner, H.; Char, K.; Ober, C. K.; DeKoven, B. M.; Bubeck, R. A.; Fischer, D. A.; Sambasivan, S. *Langmuir* **2000,** *16*, 1993.

26. Fischer, D. A.; Efimenko, K.; Bhat, R. R.; Sambasivan, S.; Genzer, J. *Macromolecular Rapid Communications* **2004,** *25*, 141.

27. Stohr, J., *NEXAFS Spectroscopy*. Springer: Berlin, 1992, p 158.

28. Shaporenko, A.; Adlkofer, K.; Johansson, L. S. O.; Ulman, A.; Grunze, M.; Tanaka, M.; Zharnikov, M. *Journal of Physical Chemistry B* **2004,** *108*, 17964.

29. Banerjee, S.; Hemraj-Benny, T.; Sambasivan, S.; Fischer, D. A.; Misewich, J. A.; Wong, S. S. *Journal of Physical Chemistry B* **2005,** *109*, 8489.

30. Kinzler, M.; Schertel, A.; Haehner, G.; Woell, C.; Grunze, M.; Albrecht, H.; Holzhueter, G.; Gerber, T. *Journal of Chemical Physics* **1994,** *100*, 7722.

31. Outka, D. A.; Stoehr, J.; Rabe, J. P.; Swalen, J. D. *Journal of Chemical Physics* **1988,** *88*, 4076.

32. Frey, S.; Stadler, V.; Heister, K.; Eck, W.; Zharnikov, M.; Grunze, M.; Zeysing, B.; Terfort, A. *Langmuir* **2001,** *17*, 2408.

33. Himmel, H.-J.; Terfort, A.; Woell, C. *Journal of the American Chemical Society* **1998,** *120*, 12069.

34. Trotter, J. *Acta Crystallographica* **1961,** *14*, 1135.

35. Shaporenko, A.; Adlkofer, K.; Johansson, L. S. O.; Tanaka, M.; Zharnikov, M. *Langmuir* **2003,** *19*, 4992.

36. Corish, J.; Morton-Blake, D. A.; O'Donoghue, F.; Baudour, J. L.; Beniere, F.; Toudic, B. *Theochem* **1995,** *358*, 29.

37. Cailleau, H.; Baudour, J. L.; Zeyen, C. M. E. *Acta Crystallographica, Section B: Structural Crystallography and Crystal Chemistry* **1979,** *B35*, 426.

38. Baudour, J. L.; Delugeard, Y.; Rivet, P. *Acta Crystallographica, Section B: Structural Crystallography and Crystal Chemistry* **1978,** *B34*, 625.

39. Stapleton, J. J.; Harder, P.; Daniel, T. A.; Reinard, M. D.; Yao, Y.; Price, D. W.; Tour, J. M.; Allara, D. L. *Langmuir* **2003,** *19*, 8245.

40. Hacker, C. A.; Batteas, J. D.; Garno, J. C.; Marquez, M.; Richter, C. A.; Richter, L. J.; Van Zee, R. D.; Zangmeister, C. D. *Langmuir* **2004,** *20*, 6195.

41. Nuzzo, R. G.; Dubois, L. H.; Allara, D. L. *Journal of the American Chemical Society* **1990,** *112*, 558.

42. Niklewski, A.; Azzam, W.; Strunskus, T.; Fischer, R. A.; Woell, C. *Langmuir* **2004,** *20*, 8620.

43. Krapchetov, D. A.; Ma, H.; Jen, A. K. Y.; Fischer, D. A.; Loo, Y.-L. *Langmuir* **2006,** *22*, 9491.

44. Tolstoy, V. P.; Chernyshova, I. V.; Skryshevsky, V. A., *Handbook of Infrared Spectroscopy of Ultrathin Films*. John Wiley & Sons, Inc.: 2003, pp 82-87.

45. Lebedev, M. V.; Mayer, T.; Jaegermann, W. *Surface Science* **2003,** *547*, 171.

46. Cranstoun Stephen, D.; Ombao Hernando, C.; von Sachs, R.; Guo, W.; Litt, B. *IEEE Transactions on Bio-Medical Engineering* **2002,** *49*, 988.

47. Maoz, R.; Sagiv, J.; Degenhardt, D.; Moehwald, H.; Quint, P. *Supramolecular Science* **1995,** *2*, 9.

48. Sheen, C. W.; Shi, J. X.; Maartensson, J.; Parikh, A. N.; Allara, D. L. *Journal of the American Chemical Society* **1992,** *114*, 1514.

49. Collins, R. W.; Kim, Y. T. *Analytical Chemistry* **1990,** *62,* 887A.

50. Nesher, G.; Vilan, A.; Cohen, H.; Cahen, D.; Amy, F.; Chan, C.; Hwang, J.; Kahn, A. *Journal of Physical Chemistry B* **2006,** *110*, 14363.

51. Shi, J.; Hong, B.; Parikh, A. N.; Collins, R. W.; Allara, D. L. *Chemical Physics Letters* **1995,** *246*, 90.

52. Shaporenko, A.; Elbing, M.; Blaszczyk, A.; Von Haenisch, C.; Mayor, M.; Zharnikov, M. *Journal of Physical Chemistry B* **2006,** *110*, 4307.

53. Heister, K.; Zharnikov, M.; Grunze, M.; Johansson, L. S. O. *Journal of Physical Chemistry B* **2001,** *105*, 4058.

54. Chaki, N. K.; Vijayamohanan, K. *Biosensors & Bioelectronics* **2002,** *17*, 1.

55. Zharnikov, M.; Grunze, M. *Journal of Physics: Condensed Matter* **2001,** *13*, 11333.

56. Tai, Y.; Shaporenko, A.; Rong, H. T.; Buck, M.; Eck, W.; Grunze, M.; Zharnikov, M. *Journal of Physical Chemistry B* **2004,** *108*, 16806.

57. Moulder, J. F.; Stickle, W. E.; Sobol, P. E.; Bomben, K. D., *Handbook of X-ray Photoelectron Spectroscopy*. Perkin-Elmer Corp.: Eden Prairie, MN: 1992, p 60.

58. Shirley, D. A. *Physical Review B* **1972,** *[3]5*, 4709.

59. Aronniemi, M.; Sainio, J.; Lahtinen, J. *Surface Science* **2005,** *578*, 108.

60. Surmann, P.; Zeyat, H. *Analytical and Bioanalytical Chemistry* **2005,** *383*, 1009.

Chapter 3: The Effect of Solvent Quality on the Structure of BPDT, TPDT, and QPDT Assemblies on Au and GaAs

Extensive structural characterization of alkylthiol molecular assemblies on coinage metal and GaAs surfaces has been reported.[1-10] Alkylthiols are most commonly assembled from EtOH,[1] and their final structures are sensitive to the quality of the solvent.[11] In general, when assembled from EtOH solutions, alkylthiols with backbones that consist of more than 12 methylene units[9,12,13] tend to form ordered molecular assemblies on Au,[1-4] Ag,[1,4,5] and GaAs[1,6-10] with preferentially upright orientation. Assemblies of alkylthiols with backbones consisting of less than 12 methylene units tend to be disordered.[1] In special cases, such as deposition in vacuum from the gas phase,[14] a preferentially upright orientation has been directly observed for alkylthiols with backbones as short as 4 methylene units.[14] The trend of increasingly upright molecular orientation with increasing alkyl backbone length is commonly attributed to the increase in Van der Waals intermolecular interactions between methylene units in neighboring chains.[1]

In contrast to their monofunctional counterparts, the assembly of alkyldithiols – symmetric alkane molecules with thiol termination on both ends – appears to be more sensitive to assembly conditions. For instance, it has been demonstrated by direct imaging that both 1,6-hexanedithiol[15] and 1,8-octanedithiol[16] generally lie flat on the substrate surface when assembled on Au at low adsorbate exposures from the gas phase. This preferential orientation is attributed to the strong interactions between the substrate and thiol groups at both ends of the molecule.[15,16] When assembled from EtOH solutions on Au, however, both 1,6-hexanedithiol[15] and 1,8-octanedithiol[16] tend to form disordered multilayers.[15,16]

Compared to the assembly of aliphatic thiols, the assembly of conjugated systems has only recently attracted research attention. Recent reports suggest the assembly of these materials is yet more complex than those of alkyl-based systems.[17-22] Specifically, the way in which conjugated systems organize on surfaces is affected by both the types of substrates used[21,23] and the solvents from which the molecules are assembled.[24] Similar to alkylthiols, conjugated monothiols with longer backbones (biphenyl and longer) have been shown to assemble in an upright fashion on Au,[21,25-27] Ag,[20,21,25,26] and GaAs.[22,23] The fact that conjugated thiols form ordered molecular assemblies at shorter backbone lengths than alkylthiols has been attributed to their backbone rigidity and increased intermolecular interactions, such as π—π interactions.[28] The assembly of conjugated dithiols presents an additional level of complexity. Because aromatic dithiols are prone to oxidation[29] and dimerization,[20] they are usually assembled from their acetyl-protected precursors. These acetyl-protected conjugated dithiol precursors are poorly-soluble in EtOH, a common solvent for the assembly of conjugated monothiols.[22-24] Conjugated dithiols are therefore typically assembled from THF.[18,19,30] Conjugated dithiol precursors with longer backbones have been reported to form ordered assemblies with preferentially upright orientation. For example, qualitative FTIR studies carried out by de Boer et. al.[18] suggest that both TPDT and QPDT organize in an upright fashion when assembled on Au from THF. To-date, the few reports addressing molecular assembly of conjugated dithiol precursors have focused exclusively on metal substrates.[17,18,30,31] Furthermore, the details of molecular orientation and the factors governing the organization of conjugated dithiols on either Au or GaAs have not been systematically investigated. We were therefore interested in understanding the factors governing the final molecular assembly structures of conjugated dithiols on both Au and GaAs.

In this Chapter, we examine how both the type of substrate used and the solvent quality affect the assembly of model conjugated dithiols. Specifically, we elucidated how the choices of solvent (EtOH, THF, or a cosolvent of the two) and substrate (Au or GaAs) affect the relative surface coverage and the ensemble-average orientation of BPDT, TPDT, and QPDT molecular assemblies. As described in Chapter 2, cosolvents of EtOH and THF are described in terms of EtOH fraction, EF. We employed near-edge absorption fine structure (NEXAFS) spectroscopy to quantify the relative surface coverage and the ensemble-average orientation of the molecular assemblies.

Figure 3.1 presents polarization-independent, pre-edge normalized C K-edge NEXAFS spectra of BPDT, TPDT and QPDT assembled on Au (Figures 3.1a–c) and on GaAs (Figures 3.1d–f). The major spectral features are pointed out in Figure 3.1a: the intense resonance at 285 eV (π^*) is attributed to the C1s → $\pi^*_{C=C}$ transition[32] in BPDT, TPDT, and QPDT backbones; the broad resonances at 293 and 303 eV originate from the C1s → σ_1^* and σ_2^* transitions,[32] respectively; the features at 287.4 and 288.8 eV are assigned to the R*/C-S* and the π_2^* transitions,[32] respectively. The carbon-edge jump, labeled 'jump' in Figure 3.1a, is proportional to the total carbon content on the surface.[33]

We acquired the NEXAFS spectra presented in Figure 3.1 at an x-ray incident angle of 55°, which is near the magic angle of 51°, as described in Chapter 2. Data acquired at this angle are independent of polarization details of the incident x-rays.[33] Differences in the spectra collected near the magic angle therefore reflect differences in the relative surface coverage between these assemblies. The dashed lines in Figure 3.1 represent the NEXAFS spectra of assemblies formed from EtOH-rich solutions while the solid lines represent the NEXAFS spectra of assemblies formed from THF solutions. The comparison of NEXAFS spectra of BPDT assembled on Au from EtOH and THF (Figure 3.1a) reveals that they are comparable in the overall shape and intensity. Similar comparisons for TPDT (Figure 3.1b) and QPDT (3.1c) reveal that the NEXAFS spectra of molecular assemblies formed from EtOH-rich and THF solvents on Au are also comparable. We therefore concluded that the solvent quality does not have a substantial effect on the quality of these assemblies on Au. In contrast, Figures 3.1d–f reveal drastically different NEXAFS spectra for assemblies formed from EtOH and THF on GaAs, indicating that the adsorption of BPDT, TPDT and QPDT on GaAs is sensitive to the solvent quality. Specifically, we see sharp decreases in both the π* resonance (285 eV) intensities and the overall PEY signal intensities in assemblies formed from THF, suggesting reduced surface coverages in these samples.

To examine how BPDT, TPDT, and QPDT organize on the substrate as a function of solvent quality, we quantified both the relative surface coverage and the ensemble-average molecular orientation of each of these molecular assemblies. To quantify the relative surface coverage, we employed the ratio of the π* (285 eV) integrated intensity and the magnitude of the corresponding carbon-edge jump (labeled ‘jump’ in Figure 3.1a), or π*/jump. As mentioned in Chapter 2, π*/jump represents the relative surface coverage of a conjugated dithiol molecular assembly. We have quantified π*/jump as a function of the composition of the solvent for BPDT, TPDT, and QPDT assemblies on Au and GaAs in Figures 3.2a and b, respectively. The comparison of the π*/jump ratios for BPDT, TPDT, and QPDT assemblies on Au (Figure 3.2a) reveals that the surface coverage of the molecular assemblies generally increases with increasing backbone length. That the π*/jump ratios generally increase with increasing number of rings in the n-phenyl backbone is attributed to the higher π orbital content in these assemblies. Further examination of Figure 3.2a reveals that the π*/jump ratios for BPDT, TPDT, and

QPDT do not change over the entire range of EF examined. This observation indicates that the surface coverage of each of the conjugated dithiols is independent of the solvent when assembled on Au. In contrast to adsorption on Au (Figure 3.2a), the π*/jump ratios for BPDT, TPDT, and QPDT assembled on GaAs (Figure 3.2b) increase with increasing EF. This observation indicates that the surface coverage increases with increasing EtOH content in solutions for all three conjugated dithiols, when assembled on GaAs. The π*/jump ratios for BPDT, TPDT, and QPDT assembled on GaAs at low EFs are significantly lower than the π*/jumps of the corresponding assemblies on Au, indicating that assemblies from THF-rich solvents on GaAs exhibit reduced surface coverages compared to those on Au. On the other hand, the π*/jump for BPDT, TPDT, and QPDT assembled on GaAs at high EFs approach those of the corresponding molecular assemblies on Au, indicating that assemblies carried out from EtOH-rich solvents on GaAs and Au exhibit comparable surface coverages.

We examined the ensemble-average molecular orientations of n-phenyldithiol molecular assemblies by analyzing the pre- and post-edge normalized NEXAFS spectra acquired at varying x-ray incident angles. Figures 3.3a and b contain pre- and post-edge normalized NEXAFS spectra of BPDT assembled on Au from EtOH and THF, respectively. The ensemble-average molecular orientation can be quantified by examining the angular dependence of the π* resonance. In the NEXAFS spectra in Figures 3.3a and b, very little variation is observed in the π* integrated intensities as a function of x-ray incident angle. In fact, the dichroic ratios derived from the spectra in Figures 3.3a and b, are only slightly positive (DR = 0.1). The low DRs indicate that the final structures of BPDT assemblies on Au from both EtOH and THF do not exhibit significant anisotropy. We therefore deduced that BPDT is disordered when assembled on Au from both EtOH (Figure 3.3a) and THF (Figure 3.3b). That BPDT forms disordered molecular assemblies on Au is in contrast with the case of biphenylthiol (1 thiol end group as opposed to two) assembled on Au. Specifically, biphenylthiol has been reported to form preferentially upright molecular assemblies on Au with an ensemble-average tilt angle of ≈23° away from the substrate normal.[21] We speculate that this difference in adsorption of BPDT relative to that of biphenylthiol may stem from differences in interactions between molecules during adsorption. For instance, thiolate groups have the tendency to interact with each other in solution.[20] The interaction between the additional functional groups in BPDT may compete with the molecule-substrate interactions during the adsorption process and thus affect the resulting molecular orientation. Furthermore, the additional functional group of BPDT is likely result in additional interactions at the molecular assembly surface, thus impacting the molecular orientation. For example, the interactions between COOH functional groups in COOH-terminated biphenylthiol molecular assemblies are believed to be responsible for the less upright molecular orientation of these assemblies compared to those of unsubstituted biphenylthiol.[23]

We also carried out orientation analysis of TPDT and QPDT assemblies on Au. Figures 3.4a and b contain angle-dependent NEXAFS spectra of TPDT assembled on Au from EtOH and THF, respectively. In these spectra, the π* resonance intensifies with increasing x-ray incident angle. Concomitantly, the σ* resonances subside with increasing x-ray incident angle. The angular dependence of the resonance intensities is emphasized by the difference spectra, $I(\theta) - I(20°)$, included in lower portions of the same figures. According to the NEXAFS selection rules described in Chapter 2, the trends of π* resonance intensifying and σ* resonances subsiding with increasing x-ray incident angle indicates that the TPDT molecules are oriented preferentially upright on Au surface.

We quantified the ensemble-average orientation of the assemblies both in terms of levels of anisotropy using dichroic ratios (DR) and in terms of average backbone tilt angles using the building block (BB) model.[34,35] Figures 3.4a and b include the DRs extracted from each of these data sets. TPDT assembled on Au from both EtOH and THF exhibit positive dichroic ratios, suggesting that the molecules are preferentially upright when assembled from both EtOH and THF. The TPDT assembly from EtOH is characterized by a slightly higher level of anisotropy (DR = 0.26) than the assembly from THF (DR = 0.21). This observation suggests a slightly more upright average orientation in TPDT assemblies on Au from EtOH compared to those from THF. Analysis using the BB model[34,35] provides an additional level of detail about the molecular organization in the respective TPDT assemblies. In our model used to extract the ensemble-average backbone tilt angle, we assumed a backbone twist $\varphi = 32°$ and a planar backbone (i.e., successive phenyl rings are coplanar). [21,22,27,36] Figures 3.4c and d contain the integrated π^* intensities extracted from data in Figures 3.4a and b, respectively, including their theoretical fits to Equation (2.2), as a function of x-ray incident angle. Included for reference are the graphical representations of Equation (2.2) at other specified backbone tilt angles (dotted lines). In each case, the best fit and the corresponding backbone tilt angle, ρ, are highlighted. The fitting results indicate that TPDT assemblies on Au carried out from EtOH (Figure 3.4c) adopt an ensemble-average backbone tilt of 30±3° away from the substrate normal. TPDT assemblies on Au carried out from THF (Figure 3.4d) adopt an ensemble-average backbone tilt of 32±3°away from the substrate normal. The final structures of TPDT assemblies on Au from EtOH and THF are very similar. This observation is consistent with the solvent-independent surface coverage for TPDT assembled on Au. The backbone tilt angles we obtained for TPDT assembled on Au (≈30°) are somewhat lower than the tilt of ≈20° reported for terphenylthiol assembled on

Au.[21,27,37] Similar to the case of BPDT, we attribute the reduced order of TPDT assemblies relative to those of terphenylthiol assemblies to the interactions resulting from the additional functional group in dithiol molecules. That TPDT molecular assemblies do exhibit preferentially upright molecular orientation while BPDT assemblies do not is consistent with increased intermolecular interactions between phenyl rings in the assemblies of TPDT.

The assembly of QPDT on Au is qualitatively similar to that of TPDT. Figures 3.5a and b contain angle-dependent NEXAFS spectra of QPDT assembled on Au from a cosolvent with EF = 0.9 and from THF, respectively. We were not able to assemble QPDT from pure EtOH, because of the low solubility of the acetyl-protected precursor of QPDT in EtOH. The angle-dependent spectra in Figures 3.5a and b exhibit growing π^* intensities with increasing x-ray incident angle, while the corresponding σ^* intensities subside. This trend indicates that, akin to TPDT, QPDT adsorbs on Au in a preferentially upright fashion. In fact, QPDT adsorbs on Au to form upright molecular assemblies with DR = 0.3 when assembled from both solutions of EF = 0.9 and pure THF on Au. According to calculations with the BB model, these assemblies are characterized by an ensemble-average backbone tilt of 28±3° away from the substrate normal. Similar to our observations for TPDT on Au, the ensemble-average orientation of QPDT on Au appears to be independent of the solvent composition. The calculated DRs and ensemble-average backbone tilt angles extracted from the NEXAFS data sets of both TPDT and QPDT assembled on Au at varying EFs are listed in Table 3.1. The molecular orientation of QPDT assemblies on Au is yet more upright than what we had observed for TPDT assemblies on Au, consistent with a further increase in intermolecular interactions in QPDT assemblies. Our analysis indicates that both TPDT and QPDT readily assemble on Au in a preferentially upright fashion; the surface coverage and the ensemble-average molecular orientation appear to be independent of the solvent quality. The ability of conjugated dithiols to form upright assemblies on Au is in stark contrast to alkyldithiols, which only 'lie down' on Au.[15,16] We attribute this distinction to the backbone rigidity of the conjugated dithiols and increased intermolecular interactions between the neighboring n-phenyl backbones.

We also characterized the ensemble-average molecular orientation of BPDT, TPDT, and QPDT molecular assemblies on GaAs. Figures 3.6a and b contain pre- and post-edge normalized NEXAFS spectra of BPDT assembled on GaAs from EtOH and THF, respectively. The dichroic ratios derived from each of these data sets are included. The π^* and σ^* resonance intensities of BPDT assemblies on GaAs do not exhibit significant dependence on the x-ray incident angle. The low DRs derived from these spectra suggest that BPDT is disordered when assembled on GaAs from both EtOH (Figure 3.3a) and THF (Figure 3.3b). Recall that BPDT molecular assemblies exhibit low surface coverage when assembled from THF, and the surface coverage improves with increasing EF on GaAs. Despite these increases, BPDT assemblies remain disordered. Our observation of disordered BPDT molecular assemblies on GaAs is in contrast with preferentially upright molecular orientation reported for biphenylthiol on GaAs.[23] Specifically, when assembled from EtOH on GaAs, biphenylthiol has been reported to exhibit an ensemble-average molecular tilt of $\approx 31°$. Similar to assembly on Au, this disparity between the assembly behavior of BPDT and that of biphenylthiol on GaAs can be attributed to the interactions resulting from the additional functional group in the dithiol molecules.

In contrast to the assembly of TPDT and QPDT on Au, NEXAFS experiments with TPDT and QPDT assemblies on GaAs tell a dramatically different story. Figure 3.7 contains the angle-dependent pre- and post-edge normalized NEXAFS spectra of TPDT assembled on GaAs as a function of EF. The corresponding difference spectra are included to emphasize changes in the angle dependent π* and σ* resonances as a function of EF. Unlike TPDT assemblies on Au, the assembly of TPDT on GaAs appears to be extremely sensitive to the amount of EtOH in solution. In assemblies carried out from EtOH-rich solvents (Figures 3.7a-c), the π* resonance intensifies at the expense of the σ* resonances when the x-ray incident angle is increased from 20° to 75°. This angle dependence and the resulting positive DRs suggest that TPDT assemblies are oriented preferentially upright. More specifically, analysis with the BB model of the spectra of TPDT assembled on GaAs from EtOH (Figure 3.7a) shows that these assemblies are characterized by an ensemble-average backbone tilt angle of 33±3° away from the substrate normal. In contrast, the assemblies carried out from EtOH-poor solvents exhibit little change in their respective angle-dependent NEXAFS spectra (Figures 3.7d-f). These difference spectra exhibit near-zero intensity (DR ≈ 0), suggesting disordered TPDT assemblies. The dichroic ratios and ensemble-average backbone tilt angles for TPDT assemblies on GaAs across the EF range are summarized in Table 3.2. The comparison of these results suggests EtOH to be the optimal solvent for the formation of TPDT molecular assemblies on GaAs with preferentially upright molecular orientation.

The angle-dependent pre- and post-edge normalized NEXAFS spectra of QPDT assembled on GaAs as a function of EF are shown in Figure 3.8. The dichroic ratios derived from each set of spectra are included. Additionally, the dichroic ratios and ensemble-average backbone tilt angles for QPDT assemblies on GaAs with varying EF are summarized in Table 3.2. At high EFs (> 0.5), QPDT behaves like TPDT and adopts a preferentially upright molecular orientation, as suggested by positive DRs. Analysis with the BB model results in ensemble-average backbone tilt angles of 27±3° and 24±3° for QPDT assembled on GaAs at EFs of 0.9 (Figure 3.8a) and 0.75 (Figure 3.8b), respectively. Decreasing EF, however, results in assemblies with progressively lower surface coverage, and these assemblies are largely disordered, as evident from Figures 3.8c and d. That the QPDT forms upright assemblies on GaAs from EtOH-rich solutions is consistent with increased surface coverage in these assemblies compared to those from THF. We note that the most upright QPDT assembly on GaAs was achieved at EF = 0.75. At this solvent composition, the dissolution of the acetyl-protected QPDT precursor is maximized while the EtOH content is high enough in the solvent to achieve upright final assembly structure on GaAs.

The solvent dependence of BPDT, TPDT, and QPDT assemblies on GaAs is not in itself surprising. Indeed, solvent-dependent assembly has been previously reported for conjugated systems. For instance, Ishida[24] reported phase separation when terphenylthiol was assembled from methylene chloride on Au. When terphenylthiol was assembled from EtOH, however, ordered and densely-packed structure was observed by scanning tunneling microscopy. Solvent-dependent assembly has also been reported for alkylthiol assemblies on Ni. Mekhalif and coworkers[38] reported the formation of high-quality assemblies from a polar solvent, whereas little adsorption occurred from a non polar solvent. These reports focused on assemblies on metal surfaces. What is surprising, in our case, is that such a pronounced solvent dependence occurs on GaAs, but not on Au. While the exact origin of this disparity remains uncertain, we believe it must arise from differences in solvent-molecule-substrate interactions in the two systems. Specifically, in the case of assemblies on Au, it is well known that the tendency to form S-Au bonds is very strong, with exothermic thiolate adsorption (0.3 – 0.5 eV)[39,40] resulting in covalent S-Au bonds of ~1.3 eV.[1,41] In fact, so strongly is the formation of S-Au bonds favored that thioacetyl-terminated molecules can spontaneously adsorb on Au without prior deprotection by surface-catalyzed cleaving of the acetyl protecting groups.[29] The molecule-substrate interactions therefore dominate molecule adsorption, outweighing any differences in solvent-molecule or solvent-substrate interactions, when the assembly takes place on Au. In contrast, the S-GaAs interaction is weaker (~0.81 eV).[41] Given the weaker molecule-substrate interaction, any solvent effect would be more prevalent on GaAs than on Au.

The examination of the orientation characteristics for BPDT, TPDT, and QPDT assemblies on Au (Table 3.1) and GaAs (Table 3.2) reveals that molecules with longer n-phenyldithiol backbones generally adopt a more upright orientation on both Au and GaAs. Indeed, while BPDT ($n = 2$) assemblies were always disordered regardless of the type of substrate used and the assembly solvent quality, TPDT ($n = 3$) and QPDT ($n = 4$) formed increasingly upright final structures. The observation that BPDT, TPDT, and QPDT assemblies become increasingly ordered with backbone length is consistent with the increase in the π—π intermolecular interactions.

Table 3.1. Calculated dichroic ratios and ensemble-average backbone tilt angles of BPDT, TPDT and QPDT assemblies on Au at varying solvent compositions.

	EtOH Fraction (EF)						
	0	**0.25**	**0.5**	**0.75**	**0.9**	**1**	
BPDT	**0.09**					**0.1**	DR
	DIS					**DIS**	Tilt angle
TPDT	**0.21**	**0.28**	**0.34**	**0.27**		**0.26**	DR
	32°±3°	**29°±3°**	**26°±3°**	**30°±3°**		**30°±3°**	Tilt angle
QPDT	**0.3**				**0.3**		DR
	28°±3°				**28°±3°**		Tilt angle

"DIS" denotes disordered molecular assemblies whose spectra do not exhibit significant angular dependence.

Table 3.2. Calculated dichroic ratios and ensemble-average backbone tilt angles of BPDT, TPDT and QPDT assemblies on GaAs at varying solvent compositions.

	EtOH Fraction (EF)						
	0	0.25	0.5	0.75	0.9	1	
BPDT	0.1					0	DR
	DIS					DIS	Tilt angle
TPDT	0.07	0.05	0.18	0.17		0.21	DR
	DIS	DIS	35°±3°	35°±3°		33°±3°	Tilt angle
QPDT	0.09		0.1	0.37	0.31		DR
	DIS		39°±3°	24°±3°	27°±3°		Tilt angle

"DIS" denotes disordered molecular assemblies whose spectra do not exhibit significant angular dependence.

FIGURES

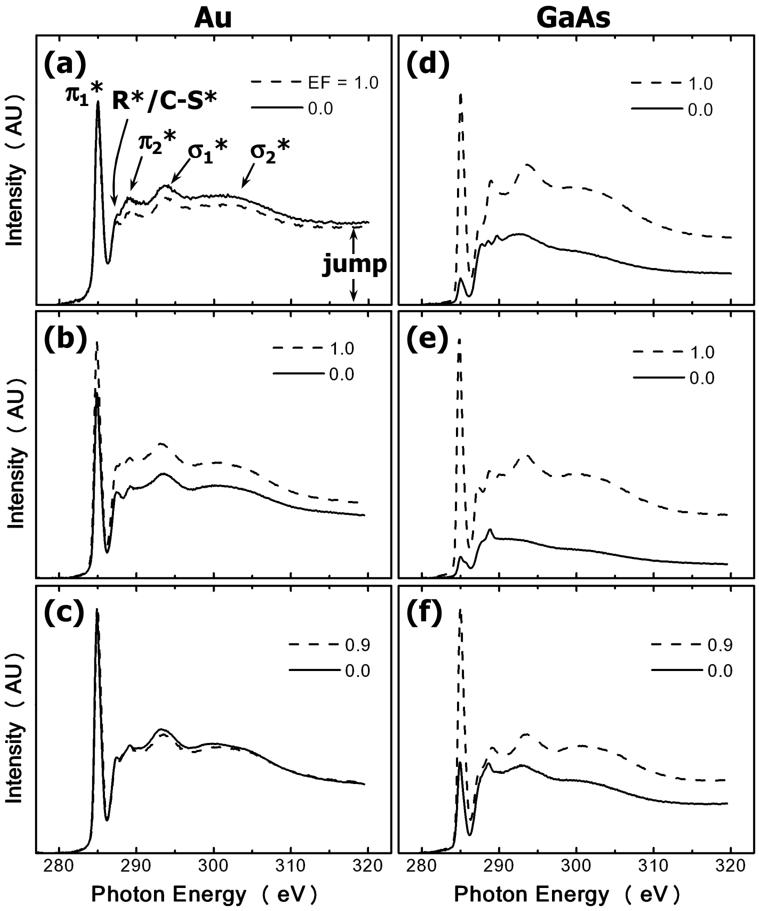

Figure 3.1. C 1s polarization-independent, pre-edge normalized NEXAFS spectra of (a) BPDT on Au, (b) TPDT on Au, (c) QPDT on Au, (d) BPDT on GaAs, (e) TPDT on GaAs, and (f) QPDT on GaAs acquired at an x-ray incident angle of 55°. BPDT and TPDT assemblies were formed from EtOH (dashed lines) or from THF (solid lines) solutions. QPDT assemblies were formed from a solution at EF = 0.9 (dashed lines) or from THF (solid lines) solutions. Relevant spectral features are identified in (a).

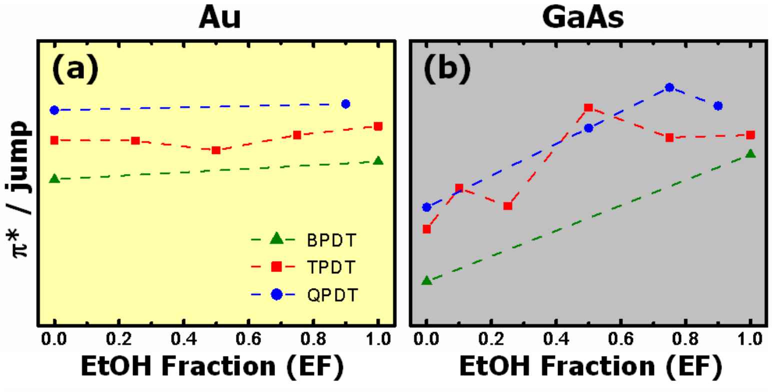

Figure 3.2. π*/jump ratios extracted from the NEXAFS spectra obtained at an x-ray incident angle of 55° of BPDT, TPDT and QPDT assembled on (a) Au and (b) GaAs as a function of ethanol fraction (EF) in the assembly solution. The π*/jumps reflect the relative surface coverages of the assemblies. At high EFs, the surface coverages of assemblies on GaAs approach those of the assemblies on Au.

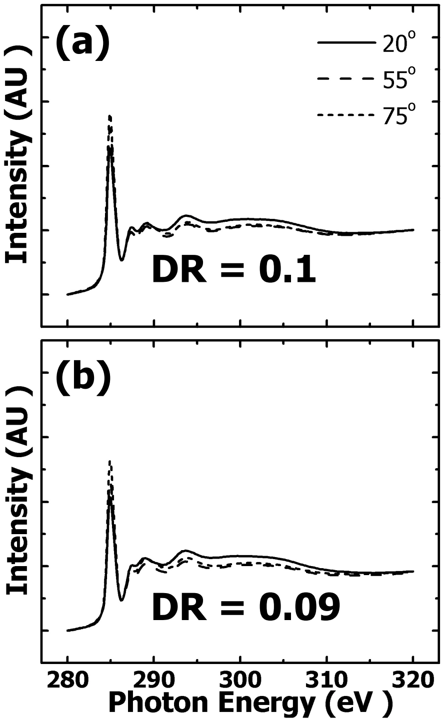

Figure 3.3. C 1s angle-dependent, pre- and post-edge normalized NEXAFS spectra of BPDT assembled on Au from (a) EtOH and (b) THF acquired at varying x-ray incident angles. Dichroic ratios derived from each set of spectra are included.

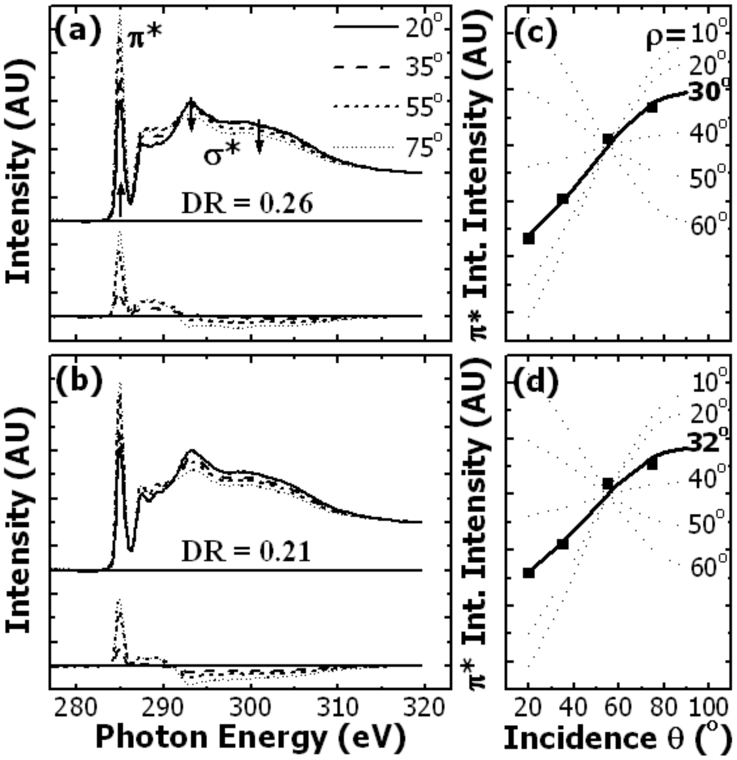

Figure 3.4. C 1s angle-dependent, pre- and post-edge normalized NEXAFS spectra of TPDT assembled on Au from (a) EtOH and (b) THF acquired at varying x-ray incident angles. The difference spectra (bottom portions of plots) emphasize angle-dependent spectral features, and are offset from the angle-dependent NEXAFS data sets along the y-axis for clarity. The dichroic ratios derived from each set of spectra are included. The π* integrated intensities extracted from the NEXAFS spectra in (a) and (b) as a function of x-ray incident angle and the corresponding theoretical fits to Equation (2.2) are presented in (c) and (d), respectively. Best fits (solid lines) and the calculated backbone tilt angles are highlighted. The dashed lines are graphical representations of Equation (2.2) at other specified backbone tilt angles.

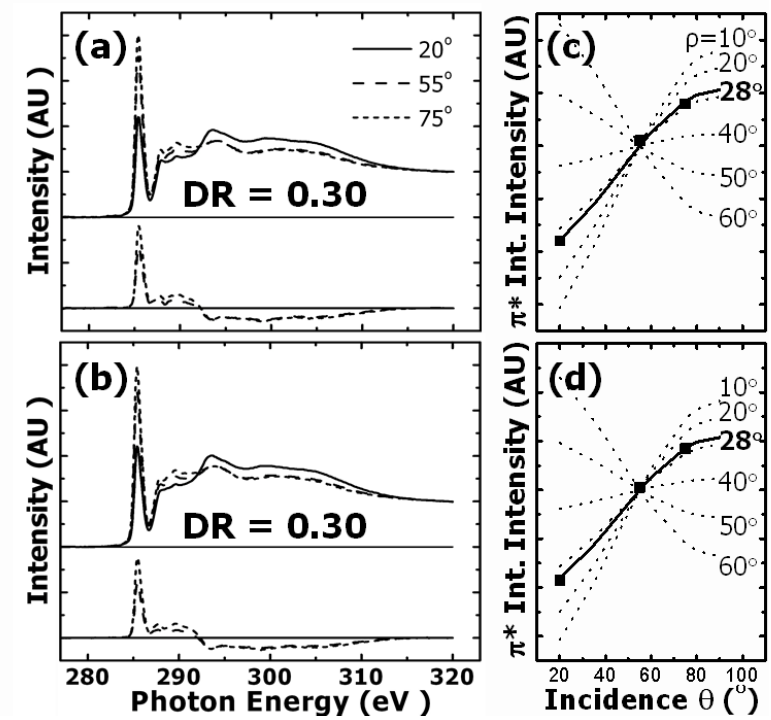

Figure 3.5. C 1s angle-dependent, pre- and post-edge normalized NEXAFS spectra of QPDT assembled on Au from (a) a cosolvent with EF = 0.9 and (b) from THF acquired at varying x-ray incident angles. The difference spectra (bottom portions of plots) emphasize angle-dependent spectral features, and are offset from the angle-dependent NEXAFS data sets along the y-axis for clarity. Dichroic ratios derived from each set of spectra are included. The π* integrated intensities extracted from the NEXAFS spectra in (a) and (b) as a function of x-ray incident angle and the corresponding theoretical fits to Equation (2.2) are presented in (c) and (d), respectively. Best fits (solid lines) and the calculated backbone tilt angles are highlighted. The dashed lines are graphical representations of Equation (2.2) at other specified backbone tilt angles.

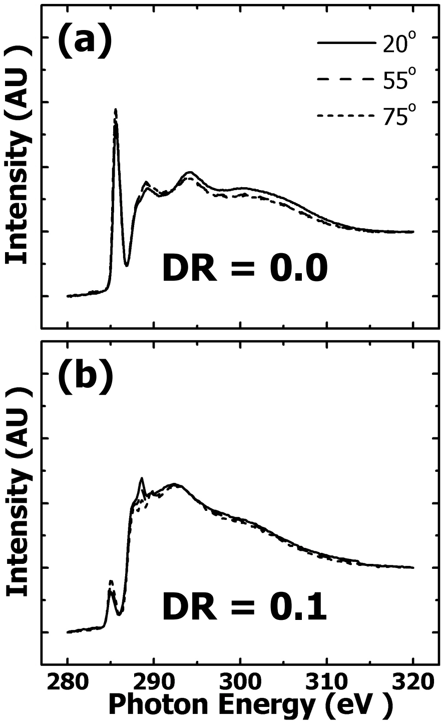

Figure 3.6. C 1s angle-dependent, pre- and post-edge normalized NEXAFS spectra of BPDT assembled on GaAs from (a) EtOH and (b) THF acquired at varying x-ray incident angles. Dichroic ratios derived from each set of spectra are included.

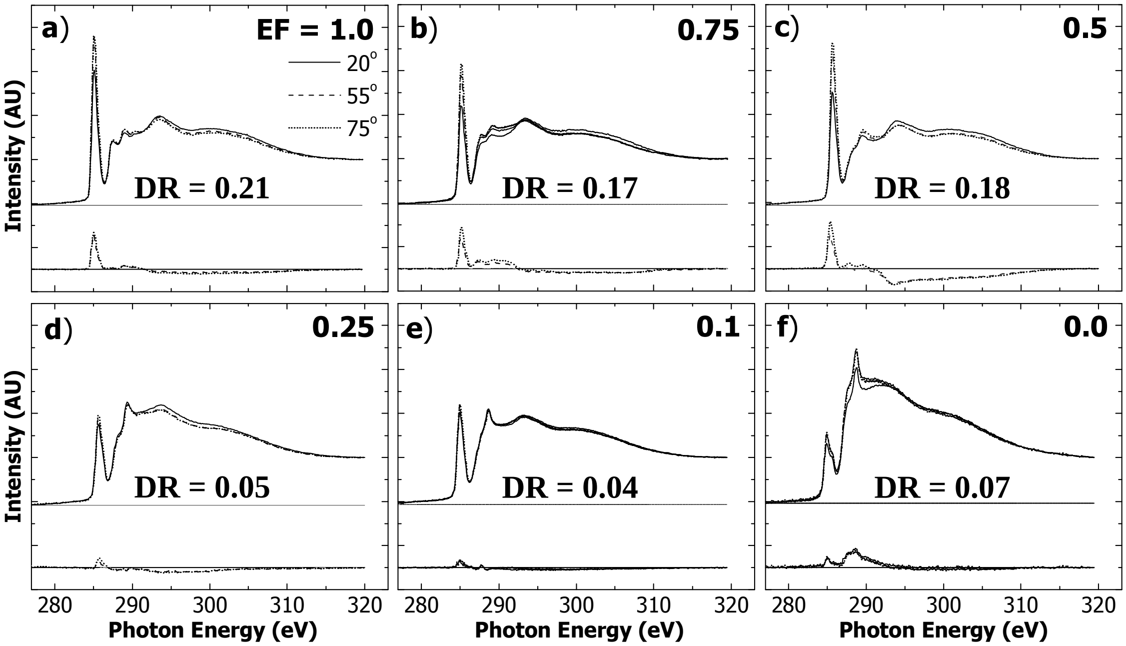

Figure 3.7. C 1s angle-dependent, pre- and post-edge normalized NEXAFS spectra of TPDT assembled on GaAs at varying EFs. The corresponding difference spectra are offset from the NEXAFS data along the y-axis for clarity. Dichroic ratios derived from each set of spectra are included.

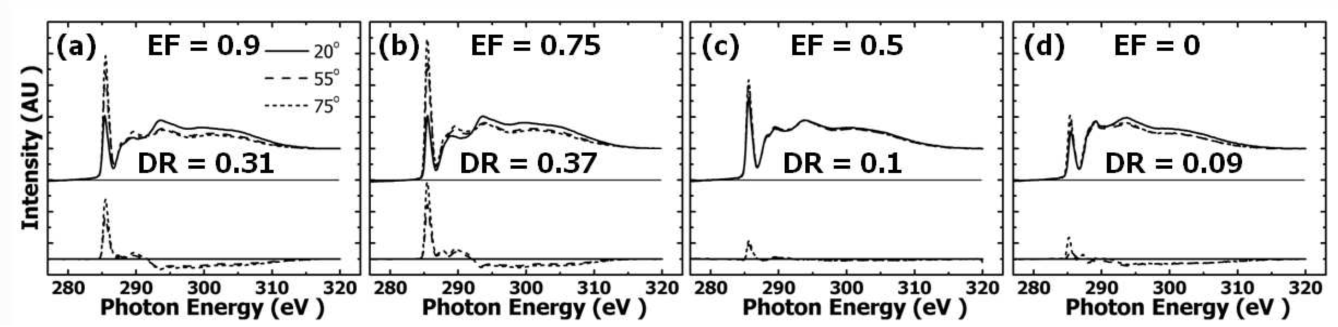

Figure 3.8. C 1s angle-dependent, pre- and post-edge normalized NEXAFS spectra of QPDT assembled on GaAs at varying EFs. The corresponding difference spectra are offset from the NEXAFS data along the y-axis for clarity. Dichroic ratios derived from each set of spectra are included.

REFERENCES

1. Ulman, A. *Chemical Reviews* **1996,** *96*, 1533.

2. Karpovich, D. S.; Blanchard, G. J. *Langmuir* **1994,** *10*, 3315.

3. Fischer, D.; Marti, A.; Hahner, G. *Journal of Vacuum Science & Technology A* **1997,** *15*, 2173.

4. Laibinis, P. E.; Whitesides, G. M.; Allara, D. L.; Tao, Y. T.; Parikh, A. N.; Nuzzo, R. G. *Journal of the American Chemical Society* **1991,** *113*, 7152.

5. Kondoh, H.; Nambu, A.; Ehara, Y.; Matsui, F.; Yokoyama, T.; Ohta, T. *Journal of Physical Chemistry B* **2004,** *108*, 12946.

6. Jun, Y.; Zhu, X. Y.; Hsu, J. W. P. *Langmuir* **2006,** *22*, 3627.

7. McGuiness, C. L.; Shaporenko, A.; Mars, C. K.; Uppili, S.; Zharnikov, M.; Allara, D. L. *Journal of the American Chemical Society* **2006,** *128*, 5231.

8. Baum, T.; Ye, S.; Uosaki, K. *Langmuir* **1999,** *15*, 8577.

9. Ye, S.; Li, G.; Noda, H.; Uosaki, K.; Osawa, M. *Surface Science* **2003,** *529*, 163.

10. Tiberio, R. C.; Craighead, H. G.; Lercel, M.; Lau, T.; Sheen, C. W.; Allara, D. L. *Applied Physics Letters* **1993,** *62*, 476.

11. Castner, D. G.; Hinds, K.; Grainger, D. W. *Langmuir* **1996,** *12*, 5083.

12. Dubois, L. H.; Nuzzo, R. G. *Annual Review of Physical Chemistry* **1992,** *43*, 437.

13. Dubois, L. H.; Zegarski, B. R.; Nuzzo, R. G. *Journal of Chemical Physics* **1993,** *98*, 678.

14. Poirier, G. E.; Pylant, E. D. *Science* **1996,** *272*, 1145.

15. Leung, T. Y. B.; Gerstenberg, M. C.; Lavrich, D. J.; Scoles, G.; Schreiber, F.; Poirier, G. E. *Langmuir* **2000,** *16*, 549.

16. Kobayashi, K.; Horiuchi, T.; Yamada, H.; Matsushige, K. *Thin Solid Films* **1998,** *331*, 210.

17. Azzam, W.; Wehner, B. I.; Fischer, R. A.; Terfort, A.; Woell, C. *Langmuir* **2002,** *18*, 7766.

18. de Boer, B.; Meng, H.; Perepichka, D. F.; Zheng, J.; Frank, M. M.; Chabal, Y. J.; Bao, Z. *Langmuir* **2003,** *19*, 4272.

19. Tai, Y.; Shaporenko, A.; Rong, H. T.; Buck, M.; Eck, W.; Grunze, M.; Zharnikov, M. *Journal of Physical Chemistry B* **2004,** *108*, 16806.

20. Weckenmann, U.; Mittler, S.; Naumann, K.; Fischer, R. A. *Langmuir* **2002,** *18*, 5479.

21. Frey, S.; Stadler, V.; Heister, K.; Eck, W.; Zharnikov, M.; Grunze, M.; Zeysing, B.; Terfort, A. *Langmuir* **2001,** *17*, 2408.

22. Shaporenko, A.; Adlkofer, K.; Johansson, L. S. O.; Tanaka, M.; Zharnikov, M. *Langmuir* **2003,** *19*, 4992.

23. Shaporenko, A.; Adlkofer, K.; Johansson, L. S. O.; Ulman, A.; Grunze, M.; Tanaka, M.; Zharnikov, M. *Journal of Physical Chemistry B* **2004,** *108*, 17964.

24. Ishida, T.; Mizutani, W.; Azehara, H.; Sato, F.; Choi, N.; Akiba, U.; Fujihira, M.; Tokumoto, H. *Langmuir* **2001,** *17*, 7459.

25. Kang, J. F.; Ulman, A.; Liao, S.; Jordan, R.; Yang, G.; Liu, G.-Y. *Langmuir* **2001,** *17*, 95.

26. Zharnikov, M.; Grunze, M. *Journal of Physics: Condensed Matter* **2001,** *13*, 11333.

27. Himmel, H.-J.; Terfort, A.; Woell, C. *Journal of the American Chemical Society* **1998,** *120*, 12069.

28. Ishida, T.; Mizutani, W.; Liang, T.-T.; Azehara, H.; Miyake, K.; Sasaki, S.; Tokumoto, H. *Annals of the New York Academy of Sciences* **2003,** *1006*, 164.

29. Tour, J. M.; Jones, L.; Pearson, D. L.; Lamba, J. J. S.; Burgin, T. P.; Whitesides, G. M.; Allara, D. L.; Parikh, A. N.; Atre, S. *Journal of the American Chemical Society* **1995,** *117*, 9529.

30. de Boer, B.; Frank, M. M.; Chabal, Y. J.; Jiang, W.; Garfunkel, E.; Bao, Z. *Langmuir* **2004,** *20*, 1539.

31. Jiang, W.; Zhitenev, N.; Bao, Z.; Meng, H.; Abusch-Magder, D.; Tennant, D.; Garfunkel, E. *Langmuir* **2005,** *21*, 8751.

32. Stohr, J.; Outka, D. A. *Physical Review B* **1987,** *36*, 7891.

33. Stohr, J., *NEXAFS Spectroscopy*. Springer: Berlin, 1992.

34. Kinzler, M.; Schertel, A.; Haehner, G.; Woell, C.; Grunze, M.; Albrecht, H.; Holzhueter, G.; Gerber, T. *Journal of Chemical Physics* **1994,** *100*, 7722.

35. Outka, D. A.; Stoehr, J.; Rabe, J. P.; Swalen, J. D. *Journal of Chemical Physics* **1988,** *88*, 4076.

36. Trotter, J. *Acta Crystallographica* **1961,** *14*, 1135.

37. Fuxen, C.; Azzam, W.; Arnold, R.; Witte, G.; Terfort, A.; Woell, C. *Langmuir* **2001,** *17*, 3689.

38. Mekhalif, Z.; Laffineur, F.; Couturier, N.; Delhalle, J. *Langmuir* **2003,** *19*, 637.

39. Schlenoff, J. B.; Li, M.; Ly, H. *Journal of the American Chemical Society* **1995,** *117*, 12528.

40. Lavrich, D. J.; Wetterer, S. M.; Bernasek, S. L.; Scoles, G. *Journal of Physical Chemistry B* **1998,** *102*, 3456.

41. Camillone, N.; Khan, K. A.; Osgood, R. M. *Surface Science* **2000,** *453*, 83.

Chapter 4: The Effect of NH_4OH Concentration and Precursor Concentration on the Structure of TPDT and QPDT Assemblies

As synthesized, conjugated dithiols are usually terminated with protecting groups because free thiols have a tendency to oxidize[1] and dimerize.[1,2] The chemistries of the protecting group include tetramethylsilylethyl[3] and, more commonly, acetyl groups.[1] These acetyl protecting groups are usually cleaved *in-situ* with the addition of a deprotecting agent. Ammonium hydroxide (NH_4OH) is the most commonly used deprotecting agent,[1,4,5] although sulfuric acid,[5] triethylamine,[6] and cesium bicarbonate[5] have also been used as deprotecting agents during conjugated dithiol assembly. While the impact of the different deprotecting agents on the final assembly structure of acetyl-protected conjugated systems has been noted,[6,7] we are not aware of any systematic studies that show how the concentration of the deprotecting agent impacts the final structure. This work aims to understand how the concentration of one such deprotection agent, i.e., NH_4OH, affects the assembly of conjugated dithiols.

The concentration of NH_4OH used in the assembly of conjugated dithiols has not been given close attention in the literature. For example, de Boer et al.[8] studied molecular assemblies of BPDT, TPDT, and QPDT on Au formed from THF using “one drop” of NH_4OH. The researchers qualitatively concluded that BPDT, TPDT, and QPDT adopted progressively more upright molecular orientations with increasing number of rings in the n-phenyl backbone. Shortly, after, Jiang et. al.[9] reported STM studies on TPDT and QPDT molecular assemblies formed on Au from THF using “a few drops” of NH_4OH, and the researchers found that TPDT and QPDT are disordered.[9] Adding to the confusing results, the molecular organization of TPDT and QPDT was not quantified in these reports.[8,9] Given the lack of understanding of how the concentration of NH_4OH can impact the structure of the molecular assembly of n-phenyldithiols, we examined the structure of the assembly of TPDT and QPDT as a function of NH_4OH concentration on both Au and GaAs. Because BPDT tends to form disordered assemblies regardless of processing conditions, we focused on TPDT and QPDT for these studies.

To understand how NH_4OH concentration impacts the final structures of TPDT and QPDT assemblies, we first examined the deprotection reaction in the assembly solvents using UV-Vis-NIR spectroscopy. Although we focused our solution studies on the case of TPDT precursor, the findings should be generally extendable to the deprotection of QPDT precursor because the deprotection mechanism is the same. The deprotection reaction, illustrated in Scheme 2.2, involves the conversion of thioacetyl end groups to thiolates with the addition of NH_4OH.[7] The reaction Scheme in 2.2 suggests that the concentration of NH_4OH should directly impact the relative concentration of thioacetyl- and thiolate-terminated molecules in solution. Given that thiolates should freely adsorb, the fraction of thiolate-terminated molecules in solution should, in turn, affect the final assembly structure. We assumed that the initial solution conditions have the most dramatic impact on the final assembly structure because the adsorption of sulfur on GaAs[10,11] and thiolates on Au[12,13] is known to occur rapidly, typically within the first few minutes of substrate immersion. We thus characterized the assembly solutions at the point of substrate immersion, i.e., 1 hour after the addition of NH_4OH to the solution. Figure 4.1a presents the UV-Vis-NIR spectra of TPDT in EtOH 1 hour after the addition of NH_4OH at varying concentrations. A spectrum of the acetyl-protected TPDT precursor in EtOH prior to the addition of NH_4OH is included for reference (solid line). The acetyl-protected TPDT precursor in EtOH exhibits an absorption band with a peak maximum at 298 nm. When NH_4OH is added, we observe the development of a new absorption band at 345 nm. We assign this new absorption band to deprotected TPDT (see Scheme 2.2), which are now terminated with thiolates ($-S^{-}NH_4^{+}$). This absorption is band attributed to thiolates, and not thiols (-SH), because thiol-terminated TPDT, obtained either by direct synthesis[14] or by deprotecting the acetyl-protected precursor with sulfuric acid,[5,7] absorbs at 302 nm in EtOH. The thiolate absorption band at 345 nm intensifies with increasing NH_4OH concentrations while the intensity of the thioacetyl absorption band at 298 nm decreases. This trend suggests an increase in thiolate fraction in EtOH with increasing NH_4OH concentration. We observe a complete disappearance of the thioacetyl absorption band at 298 nm within 60-70 minutes after the addition of NH_4OH at 160 mM, suggesting complete conversion of TPDT from its thioacetyl to thiolate form within this time period.

Figure 4.1b presents the UV-Vis-NIR spectra of TPDT in THF 1 hour after the addition of NH_4OH at varying concentrations. The spectrum of the acetyl-protected TPDT precursor in THF is also included (solid line in Figure 4.1b). We observe an absorption band attributed to the acetyl-protected precursor at 301 nm.[8] With the addition of NH_4OH, an absorption shoulder develops around 330 nm. We attribute this shoulder to thiolate-terminated TPDT because of the increased electron delocalization length of the thiolate-terminated molecule. Specifically, the additional electron density on the sulfur atoms of the thiolate-terminated molecule likely enables extended charge delocalization compared to the conjugated backbone of the thioacetyl-terminated molecule. Increased charge delocalization is expected to shift the UV-Vis-NIR absorption maximum to a higher wavelength.[15] To quantify the position of the thiolate absorption band in THF, we examined the UV-Vis-NIR spectrum of TPDT in THF 25 hours after the addition of 160 mM NH_4OH (Figure 4.1c); from this point on the time-resolved UV-Vis-NIR spectra remain unchanged, so we assumed that the deprotection reaction is complete. From this spectrum, the absorption band maximum in THF is determined to be 312 nm. While the UV-Vis-NIR data of TPDT in EtOH (Figure 4.1a) suggest complete conversion of TPDT from its thioacetyl to thiolate form 1 hour after the addition of 160 mM NH_4OH, the corresponding reaction in THF appears to be significantly slower. We were able to obtain estimates of the solution composition by fitting the absorption bands associated with thioacetyl- and thiolate-terminated molecules with Gaussian peaks, as described in Chapter 2. By examining the relative integrated intensities extracted from the fitted absorption bands of thioacetyl (301 nm) and thiolate (312 nm) in Figures 4.1a and b, we estimated that less than 50% of the thioacetyl end groups were converted to thiolates 1 hour after the addition of 160 mM NH_4OH (Figure 4.1b) in THF. In fact, at 1 mM NH_4OH, we estimated only ≈1% of the thioacetyl groups were converted to thiolates in THF as compared to ≈25% conversion in EtOH after 1 hour. The concentration of NH_4OH drastically affects the fraction of thiolates in the solution at the onset of the assembly process. Considering potential differences in chemical reactivity and end group size between these different species, the variations in their relative concentrations in solution are expected to impact the final structure of TPDT on Au and GaAs.

Figure 4.2a contains RAIRS spectra of TPDT assemblies on Au. These assemblies were formed in EtOH for 18-24 hours at NH_4OH concentrations ranging from 0 to 160 mM. Prominent resonances originating from the phenyl backbone of TPDT include the in-plane, *ip*, (1475 cm^{-1} and 1001 cm^{-1}) and out-of-plane, *op*, (807 cm^{-1}) phenyl ring vibrational modes.[8] Additionally, Figure 4.2a-i reveals features associated with the acetyl protecting group: the peaks at 1706 and 1353 cm^{-1} are assigned to C=O and CH_3 (CH_3-CO) vibrations[8,16] of the thioacetyl functionality, respectively. We observe that the acetyl-protected TPDT precursors can directly adsorb on Au from EtOH without any prior deprotection. The adsorption of acetyl-protected precursors of conjugated molecules has been previously reported on metal surfaces.[1,17,18] On Au, the adsorption was shown to proceed through spontaneous cleaving of the acetyl protecting groups catalyzed by the Au surface, followed by the formation of sulfur-Au bonds.[18] With the absence of acetyl protecting groups at the molecule-substrate interface, the associated resonances at 1706 and 1353 cm^{-1} we observe in Figure 4.2a-i must originate from acetyl protecting groups located at the assembly surface (or molecule-air interface). The intensities of the vibrations associated with the acetyl group (1706 and 1353 cm^{-1}) decrease with increasing NH_4OH concentration, suggesting a corresponding decrease in the concentration of acetyl protecting groups at the assembly surface with increasing NH_4OH concentrations. The overall spectral intensities in Figures 4.2a-ii–v are comparable, suggesting that the surface coverages are comparable in all of these assemblies. The composition of thiolates on the surface in these assemblies, however, is quite different and is dependent on the NH_4OH used during deprotection.

To gain a better understanding of the final assembly structure of TPDT on Au as a function of NH_4OH concentration, we examined the ensemble-average molecular orientation of the TPDT assemblies on Au. Specifically, we compared the relative *ip*/*op* intensities extracted from the RAIRS spectra of the TPDT assemblies to those obtained on the acetyl-protected TPDT precursor powder. We quantified the ensemble-average molecular orientation of each molecular assembly on Au by calculating the RAIRS orientation ratio, OR_r. The OR_r is a measure of anisotropy in the molecular assembly, with $OR_r > 1$ characteristic of a preferentially upright molecular orientation. Accordingly, $OR_r < 1$ indicates that molecules are generally lying flat on the substrate surface, and $OR_r \approx 1$ indicates a disordered molecular assembly. TPDT assembled on Au from EtOH with 1 mM NH_4OH (Figure 4.2a-i) exhibits $OR_r \approx 14.7$, indicating that the assembly adopts a preferentially upright orientation. Figure 4.2a-i reveals that the thioacetyl-terminated

TPDT precursor (no deprotection with NH_4OH) can also spontaneously adsorb from EtOH on Au with a preferentially upright orientation ($OR_r \approx 14.5$) that is comparable to that of TPDT assembled from EtOH at 1 mM NH_4OH (Figure 4.2a-ii). The final structures concluded from the IR spectra in Figures 4.2a-i and 4.2a-ii can be related to the thiolate fraction in the assembly solution at the point of the substrate immersion. Specifically, because no NH_4OH was added during the formation of the molecular assembly structure characterized by Figures 4.2a-i, the adsorption of TPDT must solely be due to the surface-catalyzed deprotection and adsorption[18] of thioacetyl-terminated TPDT at the Au surface. The surface of the resulting assembly is thus thioacetyl-terminated. On the other hand, the addition of 1 mM NH_4OH results in a minor (≈25%) fraction of thiolate-terminated TPDT present in solution at the point of substrate immersion, according to our UV-Vis results. The molecular assembly structure characterized by Figure 4.2a-ii therefore must be due to the competitive adsorption of TPDT thiolates produced in solution by deprotection with NH_4OH and the surface-catalyzed deprotection and adsorption of thioacetyl-terminated TPDT. In fact, the addition of 1 – 30 mM NH_4OH leads to the presence of both thiolates and thioacetyls in solution, suggesting that the final assembly structures consist of a mixture of thiolate- and thioacetyl-terminated molecules. The fact that OR_r decreases with increasing NH_4OH concentration in the assembly solution suggests that higher thiolate content in solution results in less ordered final assembly structures. Additionally, the surfaces of these assemblies are increasingly thiolate-terminated. Finally, the addition of 160 mM NH_4OH results in the complete deprotection of the TPDT precursors by the time the substrate is immersed, i.e., only thiolates are present in solution at the point of substrate immersion at this condition. The molecular assembly structure must therefore result from the sole adsorption of thiolate-terminated TPDT. The surface of this assembly is completely acetyl-free. The fact that this final structure is the least ordered ($OR_r \approx 9.6$) suggests that the adsorption of thiolate-terminated molecules results in less upright final structures compared to those resulting from competitive adsorption of thiolate- and thioacetyl-terminated molecules. Given that the assemblies consist of increasing proportion of acetyl-free molecules with increasing NH_4OH concentration, it is not surprising that the final assemblies exhibit different orientation. We speculate that the structural difference between these assemblies stems from differences in the adsorptivity of thioacetyl- and thiolate-terminated molecules on Au. First, the chemical reactivity of thioacetyl- and thiolate-terminated molecules with Au may be different. Not only will this difference in chemical reactivity result in differences in the final assembly structure, it will likely result in compositional differences between the final assembly and the solution from which the molecules adsorb. Further, the thioacetyl end group is significantly different in size compared to the thiolate end group. As the proportion of thiolate tail groups at the assembly surface increases, this tail group size disparity will certainly affect the way the molecules organize on Au.

RAIRS spectra of TPDT assembled from THF on Au at varying NH_4OH concentrations are shown in Figure 4.2b. The acetyl-protected TPDT precursor (no NH_4OH added) also spontaneously adsorbs from THF on Au (see spectrum in Figure 4.2b-i). The overall intensity of the spectrum in Figure 4.2b-i is reduced, however, compared to the corresponding spectrum in EtOH (Figure 4.2a-i). The reduced spectral intensity suggests that a lower surface coverage results when surface-catalyzed adsorption of the acetyl-protected TPDT precursor on Au occurs from THF compared to that from EtOH. The ensemble-average molecular orientation of the acetyl-protected TPDT precursor assembly from THF ($OR_r \approx 4.1$) is also significantly less upright compared to that of the corresponding assembly from EtOH ($OR_r \approx 14.5$). We speculate that the reduced surface coverage of the acetyl-protected precursor on Au from THF compared to that from EtOH stems from differences in solvent quality. Specifically, due to its high polarity, EtOH is expected be a poor solvent for thioacetyl-terminated molecules. Given that the solubility of thioacetyl-terminated molecules is low in EtOH, the tendency for surface-catalyzed spontaneous adsorption of TPDT is enhanced, thereby increasing adsorption on the surface as compared to adsorption in THF. The comparison of Figures 4.2b-i–ii reveals that, although acetyl-protected TPDT precursor adsorbs from THF on Au, its final structure is less upright ($OR_r \approx 4.1$) than when TPDT is assembled on Au from THF at 1 mM NH_4OH ($OR_r \approx 11.6$). Further comparison of Figures 4.2b-ii–v shows that, like assemblies from EtOH, OR_r decreases with increasing NH_4OH concentration in the assembly solution. The decrease in OR_r indicates correspondingly less upright molecular orientation. TPDT assembled on Au from THF at 160 mM NH_4OH exhibits $OR_r \approx 7.9$ (Figure 4.2b-v). The adsorption behavior of TPDT on Au from THF is similar to that from EtOH, although the assemblies formed from THF are less upright than those from EtOH.

To quantify the molecular orientation in each of the molecular assemblies, we carried out angle-dependent NEXAFS experiments on TPDT adsorbed on Au from EtOH and THF at varying NH_4OH concentrations. The data and dichroic ratios derived from each set of NEXAFS spectra are included in Figure 4.3. In TPDT assemblies from EtOH, we observe a maximum DR = 0.42 when the assembly is carried out with the addition of 1 mM of NH_4OH (Figure 4.3a-ii). As a point of reference, a DR of 0.42 corresponds to an ensemble-average backbone tilt of $21 \pm 3°$ away from the substrate normal according to analysis carried out with the BB model.[19] This orientation compares well with the most upright TPDT assemblies reported to-date.[14,19] Consistent with our observations from RAIRS, the acetyl-protected TPDT precursor spontaneously adsorbs from EtOH on Au

(Figure 4.3a-i), resulting in an assembly that is preferentially upright (DR = 0.4). The final structure of this assembly is slightly less upright (DR = 0.4) relative to that of TPDT assembled at 1 mM NH_4OH (DR = 0.42, Figure 4.3a-ii). The comparison of Figures 4.3a-ii–v reveals that DR decreases with increasing NH_4OH concentration, with the TPDT assembly at 160 mM NH_4OH exhibiting DR = 0.29 (Figure 4.3a-v). As a point of reference, DR = 0.42 and DR = 0.29 correspond to ensemble-average backbone tilts of 21 ± 3° and 29 ± 3° away from the substrate normal, respectively. These observations are consistent with the RAIRS results presented in Figure 4.2a.

Figure 4.3b contains angle-dependent NEXAFS spectra acquired at varying x-ray incident angles of TPDT assembled on Au from THF as a function of NH_4OH concentration. Figure 4.3b-i reveals that the π*/jump ratio, a measure of surface coverage, is ≈1.5. This π*/jump ratio is significantly lower than that obtained for the acetyl-protected TPDT precursor assembled on Au from EtOH (≈2.7), indicating a reduced adsorption of the acetyl-protected TPDT precursor on Au from THF (Figure 4.3b-i) compared to the corresponding assembly from EtOH (Figure 4.3a-i). The final structure of the assembly from THF is also poor (disordered, with DR = 0.09) relative to that of the assembly from EtOH (upright, DR = 0.4). Further comparison of the sets of NEXAFS spectra in Figures 4.3b-ii–v reveals a maximum DR of 0.31 in the assembly from THF at 1 mM NH_4OH. As a point of reference, DR = 0.31 corresponds to an ensemble-average backbone tilt of 28 ± 3° away from the substrate normal according to analysis carried out with the BB model.[14] That DR decreases with increasing NH_4OH concentration (Figures 4.3b-ii–v) indicates that the final structures of TPDT assembled on Au from THF at higher NH_4OH concentrations are less upright than those at lower NH_4OH concentrations. At the highest NH_4OH concentration of 160 mM, TPDT assembly on Au from THF exhibits DR = 0.23 (Figure 4.3b-v), which corresponds to an ensemble-average backbone tilt of 32 ± 3° away from the substrate normal. A summary of the RAIRS ORs and NEXAFS DRs extracted from our FTIR and NEXAFS data, respectively, at varying NH_4OH concentrations is shown in Figure 4.4.

The reduced structural quality of assemblies from THF on Au at high NH_4OH concentrations is consistent with reported findings.[8,20] Specifically, de Boer et. al.[8,20] have carried out the assembly of TPDT from THF on Au with the addition of "one drop" of NH_4OH per 10 mL of 50 μM solution of acetyl-protected TPDT precursor. Considering that a drop is usually on the order of 0.1 mL (100 μL), the above conditions would place the NH_4OH concentration at the high end of the concentrations we examined. Such conditions would result in assemblies of poor structural quality, as indicated by the low *ip*/*op* ratios in their reported RAIRS spectra.[20] Our observations are also consistent with the microscopy findings of Jiang et. al.[9] that reveal poor assembly of TPDT from THF on Au with the addition of "a few drops" of NH_4OH. While properly adjusting the concentration of NH_4OH in solution can help achieve more upright molecular assemblies, the surface termination of these assemblies will also depend on the NH_4OH concentration. It is therefore important to pay attention to NH_4OH concentration when making comparisons between assembly structures.

We have also examined the effect of NH_4OH concentration on the final assembly structures of TPDT on GaAs.[19] Figure 4.5a contains transmission IR spectra of TPDT assemblies from EtOH on GaAs at varying NH_4OH concentrations. Features associated with the phenyl backbone of TPDT are the in-plane, *ip*, (1475 cm^{-1} and 1001 cm^{-1}) and the out-of-plane, *op*, (807 cm^{-1}) phenyl ring vibrational modes.[8] Additionally, a weak *ip perp*[8] ring vibration is visible at 1398 cm^{-1}. The resonance associated with the C=O vibration[8,16] of the acetyl protecting group is observed at 1707 cm^{-1} in samples assembled at lower NH_4OH concentrations. Similar to the spontaneous adsorption of acetyl-protected TPDT on Au, the acetyl-protected TPDT precursor can directly adsorb on GaAs from EtOH without any prior deprotection with NH_4OH (Figure 4.5a-i). The intensity of the C=O vibration signal at 1707 cm^{-1} decreases with increasing NH_4OH concentration, indicating a corresponding decrease in the acetyl termination at the assembly surface. The intensities in Figures 4.5a-ii–v are similar, suggesting comparable surface coverage in TPDT assemblies on GaAs from EtOH across the NH_4OH concentration range we examined. Because the IR studies on Au were carried out in reflection mode while the IR studies on GaAs were carried out in transmission mode, the spectral intensities cannot be directly compared to assess the relative surface coverages between assemblies on Au and GaAs.

To determine molecular orientation, we examined the orientation ratios, OR_t, extracted from each transmission IR spectrum. These value are included in Figure 4.5. When TPDT is assembled on GaAs from EtOH with 1 mM NH_4OH, $OR_t \approx 2.6$. We observe from Figure 4.5a-i that, although the acetyl-protected TPDT precursor can also spontaneously adsorb from EtOH on GaAs, its final structure is less upright ($OR_t \approx 1.9$) compared to that of TPDT assembled from EtOH at 1 mM NH_4OH (Figure 4.5a-ii). The comparison of Figures 4.5a-ii–v reveals decreasing OR_t with increasing NH_4OH concentration in the assembly solution, indicating that the final structures of TPDT assembled on GaAs from EtOH at higher NH_4OH concentrations are less upright than those at lower NH_4OH concentrations. TPDT assembled on GaAs from EtOH at the highest NH_4OH concentration (160 mM) is characterized by $OR_t \approx 1.6$ (Figure 4.5a-v). Similar to TPDT assemblies from EtOH on Au, there appears to be an optimal NH_4OH concentration, thus an optimal thiolate fraction, in the assembly solution that results in the TPDT assembly with the most upright molecular orientation (Figure 4.5a-ii). We speculate that, like assemblies on Au, the assemblies on GaAs may be governed by differences in adsorptivity of thioacetyl- and thiolate-terminated molecules.

Transmission IR spectra of TPDT assembled on GaAs from THF at varying NH_4OH concentrations are presented in Figure 4.5b. These spectra are different from those of TPDT assemblies on GaAs from EtOH. Specifically, the transmission IR spectra of these assemblies exhibit significantly weaker overall intensities, especially at lower NH_4OH concentrations. In fact, when TPDT is assembled on GaAs from THF without any NH_4OH, very little adsorption occurs, as evinced in the featureless spectrum in Figure 4.5b-i. This observation contrasts that of the assembly on GaAs from EtOH (Figure 4.5a-i), where we observe appreciable adsorption of acetyl-protected TPDT precursors. The comparison of the remaining spectra in Figures 4.5b-ii–v shows that the overall spectral intensities increase with increasing NH_4OH concentration, suggesting an increase in surface coverage. Concomitantly, the orientation characteristics improve to result in $OR_r \approx 1.5$ at 160 mM NH_4OH (Figure 4.5b-v). Unlike adsorption from EtOH, our transmission IR experiments suggest that only thiolate-terminated TPDT molecules adsorb significantly on GaAs when assembled from THF. We thus have to assemble TPDT at high NH_4OH concentrations in THF in order to achieve decent surface coverage. These assemblies on GaAs from THF, however, are never as ordered as TPDT on GaAs assembled from EtOH.

We carried out angle-dependent NEXAFS experiments on the TPDT assemblies on GaAs from EtOH and THF across the NH_4OH concentration range. Figure 4.6a contains pre- and post-edge normalized angle-dependent NEXAFS spectra of TPDT assembled from EtOH at varying NH_4OH concentrations, along with the extracted dichroic ratios. We observe a maximum DR = 0.32 when the assembly is carried out with 1 mM of NH_4OH (Figure 4.6a-ii). As a reference, analysis with the BB model of this assembly results in an ensemble-average backbone tilt of 27 ± 3° away from the substrate normal. Consistent with what was observed by transmission IR, the acetyl-protected TPDT precursor spontaneously adsorbs on GaAs from EtOH (Figure 4.6a-i). Its final structure, however, is less upright (DR = 0.12) compared to that of TPDT assembled on GaAs from EtOH with 1 mM NH_4OH (Figure 4.6a-ii). Further comparison of Figures 4.6a-ii–v reveals decreasing DR with increasing NH_4OH concentration, with DR = 0.19 at 160 mM NH_4OH (Figure 4.6a-v). These observations are again consistent with the transmission IR results presented in Figure 4.5a.

Pre- and post-edge normalized NEXAFS spectra acquired at varying x-ray incident angles for assemblies of TPDT from THF as a function of NH_4OH concentration are shown in Figure 4.6b. From Figure 4.6b-i, we observe that the assembly of acetyl-protected TPDT precursor on GaAs from THF exhibits a π^*/jump ratio ($\approx$1.3) that is substantially lower than that ($\approx$3.3) from EtOH (Figure 4.6a-i). The lower π^*/jump ratio indicates reduced adsorption of the acetyl-terminated TPDT precursor on GaAs from THF. That TPDT does not adsorb significantly from THF was previously observed by transmission IR. Further comparison of the NEXAFS data sets in Figures 4.6b-ii–v reveals that the π^*/jump ratios increase with increasing NH_4OH concentrations, suggesting an increase in surface coverage. The spectra of TPDT assembled on GaAs from THF at the highest NH_4OH concentration of 160 mM (Figure 4.6b-v) exhibit a π^*/jump $\approx$ 2.9. Also consistent with transmission IR data, we observe a moderate increase in DR to DR = 0.19 at 160 mM NH_4OH (Figure 4.6b-v), suggesting a modest improvement in the final structure of the assemblies at high NH_4OH concentrations. A summary of the OR_t and DR extracted from the transmission IR and NEXAFS data, respectively, at varying NH_4OH concentrations is presented in Figure 4.7.

We investigated whether NH_4OH concentration had a similar impact on the molecular assemblies of QPDT formed on GaAs from EtOH-rich solutions. We found that, similar to TPDT assemblies on GaAs, the final structure of QPDT assemblies on GaAs is dependent on NH_4OH concentration. Figure 4.8 contains transmission IR spectra of QPDT assembled on GaAs from EtOH-rich (EF = 0.75) with the addition of 10 mM (a) and 160 mM (b) of NH_4OH. The spectrum in Figure 4.8a reveals the C=O peak at 1706 cm^{-1}, indicating that QPDT assembled with the addition of NH_4OH at 10 mM is largely acetyl-terminated at the surface. Acetyl assembly surface termination was also observed for TPDT assemblies on GaAs carried out from EtOH at low NH_4OH concentrations (Figure 4.5a-i–ii). On the other hand, QPDT assembled with the addition of NH_4OH at 160 mM is free of acetyl termination at the assembly surface, as evidenced by the absence of the C=O peak at 1706 cm^{-1} in Figure 4.8b. QPDT assembled on GaAs at 10 mM NH_4OH exhibits an $OR_t \approx 4$, suggesting preferentially upright molecular orientation. The molecular orientation of QPDT assembled on GaAs at 160 mM NH_4OH is significantly less upright, as indicated by a lower $OR_t \approx 2$. We therefore concluded that the molecular orientation of QPDT assembled on GaAs from EtOH-rich solutions is more upright at low NH_4OH concentrations than at high NH_4OH concentrations. The $OR_t \approx 4$ comparison of the most upright TPDT assemblies on GaAs from EtOH ($OR_t \approx 2.6$) and the most upright QPDT assemblies on GaAs from EtOH-rich solutions ($OR_t \approx 4$) achieved at low NH_4OH concentrations reveals that QPDT is more upright than TPDT. This observation is consistent with an increase in preferential orientation due to increased backbone length of QPDT.

We also carried out NEXAFS experiments on QPDT assembled on GaAs from EtOH-rich (EF = 0.75) solutions at varying NH_4OH concentrations. Figure 4.9 contains pre- and post-edge normalized angle-dependent NEXAFS spectra of QPDT assembled without any NH_4OH added, and at NH_4OH concentrations ranging from 1 to 160 mM. Figure 4.9a indicates that the acetyl-protected QPDT precursor tends to spontaneously adsorb on GaAs and exhibits a preferentially upright final structure with DR = 0.29. According to analysis with the BB model,[14] DR = 0.29 corresponds to an ensemble-average backbone tilt of 29 ± 3° away from the substrate normal. Its final structure, however, is less upright compared to that of QPDT assembled on GaAs at 1 mM NH_4OH (DR = 0.44, Figure 4.9b). Further comparison of Figures 4.9b-e reveals DRs that decrease with increasing NH_4OH concentration, similar to the trend observed for TPDT assembled on GaAs from EtOH. The DR exhibited by QPDT assembled on GaAs from EtOH-rich solutions at 1 mM NH_4OH (DR = 0.44) is higher than that exhibited by TPDT assembled on GaAs from EtOH 1 mM NH_4OH (DR = 0.32). This observation indicates that QPDT assemblies on GaAs are generally more upright than those of TPDT. The impact of NH_4OH concentration on the final structure of QPDT assemblies on GaAs from EtOH-rich solutions (Figure 4.9) also appears to be less pronounced than that observed for TPDT assemblies on GaAs from EtOH (Figure 4.6). Specifically, QPDT assemblies on GaAs from EtOH-rich solvents exhibit upright preferential orientation across a wider range of NH_4OH concentrations (1 – 30 mM) than TPDT assemblies on GaAs from EtOH (1 mM). We attribute the reduced impact of NH_4OH concentration on the assembly of QPDT on GaAs from EtOH-rich solutions to increased intermolecular interactions between the longer QPDT backbones. The strong intermolecular interactions in QPDT molecular assemblies strongly favor ordered molecular assembly structures, outweighing competing effects, such as increased NH_4OH concentrations.

In addition to the type of substrate used, the quality of the solvent, and the concentration of the deprotecting agent, the concentration of the acetyl-protected precursor in solution can also potentially impact the final structure. For instance, the adsorption of alkylthiols on both Au[12,21] and GaAs[22] has been reported to be concentration dependent. Specifically, Dannenberger et. al.[21] observed that 1-docosanethiol exhibited near-monolayer coverage on Au after ~1000 s when adsorbed from a 0.5 μM solution in hexane. The same coverage was observed in ~100 s when the adsorption of 1-docosanethiol on Au was carried out from a 10 μM solution.[21] Similarly, Jun et. al.[22] reported final assembly thicknesses of 5 and 11Å for 1-hexadecanethiol adsorbed on GaAs from 1 and 50 mM solutions in ethanol, respectively. The concentration of conjugated thiols has also been shown to impact their adsorption on Au. For example, Liao et. al.[13] observed that 4'-methylmercapto-4-mercaptobiphenyl exhibited equilibrium coverage on Au after ~600 s when adsorbed from a 60 μM solution in toluene. The same molecule exhibited equilibrium coverage in ~150 s when the adsorption on Au was carried out from a 256 μM solution in toluene,[13] indicating that higher molecule concentrations generally lead to faster assembly. Although different molecular orientations were implied with varying precursor concentration, the molecular orientation of the molecular assemblies was not actually quantified.[12,21,22] In what follows, we will specifically address how the concentration of the acetyl-protected precursor influences the final surface coverage and ensemble-average orientation of TPDT and QPDT molecular assemblies. Here, we focused on assemblies on GaAs. We also held the NH_4OH concentrations constant at concentrations that were previously determined to yield the most ordered assemblies. Specifically, we used 1 mM NH_4OH to examine how the concentration of acetyl-protected TPDT precursor affects the assembly on GaAs from EtOH. We used 160 mM NH_4OH to examine how the acetyl-protected TPDT and QPDT precursor concentration affects the assembly on GaAs from THF.

Figure 4.10a contains transmission IR spectra of TPDT assemblies on GaAs formed from EtOH using 1 mM NH_4OH. The concentration of the acetyl-protected TPDT precursor ranged from 50 to 375 μM in the assembly solution. OR_t extracted from each of the spectra are included. The comparison of Figures 4.8a-i–iv reveals that OR_t increases with increasing TPDT precursor concentration in the assembly solution, with the most upright (OR_t = 2.4) assembly from solutions at precursor concentration of 250 μM. When the precursor concentration is further increased to 375 μM (Figure 4.10a-v), the final structure becomes less upright (OR_t = 2.0). We concluded that there exists an optimal acetyl-protected TPDT precursor concentration which results in most upright final assembly structure. The existence of an optimal acetyl-protected TPDT precursor concentration can be understood in terms of the optimal thiolate fraction in solution. Since both thiolate- and thioacetyl-terminated TPDT molecules adsorb on GaAs from EtOH, the final structure of these assemblies must be a result of simultaneous adsorption of the thiolate- and thioacetyl-terminated species. We speculate that there exists an optimal balance of the thiolate- and thioacetyl-terminated species which results in the most upright final assembly structures. The fraction of thiolates in solution depends on both the NH_4OH and the acetyl-protected precursor concentrations. Accordingly, a given thiolate fraction at the point of substrate immersion can be achieved by (1) by fixing the acetyl-protected precursor concentration and adjusting the NH_4OH concentration or (2) by fixing the NH_4OH concentration and adjusting the acetyl-protected precursor concentration. That we observed an optimal NH_4OH concentration (1 mM) during our studies (Figure 4.5a) is consistent with achieving an optimal thiolate fraction via (1). That we observed an optimal acetyl-protected precursor concentration (250 μM) during our studies (Figure 4.10a) is consistent with achieving an optimal thiolate fraction via (2).

Figure 4.10b contains transmission IR spectra of TPDT assembled on GaAs from THF using 160 mM NH_4OH. The acetyl-protected TPDT precursor concentration ranged from 80 to 500 μM in these assembly solutions. OR_t extracted from each of the spectra are included. The comparison of Figures 4.10b-i–iii reveals that OR_t increase with increasing acetyl-protected TPDT precursor concentrations, with the most upright (OR_t = 1.9) assembly resulting at the highest precursor concentration of 500 μM. Since only thiolate-terminated TPDT molecules adsorb on GaAs from THF, a high thiolate content in solution is required to achieve decent surface coverages and structural organization. High thiolate content in solution could result from both (1) increasing NH_4OH concentration and (2) increasing acetyl-protected precursor concentration at a given NH_4OH concentration. As demonstrated in our NH_4OH concentration studies (Figure 4.5b) the highest NH_4OH concentration of 160 mM resulted in the most upright molecular assembly structure. The observation of the most upright molecular assembly structure at the highest NH_4OH concentration is consistent with achieving the highest thiolate content in solution via (1). As we observed in this TPDT precursor concentration study, the highest acetyl-protected TPDT precursor concentration of 500 μM led to the most upright molecular assembly structure (Figure 4.10b). The occurrence of the most upright molecular assembly structure at the highest TPDT precursor concentration is consistent with achieving the highest thiolate content in solution via (2).

We examined the impact of the QPDT precursor concentration on its final structure when assembled on GaAs from THF. Figure 4.11 contains transmission IR spectra of QPDT assembled on GaAs from THF using 160 mM NH_4OH. We explored the precursor concentration ranging from 50 to 200 μM. OR_t extracted from each of the spectra are included. The comparison of Figures 4.11a-d reveals that OR_t increase with increasing acetyl-protected QPDT precursor concentrations in the assembly solution. A maximum OR_t = 4.5 was determined at the highest precursor concentration of 200 μM. Similar assembly behavior, where more upright assembly structures resulted at higher precursor concentrations, was observed for TPDT assembled on GaAs from THF (Figure

4.10b). Similar to TPDT assembly on GaAs from THF, we attribute this trend to an increased thiolate fraction in solution at elevated acetyl-protected QPDT precursor concentrations.

In this Chapter, we demonstrated that both NH_4OH and thioacetyl precursor concentrations affect the final assembly structures of TPDT. For assemblies on Au, we found that the high NH_4OH concentrations (we estimate above 100 mM)[8,9] commonly used for conjugated thiol assembly on Au actually result in some of the least ordered final structures. We found that the most upright TPDT assemblies on Au from both EtOH and THF are, in fact, achieved when a low (1 mM) NH_4OH concentration is used to deprotect the molecules. At these conditions, the assembly formation appears to be dominated by the surface-catalyzed adsorption of thioacetyl-terminated molecules. These assemblies become less upright when increased NH_4OH concentrations are used. At these conditions, the assembly formation appears to be dominated by the adsorption of thiolate-terminated molecules produced in solution by the deprotection reaction. Because increasing NH_4OH concentration increases the fraction of thiolates in solution, the surfaces of the resulting assemblies become increasingly thiolate-terminated as the NH_4OH concentration used is increased. TPDT assemblies on GaAs carried out from EtOH exhibit a NH_4OH concentration dependence similar to that on Au. Specifically, the final structure of TPDT assembled on GaAs from EtOH is upright at low (1 mM) NH_4OH concentration. The assemblies become less upright with increasing NH_4OH concentration. TPDT assemblies on GaAs carried out from THF are drastically different from those carried out from EtOH. Specifically, TPDT assemblies on GaAs carried out from THF at low NH_4OH concentrations exhibit negligible surface coverage. The surface coverage and structural organization of TPDT assemblies on GaAs carried out from THF improve with increasing NH_4OH concentrations.

We then selected the NH_4OH concentrations that yielded the most oriented assemblies and examined the effect of thioacetyl TPDT precursor concentration on the final assembly structure at these conditions. We found that the thioacetyl precursor concentration also affects the final assembly structure of TPDT. TPDT assemblies on GaAs carried out from EtOH at 1 mM NH_4OH were found to exhibit the most upright final structure when an optimal thioacetyl precursor concentration of 250 μM was used. We attributed the formation of the most upright final assembly structures to the likely occurrence of an optimal thiolate fraction in solution at this precursor concentration. TPDT assemblies on GaAs carried out from THF at 160 mM NH_4OH were found to exhibit the most upright final structure at the highest acetyl-precursor concentration explored (500 μM). We attributed the formation of the most upright final assembly structures to the highest thiolate contents in solution at these conditions.

We also examined the effects of both the NH_4OH and the thioacetyl precursor concentrations on the final structures of select assemblies of QPDT on GaAs. Specifically, we showed that the assembly of QPDT on GaAs from EtOH-rich solvent (EF = 0.75) is sensitive to NH_4OH concentration. When assembled at low NH_4OH concentrations (1 – 30 mM), the QPDT assemblies on GaAs exhibit the desired preferentially upright orientation. On the other hand, at the highest NH_4OH concentration (160 mM), QPDT assembled on GaAs from the EtOH-rich solvent was found to be largely disordered. We also examined the effect of thioacetyl QPDT precursor on the final structure of QPDT assembled on GaAs from THF at high NH_4OH concentrations (160 mM). QPDT assembled on GaAs from THF at this condition exhibits the most upright final structures at 200 μM thioacetyl precursor concentration.

Our results emphasize that the final assembly structures of even the simplest conjugated molecules like n-phenyldithiols are extremely sensitive to the assembly conditions, including the type of substrate, the assembly solvent quality, and the NH_4OH and thioacetyl precursor concentrations. The consideration of each and all of these conditions is essential for achieving a highly ordered assembly structure. Compared to the assembly of alkylthiol molecules, the assembly of conjugated dithiols is complex for a number of reasons. First, the assembly of conjugated molecules requires a deprotecting agent. The use of a deprotecting agent (NH_4OH) in the assembly of conjugated molecules adds an extra layer of complexity, as suggested by the pronounced effects of its concentration on the final assembly structures we demonstrated.[19] These molecular assemblies appear to form by the competing adsorption of thiolate-terminated molecules and thioacetyl-terminated molecules. The concentration balance between the thiolates and the thioacetyls in solution at the point of the substrate immersion depends on both the concentration of NH_4OH and the concentration of the acetyl-terminated precursor in solution. The details of this concentration balance affect the surface termination of the resulting assemblies. Furthermore, the tendency of each of the two species to adsorb is governed by both the solvent quality and the type of substrate on which the adsorption occurs. As a result, the details of the final assembly structure are affected by a complex interplay of all these parameters. Finally, the size of the processing condition window leading to ordered final assembly structures appears to depend on the strength of intermolecular interactions between the adsorbed molecules. If the intermolecular interactions are weak, such as in the case of the shorter BPDT molecules, no combination of processing conditions appears to lead to ordered final assembly structures. When the intermolecular interactions are stronger, as is in the case of the longer TPDT molecules, a narrow window of processing parameters leads to ordered final assembly structures. If the intermolecular interactions are yet stronger, such as in the case of the yet longer

QPDT molecules, ordered final assembly structures result across a wider range of processing conditions.

FIGURES

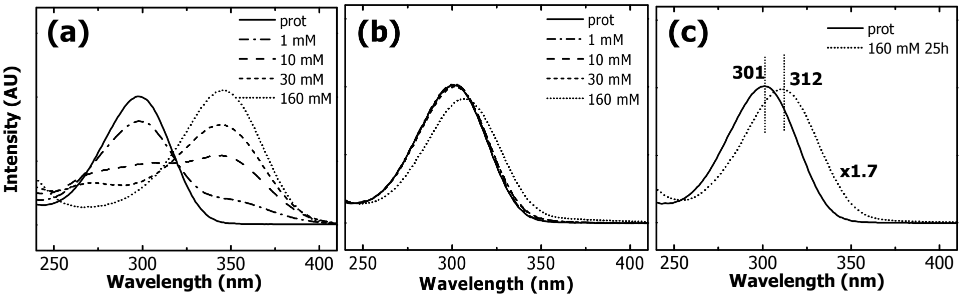

Figure 4.1. UV-Vis-NIR spectra of TPDT dissolved in (a) EtOH and (b) THF with the addition of NH_4OH at varying concentrations 1h after injection. Spectra of acetyl-protected TPDT precursor dissolved in EtOH and THF are included as solid lines in (a) and (b) for reference. Panel (c) contains UV-Vis-NIR spectra of acetyl-protected TPDT precursor (solid line) and TPDT dissolved in THF after 25 hours of NH_4OH injection at 160 mM (dashed line). The latter spectrum was scaled for clarity.

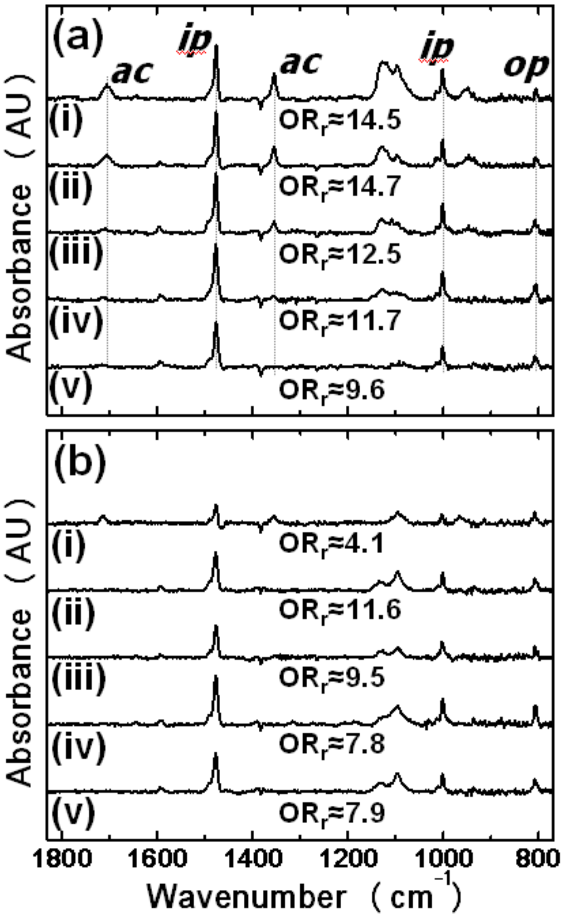

Figure 4.2. RAIRS spectra of TPDT assembled on Au from (a) EtOH and (b) THF with (i) no NH_4OH added, and with the addition of (ii) 1, (iii) 10, (iv) 30, and (v) 160 mM of NH_4OH. OR_r extracted from each of the spectra are included. Major vibrations are identified in (a).

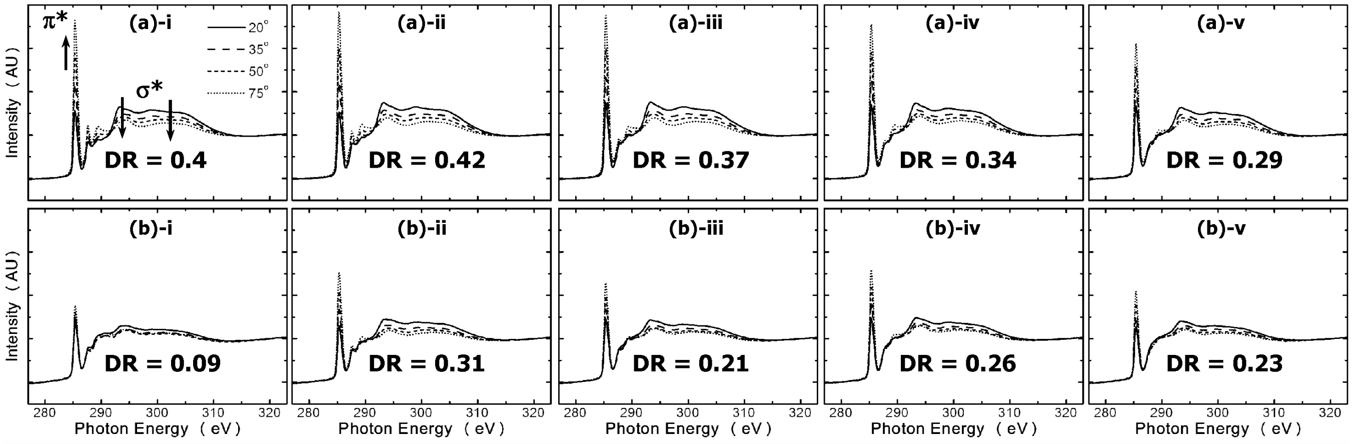

Figure 4.3. C 1s angle-dependent, pre- and post-edge normalized NEXAFS spectra of TPDT assembled on Au from (a) EtOH and (b) THF with (i) no NH_4OH added, and with the addition of (ii) 1, (iii) 10, (iv) 30, and (v) 160 mM NH_4OH. The dichroic ratios derived from each set of spectra are included.

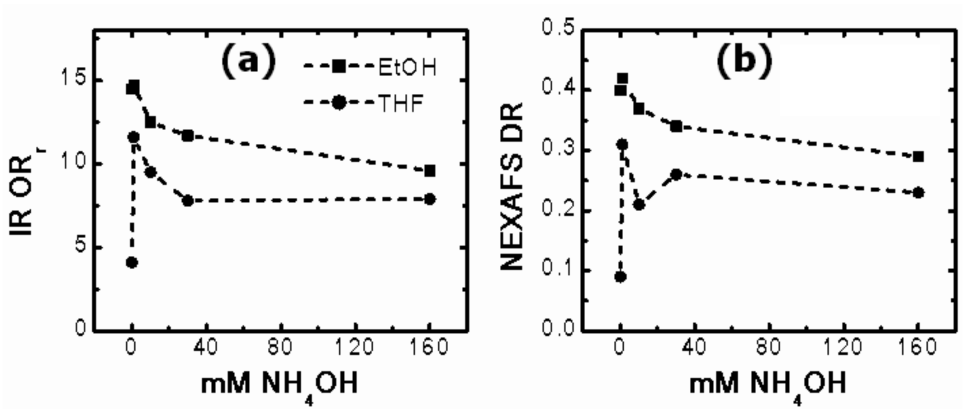

Figure 4.4. Orientation parameters and dichroic ratios derived from (a) RAIRS and (b) NEXAFS spectra, respectively, for TPDT assembled on Au from EtOH and THF as a function of NH_4OH concentration.

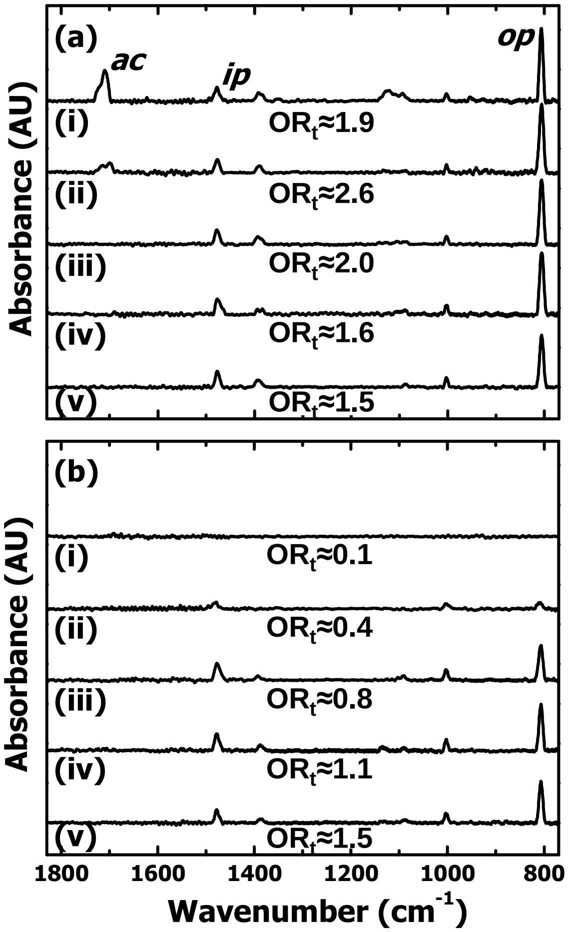

Figure 4.5. Transmission IR spectra of TPDT assembled on GaAs from (a) EtOH and (b) THF with (i) no NH_4OH added, and with the addition of (ii) 1, (iii) 10, (iv) 30, and (v) 160 mM NH_4OH. OR_t extracted from each of the spectra are included. Major vibrations are identified in (a).

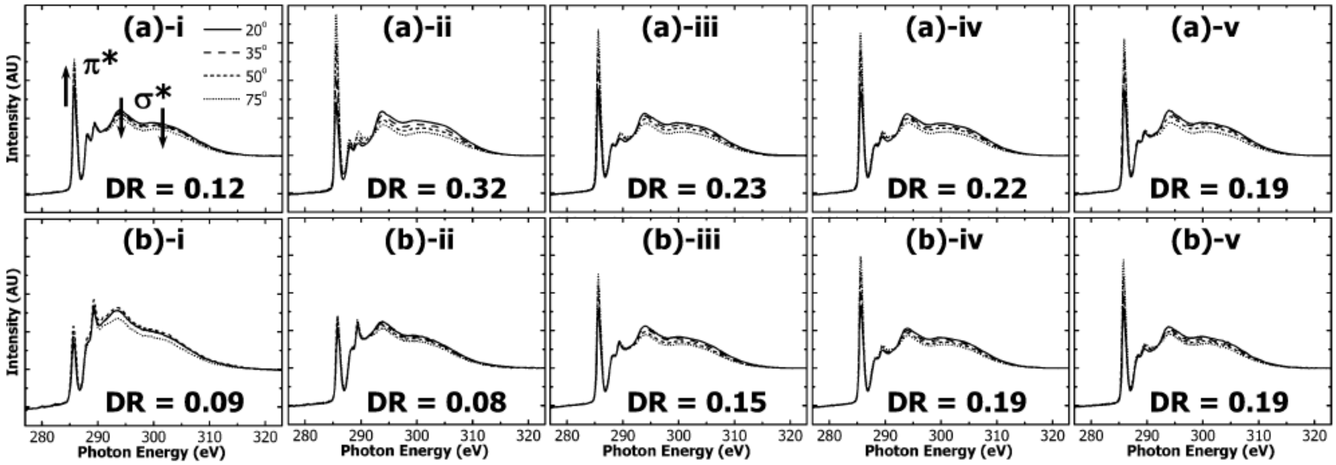

Figure 4.6. C 1s angle-dependent, pre- and post-edge normalized NEXAFS spectra of TPDT assembled on GaAs from (a) EtOH and (b) THF with (i) no NH_4OH added, and with the addition of (ii) 1, (iii) 10, (iv) 30, and (v) 160 mM NH_4OH. The dichroic ratios derived from each set of spectra are included.

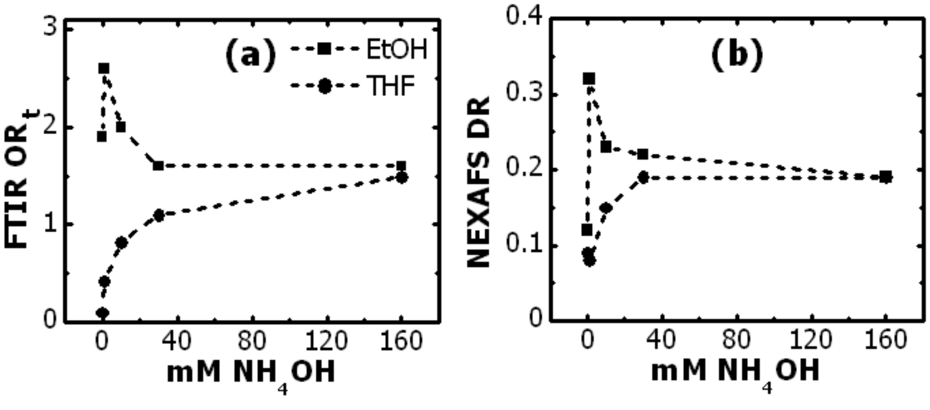

Figure 4.7. Orientation parameters and dichroic ratios derived from (a) transmission IR and (b) NEXAFS spectra, respectively, for TPDT assembled on GaAs from EtOH and THF as a function of NH_4OH concentration.

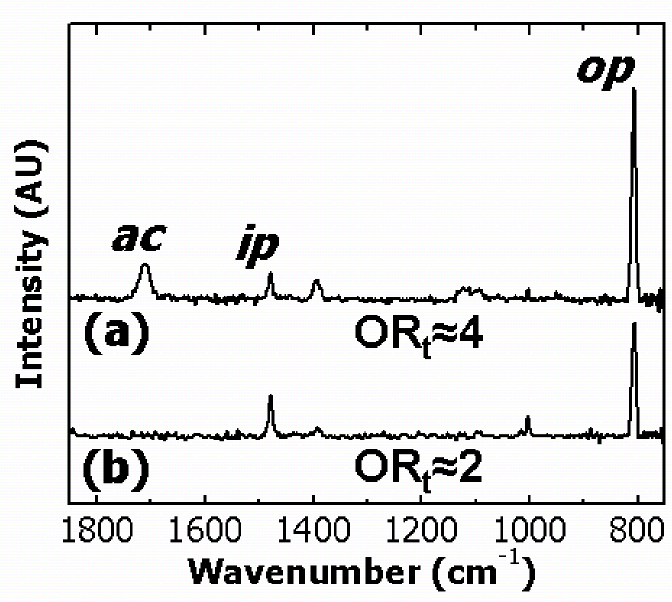

Figure 4.8. Transmission IR spectra of QPDT assembled on GaAs from a cosolvent with EF = 0.75 with the addition of (a) 10 and (b) 160 mM of NH_4OH. OR_t extracted from each of the spectra are included. Major vibrations are identified in (a).

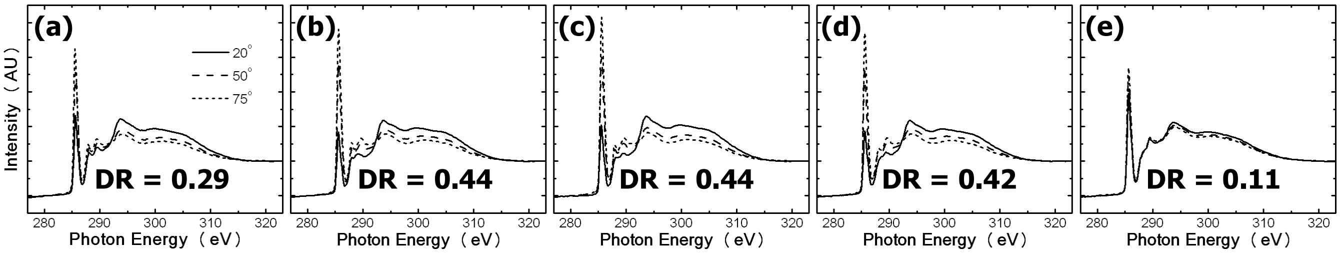

Figure 4.9. C 1s angle-dependent, pre- and post-edge normalized NEXAFS spectra of QPDT assembled on GaAs from a cosolvent with EF = 0.75 with (a) no NH_4OH added, and with the addition of (b) 1, (c) 10, (d) 30, and (e) 160 mM NH_4OH. The dichroic ratios derived from each set of spectra are included.

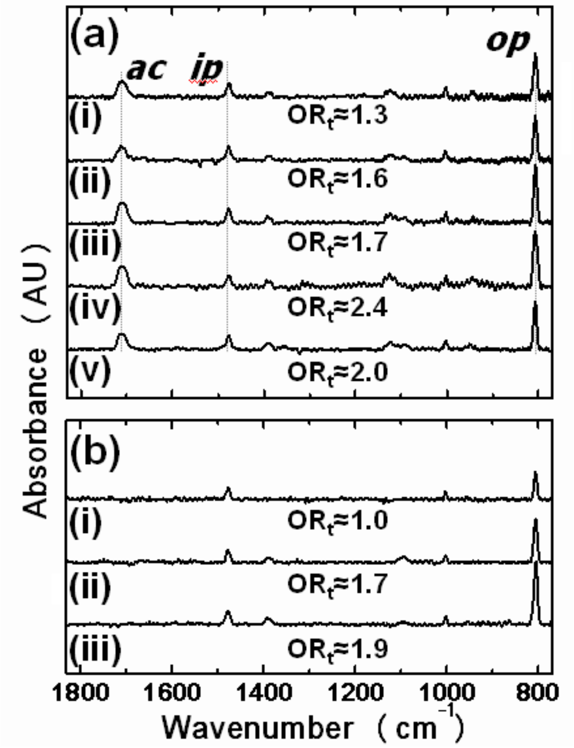

Figure 4.10. Transmission IR spectra of TPDT assembled on GaAs from (a) EtOH with the addition of 1 mM NH_4OH and (b) THF with the addition of 160 mM NH_4OH. The TPDT precursor concentration varied from (i) 50, (ii) 80, (iii) 125, (iv) 250, to (v) 375 μM for the assemblies from EtOH and from (i) 80, (ii) 200, to (iii) 500 μM for the assemblies from THF. OR_t extracted from each of the spectra are included. Major vibrations are identified in (a).

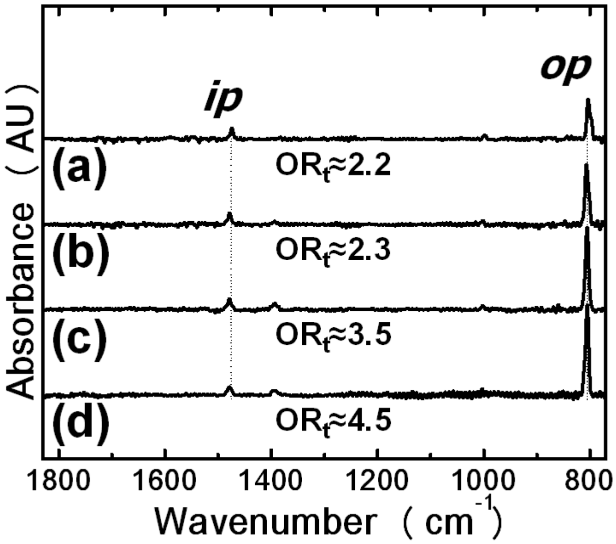

Figure 4.11. Transmission IR spectra of QPDT assembled on GaAs from THF with the addition of 160 mM NH_4OH and QPDT precursor concentration of (a) 50, (b) 100, (c) 150, and (d) 200 μM. OR_t extracted from each of the spectra are included. Major vibrations are identified in (a).

REFERENCES

1. Tour, J. M.; Jones, L.; Pearson, D. L.; Lamba, J. J. S.; Burgin, T. P.; Whitesides, G. M.; Allara, D. L.; Parikh, A. N.; Atre, S. *Journal of the American Chemical Society* **1995,** *117*, 9529.

2. Weckenmann, U.; Mittler, S.; Naumann, K.; Fischer, R. A. *Langmuir* **2002,** *18*, 5479.

3. Pollack, S. K.; Naciri, J.; Mastrangelo, J.; Patterson, C. H.; Torres, J.; Moore, M.; Shashidhar, R.; Kushmerick, J. G. *Langmuir* **2004,** *20*, 1838.

4. Donhauser, Z. J.; Mantooth, B. A.; Kelly, K. F.; Bumm, L. A.; Monnell, J. D.; Stapleton, J. J.; Price Jr, D. W.; Rawlett, A. M.; Allara, D. L.; Tour, J. M.; Weiss, P. S. *Science* **2001,** *292*, 2303.

5. Cai, L.; Bahr, J. L.; Yao, Y.; Tour, J. M. *Chemistry of Materials* **2002,** *14*, 4235.

6. Shaporenko, A.; Elbing, M.; Blaszczyk, A.; Von Haenisch, C.; Mayor, M.; Zharnikov, M. *Journal of Physical Chemistry B* **2006,** *110*, 4307.

7. Cai, L.; Yao, Y.; Yang, J.; Price, D. W., Jr.; Tour, J. M. *Chemistry of Materials* **2002,** *14*, 2905.

8. de Boer, B.; Meng, H.; Perepichka, D. F.; Zheng, J.; Frank, M. M.; Chabal, Y. J.; Bao, Z. *Langmuir* **2003,** *19*, 4272.

9. Jiang, W.; Zhitenev, N.; Bao, Z.; Meng, H.; Abusch-Magder, D.; Tennant, D.; Garfunkel, E. *Langmuir* **2005,** *21*, 8751.

10. Lebedev, M. V.; Mayer, T.; Jaegermann, W. *Surface Science* **2003,** *547*, 171.

11. Ke, Y.; Milano, S.; Wang, X. W.; Tao, N.; Darici, Y. *Surface Science* **1998,** *415*, 29.

12. Bain, C. D.; Troughton, E. B.; Tao, Y. T.; Evall, J.; Whitesides, G. M.; Nuzzo, R. G. *Journal of the American Chemical Society* **1989,** *111*, 321.

13. Liao, S.; Shnidman, Y.; Ulman, A. *Journal of the American Chemical Society* **2000,** *122*, 3688.

14. Krapchetov, D. A.; Ma, H.; Jen, A. K. Y.; Fischer, D. A.; Loo, Y.-L. *Langmuir* **2005,** *21*, 5887.

15. L.G. Wade, J., *Organic Chemistry*. Prentice-Hall, Inc.: Upper Saddle River, New Jersey, 1999, p 649.

16. Niklewski, A.; Azzam, W.; Strunskus, T.; Fischer, R. A.; Woell, C. *Langmuir* **2004,** *20*, 8620.

17. Kushmerick, J. G.; Holt, D. B.; Yang, J. C.; Naciri, J.; Moore, M. H.; Shashidhar, R. *Physical Review Letters* **2002,** *89*, 086802/1.

18. Lau, K. H. A.; Huang, C.; Yakovlev, N.; Chen, Z. K.; O'Shea, S. J. *Langmuir* **2006,** *22*, 2968.

19. Krapchetov, D. A.; Ma, H.; Jen, A. K. Y.; Fischer, D. A.; Loo, Y.-L. *Langmuir* **2008,** *24*, 851.

20. de Boer, B.; Frank, M. M.; Chabal, Y. J.; Jiang, W.; Garfunkel, E.; Bao, Z. *Langmuir* **2004,** *20*, 1539.

21. Dannenberger, O.; Buck, M.; Grunze, M. *Journal of Physical Chemistry B* **1999,** *103*, 2202.

22. Jun, Y.; Zhu, X. Y.; Hsu, J. W. P. *Langmuir* **2006,** *22*, 3627.

Chapter 5: Deposition of Top Metal Electrode and Characterization of the Molecule-Electrode Interface in Model Conjugated Assemblies on GaAs

Nano-scale electronics where single molecules or molecular assemblies comprise the electrically-active component[1] require the ability to reliably 'wire' the molecules. One of the common approaches of wiring the molecules involves covalently attaching the molecules to a substrate which can then act as the electrode for self assembly, followed by placing a second electrode, usually Au, in contact with the molecular assembly surface. To-date, several approaches of depositing the top electrode on molecular assembly surfaces have been developed.[2-5] One of these approaches involves evaporating a metal layer directly onto a molecular assembly surface.[6-8] The metal source and the assembly surface are placed within a direct line of sight relative to each other during evaporation.[6-8] Direct metal evaporation, however, often results in the evaporated metal penetrating through the molecular assembly to the substrate surface,[6,9,10] resulting in electrical shorts between the evaporated top electrode and the substrate. To reduce the occurrence of metal penetration, an indirect evaporation approach has been developed.[10,11] In indirect evaporation, the metal is evaporated onto the molecular assembly surface by placing the metal source and the molecular assembly out of direct line of sight relative to each other. Such placement minimizes the impingement of direct metal flux on the molecular assembly surface. Although indirect evaporation helps to reduce the occurrence of metal atom penetration through the molecular assembly, electrical shorts still occur because metal atoms reach the substrate through pinholes in the molecular assembly.[11-13]

It is also possible to place a pre-fabricated metal film in contact with the molecular assembly surface. The lift-off, float-on (LOFO)[14] process is one such example. In this approach, a Au film is first evaporated onto a sacrificial low-adhesion surface, such as octadecyltrichlorosilane-treated glass.[14] The evaporated Au film then delaminates from the sacrificial low-adhesion surface when placed in a solvent. Provided that the surface tension of the solvent is sufficiently high,[14] the detached Au film floats on the solvent surface. The Au leaf is then lifted from the solvent surface onto a molecular assembly adsorbed on a separate substrate. A gentle molecule-Au contact results as the solvent evaporates from the interface between the Au film and the molecular assembly surface.[14] The quality of the molecule-Au contact, however, is difficult to control because the flotation of the Au film often results in wrinkles.[3,14] The polymer-assisted lift-off (PALO) process[3] takes the idea of float-on contacts a step further. Largely similar to LOFO, PALO involves spin-casting a polymer support layer onto the evaporated metal film so that when the metal delaminates from the sacrificial low-adhesion surface, it is supported by the polymer film. The polymer holds the Au film intact during flotation and allows wrinkle-free transfer.[3] While continuous, wrinkle-free Au films can be transferred onto assembly surfaces using this modified float-on approach, the placement of the Au film remains difficult to control.

Another common approach for transferring metal electrodes onto molecular assembly surfaces is nano-transfer printing, nTP.[15] Described in detail in Chapter 2, nTP involves evaporating a layer of Au 5-20 nm thick onto a sacrificial elastomeric poly(dimethylsiloxane) (PDMS) stamp. The elastomeric stamp is then brought in contact with a dithiol molecular assembly separately formed on a GaAs substrate. The intimate contact between the stamp and the substrate allows the free thiol end groups to covalently bond to the metal that is on the stamp surface.[16] When the stamp is removed, the Au layer remains on the molecular assembly surface.

Regardless of the approach that is used to deposit the top metal electrode, the formation of covalent bonds between the functional groups at the molecular assembly surface and the top metal electrode is often sought.[2,17-19] The formation of covalent bonds between the molecular assembly surface and the metal electrode is expected to facilitate reliable electrical contact.[18,19] The determination of whether these bonds actually form, however, has proven to be challenging. The fact that the molecule-metal interface is buried under the metal layer presents clear spectroscopic challenges. Given the difficulty of direct analysis of the buried molecule-metal interface, the nature of the this interface is often assumed[20] or speculated indirectly.[21] For example, in the case of GaAs—dithiol—Au junctions, the Scotch tape test[22] is a dominant, albeit indirect, method used to speculate the nature of the top dithiol-Au interface. In this test, Scotch tape is attached to the top Au electrode and then pulled off. One surmises the presence of covalent S-Au bonds at the dithiol-Au interface if the Au electrode remains on the assembly surface after the Scotch tape is pulled off.

Several attempts to verify the presence of S-Au bonds directly through *in-situ* spectroscopic analysis have been reported. For example, Ohgi et. al.,[9] used x-ray photoelectron spectroscopy (XPS) to observe the interaction between the thiol groups located at the surface of 1,8-octanedithiol molecular assemblies on Au substrates and small clusters of Au formed as a result of direct evaporation on the molecular assembly surface. By examining the 1,8-octanedithiol molecular assemblies on Au prior to Au cluster deposition, the researchers were able to observe evidence for S-Au bonds at the molecule-substrate interface. Upon evaporating Au clusters onto the 1,8-octanedithiol molecular assembly surfaces, broadening of the XPS signal associated with the S-Au interaction was observed. This XPS signal broadening was attributed to the presence of S-Au bonds between the thiol groups located at the 1,8-octanedithiol molecular assembly surface and the evaporated Au clusters. Because Au was also used as the substrate, the signal associated with S-Au bonds at the molecule-substrate interface could not be easily decoupled from that associated with S-Au bonds at the top molecule-Au interface.

Inspired by the experiments of Ohgi et. al.,[9] we extended this direct spectroscopic characterization to examine the buried dithiol-Au interface in molecular assemblies on GaAs. Specifically, we first formed dithiol molecular assemblies on GaAs. We then deposited very thin ≈15Å Au by nTP to simulate the top Au electrodes that are generally much thicker (10-15 nm) in the GaAs—dithiol—Au junctions. Because the bottom substrate is GaAs and not Au, we were able to more easily decouple the signal associated with S-GaAs compared to S-Au. We examined the samples using grazing-incidence XPS at a grazing angle of 15° relative to the surface. This configuration was used to enhance the sensitivity of the sample surface. The Au thickness of ≈15Å was chosen so that we could obtain XPS signal through printed Au. We focused on GaAs as the substrate for our spectroscopic studies because the S-GaAs bonds are energetically different from the S-Au bonds.[23,24] Specifically, the S-GaAs bonds are commonly observed at the S 2p binding energy of ≈162.6 eV in molecular assemblies of both saturated[25,26] and conjugated[27,28] thiols. The S-Au bonds are observed at the S 2p binding energy of ≈161.9-162.1 eV[29-31] for both saturated and conjugated assemblies. Additionally, unbound thiol, thiolate or thioacetyl groups are observed at the S 2p binding energy of ≈163.5-164 eV in molecular assemblies of both saturated[32-36] and conjugated[28,37-39] molecules.

We first studied 1,8-octanedithiol assembled on both GaAs and Au substrates. Figure 5.1a contains an XPS spectrum of the S 2p region of 1,8-octanedithiol assembled on GaAs. The spectrum can be fitted with two S 2p doublets, located at 162.8-162.9 eV and 163.8 eV (see fitting parameters detailed in Chapter 2). Per literature,[25-28,37,38] we assigned these doublets to S-GaAs bonds at the dithiol-GaAs interface and unbound thiol groups at the assembly surface, respectively. The S 2p XPS spectrum in Figure 5.1a also contains the Ga 3s peak at ≈160.5 eV. Generally, the intensity of the Ga 3s peak overwhelms the nearby S 2p signal intensity.[25,40] The Ga 3s intensity in our XPS spectra is minimized because of increased surface sensitivity of the grazing x-ray incidence configuration we employed, allowing the observation of the nearby S 2p signal. The integrated intensity of the S-GaAs signal accounts for ≈28% of the total S 2p intensity, with the remaining S 2p intensity attributed to the unbound thiol groups. Figure 5.1b contains an XPS spectrum of the S 2p region of 1,8-octanedithiol assembled on Au. The spectrum was fitted using two S 2p doublets, located at 162.1 eV and 164 eV. We attributed these doublets to the S-Au bonds at the dithiol-Au interface and the unbound S at the assembly surface, respectively.[29-32] The combination of the spectra in Figures 5.1a and b allowed us to verify the binding energy positions of each of the three sulfur environments likely to occur after Au transfer onto a 1,8-octanedithiol molecular assembly on GaAs: 162.1 eV (S-Au bond), 162.9 eV (S-GaAs bond), and 164 eV (unbound thiol).

We then examined the XPS spectrum of the S 2p region of 1,8-octanedithiol assembled on GaAs after ≈15Å Au was deposited using nTP on the molecular assembly surface. The S 2p XPS spectrum is shown in Figure 5.1c, with the corresponding Au 4f XPS spectrum provided in the inset. The Au 4f XPS signal originates from the deposited Au, and its integrated intensity is proportional to how much Au was transferred onto the assembly surface. The S 2p spectrum in Figure 5.1c was fitted with three doublets. Specifically, we fitted the spectrum with the doublet associated with S-GaAs bonds at the dithiol-GaAs interface (≈162.9 eV), the doublet associated with the unbound S at the assembly surface (≈164 eV), and a third doublet associated with S-Au bonds (≈162 eV). The integrated intensity of the S-GaAs signal derived from our fit accounts for ≈26% of the total S 2p intensity, with the rest of S 2p signal attributed to unbound S (≈40%) and S-Au (≈34%). The S-GaAs intensity accounts for a similar fraction of the total S 2p signal before (≈28%, Figure 5.1a) and after (≈26%, Figure 5.1c) Au deposition. Since the S-GaAs relative intensity is unchanged, and the relative intensity attributed to the unbound thiol groups before Au deposition decreased, we deduced that a fraction of the unbound thiol groups at the molecular assembly surface bonded with the deposited Au.

We calculated the fraction of the unbound thiol groups that have formed S-Au bonds with the deposited Au, or the S-Au conversion, as:

$$\text{S}-\text{Au conversion} = \frac{I_{S-Au}}{I_{S-Au} + I_{S-unbound}} \qquad \text{Equation (5.1)}$$

In Equation (5.1), $I_{S\text{-}Au}$ is the integrated intensity of the S-Au signal at ≈162 eV after Au deposition; $I_{S\text{-}unbound}$ is the integrated intensity of the unbound S signal at ≈164 eV before Au deposition. Applying Equation (5.1) to the integrated intensities extracted from Figure 5.1c shows that, out of ≈75% S 2p integrated intensity attributed to unbound thiols before printing Au, a fraction of roughly 34/(40+34) ≈ 45% appears to have formed S-Au bonds after Au deposition. The observation that this fraction is not 100% can be explained by the reduced coverage of the deposited Au. Specifically, we found the ≈15Å Au deposited on the 1,8-octanedithiol assembly surface using nTP is discontinuous. In fact, we estimated that the coverage is only 40-45% by scanning electron microscopy. If normalized by the coverage of deposited Au, the fraction of the unbound thiol groups that have formed S-Au bonds with the deposited Au, is ≈100%. Our results suggest that we are able to directly observe the S-Au bonds formed between the unbound thiol groups of 1,8-octanedithiol assembled on GaAs and Au deposited by nTP onto the assembly surface.

Having established the ability to observe S-Au bonds at the buried dithiol-Au interface prepared by transferring thin Au onto 1,8-octanedithiol assembled on GaAs, we characterized a comparable interface prepared by transferring thin Au onto molecular assemblies of QPDT on GaAs. QPDT was assembled on GaAs from a cosolvent with EF = 0.75 using 10 mM NH_4OH. As shown in Chapter 4, these processing conditions result in a largely acetyl-terminated molecular assembly, with an ensemble-average QPDT backbone tilt of 20±3° away from the substrate normal. We focused on these preferentially upright molecular assemblies in an effort to maximize the amount of functional groups potentially available for S-Au bond formation at the assembly surface. We deposited Au on the assembly surfaces using our ‘wet’ nTP approach in dichloroethane (DCE), as described in Chapter 2.

Figure 5.2a contains an XPS spectrum of the S 2p region of QPDT assembled on GaAs. The spectrum was fitted with two S 2p doublets, located at ≈162.8 and ≈164 eV. Similar to the 1,8-octanedithiol molecular assemblies, we attributed the doublet at ≈162.8 eV to S-GaAs bonds at the QPDT-GaAs interface. The doublet at ≈164 eV was attributed to the unbound thiolate/thioacetyl groups at the QPDT molecular assembly surface.[27,28] Additionally, the signal associated with the Ga 3s is located at ≈160.5 eV. The integrated intensity of the S-GaAs signal in the S 2p spectrum in Figure 5.2a accounts for ≈19% of the total S 2p intensity, with the remaining ≈81% from the unbound S at the molecular assembly surface. The higher intensity of the unbound S relative to the S-GaAs is attributed to the attenuation of the S-GaAs signal by the QPDT assembly and to the increased surface sensitivity of the grazing x-ray incidence configuration.

Figure 5.2b contains an XPS spectrum of the S 2p region of QPDT assembled on GaAs after the deposition of ≈15Å Au on the molecular assembly surface by 'wet' nTP. The corresponding Au 4f XPS spectrum is provided in the inset. We fitted the S 2p spectrum using 3 S 2p doublets. The doublets at ≈162.8 eV and ≈164 eV were assigned to S-GaAs bonds at the QPDT-GaAs interface and the unbound thiolates/thioacetyls at the assembly surface, similar to those observed for the 'bare' QPDT molecular assembly on GaAs (Figure 5.2a). The binding energy of the third S 2p doublet, ≈162 eV, corresponds to that of S-Au bonds observed in molecular assemblies of conjugated thiols on Au substrates.[29,41] This intensity must therefore stem from the formation of S-Au bonds at the buried QPDT-Au interface. The integrated intensity of the S-GaAs signal derived from our fit accounts for ≈22% of the total S 2p intensity, with the rest of S 2p signal attributed to unbound thiolates/thioacetyls (≈43%) and S-Au (≈35%). The fact that the S-GaAs intensity accounts for a similar fraction of the total S 2p signal before (≈19%, Figure 5.2a) and after (≈22%, Figure 5.2b) Au deposition is consistent with some of the unbound functional groups at the molecular assembly surface bonding with the deposited Au, while the QPDT-GaAs interface remains unchanged.

Out of ≈81% S 2p integrated intensity attributed to unbound S before printing Au, roughly 35/(43+35) ≈ 44% reacted with the printed Au to form S-Au bonds. We estimated the coverage of the Au transferred on the QPDT assembly surface to be 35-45% using scanning electron microscopy. Accordingly, if normalized by the coverage of deposited Au, the fraction of the surface groups that appear to form S-Au bonds with deposited Au is ≈100%. Our results suggest that, despite a largely acetyl-terminated surface, S-Au bonds form when Au is deposited onto QPDT assembled on GaAs using 'wet' nTP in DCE.

Because Au was transferred onto the QPDT molecular assembly surfaces in DCE rather than at ambient conditions, we examined whether the brief immersion of the samples in DCE affected the integrity of the QPDT molecular assemblies. Figure 5.3a contains an XPS spectrum of the S 2p region of QPDT assembled on GaAs after a brief immersion in DCE. The S 2p spectrum closely resembles that of the QPDT molecular assembly before immersion in DCE (Figure 5.2a). In fact, the integrated S-GaAs intensity accounts for ≈20% of the total S 2p intensity, compared to the corresponding case of ≈19% before immersion in DCE. The comparable intensities of the S-GaAs signal and the unbound thiolate/thioacetyl signal in QPDT molecular assemblies before and after DCE immersion suggest that exposure to DCE does not induce any changes in these molecular assemblies. We also examined the C 1s region of QPDT assembled on GaAs before (open circles) and after (filled circles) immersion in DCE, shown in Figure 5.3b. The C 1s spectra of the QPDT molecular assemblies on GaAs are comparable before (open circles) and after (filled circles) DCE immersion, suggesting that the corresponding carbon surface coverages remained unaffected by the immersion. Similarly, the Ga 2p spectra of QPDT molecular assemblies on GaAs before and after immersion in DCE (Figure 5.3c) do no exhibit detectable differences. This observation suggests constant substrate Ga 2p signal attenuation and therefore constant QPDT surface coverage before and after DCE immersion. Finally, there is negligible intensity in the Cl 2p XPS signal (inset in Figure 5.3c) before and after DCE immersion, indicating no detectable Cl contamination of the QPDT molecular assembly. Based on the combination of observations from Figure 5.3, we concluded that the brief immersion of QPDT molecular assemblies on GaAs in DCE during ‘wet’ nTP did not compromise the integrity of the QPDT molecular assemblies.

To determine whether the presence of DCE is necessary for S-Au bond formation between the largely acetyl-terminated QPDT molecular assembly surfaces and the transferred Au, we examined samples prepared by depositing thin Au onto QPDT assembled on GaAs using nTP at ambient conditions. We discovered drastic differences between the samples where Au was transferred onto QPDT assembled on GaAs using 'wet' nTP in DCE and those whose Au was deposited using nTP at ambient conditions. Specifically, we found significant sample-to-sample variations in XPS spectra collected from QPDT molecular assemblies on GaAs after depositing Au on the assembly surfaces using nTP at ambient conditions. Figures 5.4a and b contain S 2p XPS spectra of samples prepared on different days with nominally the same protocol wherein thin Au was deposited on QPDT assemblies on GaAs using nTP at ambient conditions. The S-Au conversions derived from these spectra using Equation (5.1) vary significantly from ≈7% (Figure 5.4a) to ≈25% (Figure 5.4b). The intensities of the corresponding Au 4f XPS signals shown in the insets also vary tremendously, indicating large variations in how much Au actually transferred from the stamp on the assembly surface. In fact, we estimated the coverage of transferred Au to be ≈13% and ≈23% for the samples whose XPS spectra are shown in Figures 5.4a and b, respectively. Normalizing the S-Au conversions by the coverages of the deposited Au reveals that, although relatively little Au was transferred on the QPDT assemblies by nTP at ambient conditions, the fraction of the surface groups that formed S-Au bonds with the deposited Au is still ≈100%. Given that the QPDT assembly surface is largely thioacetyl-terminated, the formation of S-Au bonds must proceed via surface-catalyzed cleaving of the acetyl groups.[42] This reaction is likely to be sensitive to processing conditions. While S-Au bond formation in solution takes place within seconds,[43,44] we suspect that this process may be prolonged in air. As such, operator variation in stamp liftoff speed[45] and stamp contact duration[46] may impact the formation of S-Au bonds and the area coverage of the Au transfer on the assembly surface. Additionally, day-to-day variations of ambient conditions, such as humidity and temperature, may also impact the formation of S-Au bonds at the top QPDT-Au interface. When Au is deposited onto a highly-reactive thiol-terminated assembly surface, however, such as 1,8-octanedithiol, processing conditions matter less, as evinced in our XPS results in Figure 5.1.

In this Chapter, we demonstrated a direct spectroscopic approach to test for the presence of the S-Au bonds at the buried dithiol-Au interface in samples prepared by depositing Au on molecular assembly surfaces of dithiols adsorbed on GaAs. We showed that the conditions under which Au is deposited onto the molecular assembly surface can affect the nature of the dithiol-Au interaction. Specifically, the deposition of Au on the largely acetyl-terminated QPDT assemblies on GaAs using ‘wet’ nTP results in reproducible formation of S-Au bonds at the QPDT-Au interface. In contrast, the deposition of Au on these assemblies using conventional nTP at ambient conditions resulted in reduced and irreproducible formation of S-Au bonds at the QPDT-Au interface.

FIGURES

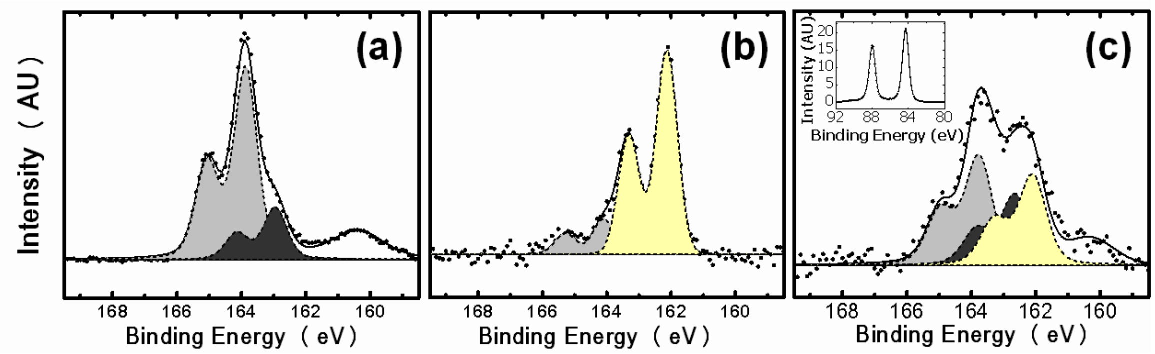

Figure 5.1. XPS spectra of the S 2p region of 1,8-octanedithiol molecular assemblies on (a) GaAs and (b) on Au; (c) contains the S 2p spectrum of 1,8-octanedithiol assembled on GaAs after the deposition of ≈15Å Au using nTP at ambient conditions. Inset in (c) contains the Au 4f spectrum of the corresponding sample. The S 2p spectra are fitted with individual S 2p doublets: light gray, unbound thiol groups at the assembly surface; dark gray, S-GaAs bonds at the dithiol-GaAs interface; yellow, S-Au bonds formed at the dithiol-Au interface.

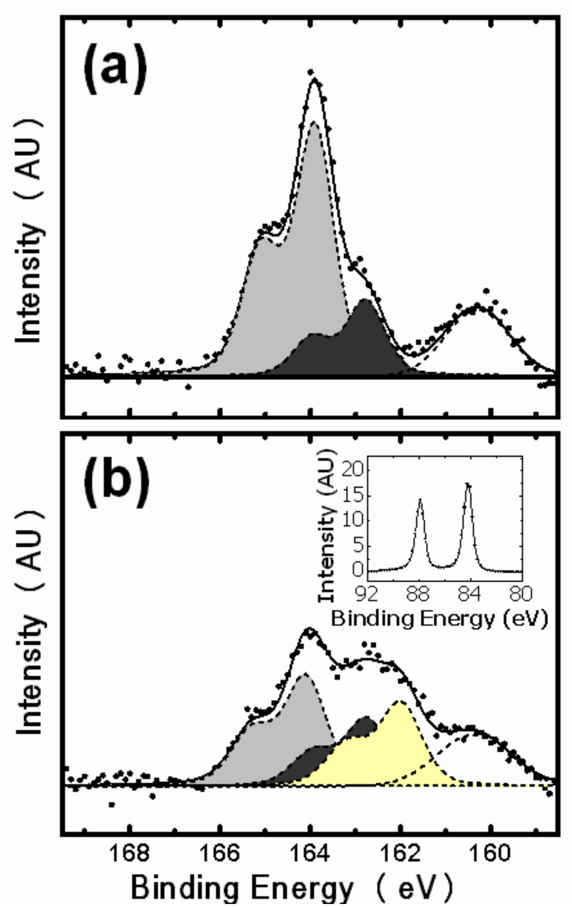

Figure 5.2. XPS spectra of the S 2p region of QPDT molecular assembly on GaAs (a) before and (b) after the deposition of ≈15Å Au using 'wet' nTP in DCE. Inset in (b) contains the Au 4f spectrum of the corresponding sample. The S 2p spectra are fitted with individual S 2p doublets: light gray, unbound thiolate/thioacetyl groups at the assembly surface; dark gray, S-GaAs bonds at the dithiol-GaAs interface; yellow, S-Au bonds formed at the dithiol-Au interface.

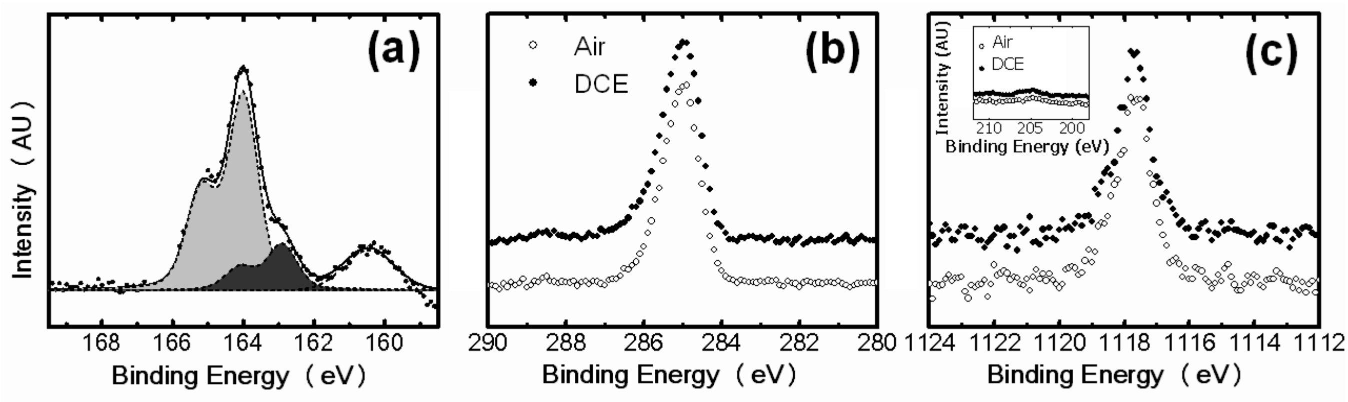

Figure 5.3. XPS spectra of (a) the S 2p region of QPDT molecular assembly on GaAs after immersion in DCE; (b) C 1s and (c) Ga 2p regions before and after immersion in DCE. Inset in (c) contains Cl 2p spectra of the QPDT assembly before and after immersion in DCE. Spectra in (b) and (c) are vertically offset for clarity. The S 2p spectrum is fitted with individual S 2p doublets: light gray, unbound thiolate/thioacetyl groups at the assembly surface; dark gray, S-GaAs bonds at the dithiol-GaAs interface.

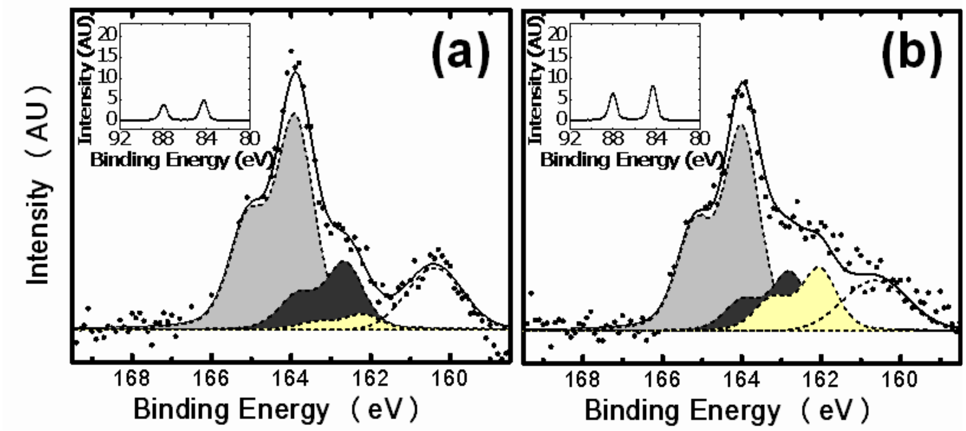

Figure 5.4. XPS spectra of the S 2p region of QPDT molecular assemblies on GaAs prepared on different days after the deposition of ≈15Å Au using nTP at ambient conditions. The significant sample-to-sample variations are illustrated by different S-Au conversions of ≈7% and ≈25% calculated for the specimens in (a) and (b). Insets contain XPS Au 4f spectra of the corresponding samples. The S 2p spectra are fitted with individual S 2p doublets: light gray, unbound thiolate/thioacetyl groups at the assembly surface; dark gray, S-GaAs bonds at the dithiol-GaAs interface; yellow, S-Au bonds formed at the dithiol-Au interface.

REFERENCES

1. Aviram, A.; Ratner, M. A. *Chemical Physics Letters* **1974,** *29*, 277.

2. Akkerman Hylke, B.; Naber Ronald, C. G.; Jongbloed, B.; van Hal Paul, A.; Blom Paul, W. M.; de Leeuw Dago, M.; de Boer, B. *Proceedings of the National Academy of Sciences of the United States of America* **2007,** *104*, 11161.

3. Shimizu, K. T.; Fabbri, J. D.; Jelincic, J. J.; Melosh, N. A. *Advanced Materials* **2006,** *18*, 1499.

4. Akkerman Hylke, B.; Blom Paul, W. M.; de Leeuw Dago, M.; de Boer, B. *Nature* **2006,** *441*, 69.

5. Nesher, G.; Shpaisman, H.; Cahen, D. *Journal of the American Chemical Society* **2007,** *129*, 734.

6. Ohgi, T.; Sheng, H. Y.; Nejoh, H. *Applied Surface Science* **1998,** *130-132*, 919.

7. de Boer, B.; Frank, M. M.; Chabal, Y. J.; Jiang, W.; Garfunkel, E.; Bao, Z. *Langmuir* **2004,** *20*, 1539.

8. Guerin, D.; Merckling, C.; Lenfant, S.; Wallart, X.; Pleutin, S.; Vuillaume, D. *Journal of Physical Chemistry C* **2007,** *111*, 7947.

9. Ohgi, T.; Sheng, H. Y.; Dong, Z. C.; Nejoh, H.; Fujita, D. *Applied Physics Letters* **2001,** *79*, 2453.

10. Walker, A. V.; Tighe, T. B.; Cabarcos, O. M.; Reinard, M. D.; Haynie, B. C.; Uppili, S.; Winograd, N.; Allara, D. L. *Journal of the American Chemical Society* **2004,** *126*, 3954.

11. Haick, H.; Ghabboun, J.; Niitsoo, O.; Cohen, H.; Cahen, D.; Vilan, A.; Hwang, J.; Wan, A.; Amy, F.; Kahn, A. *Journal of Physical Chemistry B* **2005,** *109*, 9622.

12. Haick, H.; Ambrico, M.; Ghabboun, J.; Ligonzo, T.; Cahen, D. *Physical Chemistry Chemical Physics* **2004,** *6*, 4538.

13. Haick, H.; Ghabboun, J.; Cahen, D. *Applied Physics Letters* **2005,** *86*, 042113/1.

14. Vilan, A.; Cahen, D. *Advanced Functional Materials* **2002,** *12*, 795.

15. Loo, Y.-L.; Willett, R. L.; Baldwin, K. W.; Rogers, J. A. *Applied Physics Letters* **2002,** *81*, 562.

16. Hsu, J. W. P.; Loo, Y. L.; Lang, D. V.; Rogers, J. A. *Journal of Vacuum Science & Technology B* **2003,** *21*, 1928.

17. Hipps, K. W. *Science* **2001,** *294*, 536.

18. Zhou, C.; Deshpande, M. R.; Reed, M. A.; Jones, K., II; Tour, J. M. *Applied Physics Letters* **1997,** *71*, 611.

19. Schumm, J. S.; Pearson, D. L.; Jones, L., II; Hara, R.; Tour, J. M. *Nanotechnology* **1996,** *7*, 430.

20. Salomon, A.; Boecking, T.; Gooding, J. J.; Cahen, D. *Nano Letters* **2006,** *6*, 2873.

21. Kushmerick, J. G.; Holt, D. B.; Yang, J. C.; Naciri, J.; Moore, M. H.; Shashidhar, R. *Physical Review Letters* **2002,** *89*, 086802/1.

22. Loo, Y.-L.; Lang, D. V.; Rogers, J. A.; Hsu, J. W. P. *Nano Letters* **2003,** *3*, 913.

23. Camillone, N.; Khan, K. A.; Osgood, R. M. *Surface Science* **2000,** *453*, 83.

24. Ulman, A. *Chemical Reviews* **1996,** *96*, 1533.

25. McGuiness, C. L.; Shaporenko, A.; Mars, C. K.; Uppili, S.; Zharnikov, M.; Allara, D. L. *Journal of the American Chemical Society* **2006,** *128*, 5231.

26. McGuiness, C. L.; Shaporenko, A.; Zharnikov, M.; Walker, A. V.; Allara, D. L. *Journal of Physical Chemistry C* **2007,** *111*, 4226.

27. Shaporenko, A.; Adlkofer, K.; Johansson, L. S. O.; Tanaka, M.; Zharnikov, M. *Langmuir* **2003,** *19*, 4992.

28. Shaporenko, A.; Adlkofer, K.; Johansson, L. S. O.; Ulman, A.; Grunze, M.; Tanaka, M.; Zharnikov, M. *Journal of Physical Chemistry B* **2004,** *108*, 17964.

29. Heister, K.; Zharnikov, M.; Grunze, M.; Johansson, L. S. O. *Journal of Physical Chemistry B* **2001,** *105*, 4058.

30. Laibinis, P. E.; Whitesides, G. M.; Allara, D. L.; Tao, Y. T.; Parikh, A. N.; Nuzzo, R. G. *Journal of the American Chemical Society* **1991,** *113*, 7152.

31. Zharnikov, M.; Grunze, M. *Journal of Physics: Condensed Matter* **2001,** *13*, 11333.

32. Castner, D. G.; Hinds, K.; Grainger, D. W. *Langmuir* **1996,** *12*, 5083.

33. Esplandiu, M. J.; Noeske, P. L. M. *Applied Surface Science* **2002,** *199*, 166.

34. Deng, W.; Yang, L.; Fujita, D.; Nejoh, H.; Bai, C. *Applied Physics A* **2000,** *71*, 639.

35. Rieley, H.; Kendall, G. K.; Zemicael, F. W.; Smith, T. L.; Yang, S. *Langmuir* **1998,** *14*, 5147.

36. Xu, L.; Liao, J.; Huang, L.; Gu, N.; Zhang, H.; Liu, J. *Applied Surface Science* **2003,** *211*, 184.

37. Tai, Y.; Shaporenko, A.; Rong, H. T.; Buck, M.; Eck, W.; Grunze, M.; Zharnikov, M. *Journal of Physical Chemistry B* **2004,** *108*, 16806.

38. Azzam, W.; Wehner, B. I.; Fischer, R. A.; Terfort, A.; Woell, C. *Langmuir* **2002,** *18*, 7766.

39. Tour, J. M.; Jones, L.; Pearson, D. L.; Lamba, J. J. S.; Burgin, T. P.; Whitesides, G. M.; Allara, D. L.; Parikh, A. N.; Atre, S. *Journal of the American Chemical Society* **1995,** *117*, 9529.

40. Moulder, J. F.; Stickle, W. E.; Sobol, P. E.; Bomben, K. D., *Handbook of X-ray Photoelectron Spectroscopy*. Perkin-Elmer Corp.: Eden Prairie, MN: 1992, p 60.

41. Shaporenko, A.; Roessler, K.; Lang, H.; Zharnikov, M. *Journal of Physical Chemistry B* **2006,** *110*, 24621.

42. Lau, K. H. A.; Huang, C.; Yakovlev, N.; Chen, Z. K.; O'Shea, S. J. *Langmuir* **2006,** *22*, 2968.

43. Bain, C. D.; Troughton, E. B.; Tao, Y. T.; Evall, J.; Whitesides, G. M.; Nuzzo, R. G. *Journal of the American Chemical Society* **1989,** *111*, 321.

44. Bensebaa, F.; Voicu, R.; Huron, L.; Ellis, T. H.; Kruus, E. *Langmuir* **1997,** *13*, 5335.

45. Feng, X.; Meitl, M. A.; Bowen, A. M.; Huang, Y.; Nuzzo, R. G.; Rogers, J. A. *Langmuir* **2007,** *23*, 12555.

46. Hur, S.-H.; Khang, D.-Y.; Kocabas, C.; Rogers, J. A. *Applied Physics Letters* **2004,** *85*, 5730.

Chapter 6: The Effects of Assembly Structure on Charge Transport Across BPDT, TPDT, and QPDT Assemblies on GaAs

The idea of molecular electronics[1,2] has motivated strong research interest in understanding the electrical response of molecules. To this end, various methods of making macroscopic and local electrical contacts to molecular assemblies have been developed.[2-8] The electrical conduction of molecular assemblies is commonly measured in a two-electrode architecture. In this architecture, the molecular assemblies are first formed on a substrate that acts as the bottom electrode, and then the molecules are 'wired' to a top electrode. There are two distinct approaches to 'wiring' the molecules. One involves making direct electrical contact to the molecules with the probe of interest, eliminating the use of a separate top contact. The other approach involves depositing a top electrode, and then making an ohmic contact to the pre-deposited top electrode.

Examples of the electrode-less approach include scanning tunneling microscopy (STM),[9] conductive atomic force microscopy (CAFM),[7] and hanging-drop mercury (Hg) electrode.[10] STM employs an atomically-sharp tip (schematically illustrated in Figure 6.1a) which hovers in proximity to the target surface guided by a piezo measuring the tunneling current between the tip and the target surface.[7,11,12] While STM allows the measuring of tunneling currents with atomic resolution,[9] its use is intrinsically limited to measurements on conductive substrates that are atomically-flat.[13-15] CAFM involves making direct microscopic contact to single molecules or a small number of molecules in molecular assemblies using a conductive tip[3,16] several nanometers in size (schematically illustrated in Figure 6.1b). CAFM has been used successfully for molecular conductance studies of assemblies on a variety of coinage metal substrates.[16,17] Because a physical contact is made to the molecules, CAFM measurements are extremely sensitive to both the force applied to the tip[3,18,19] and the topographical details of the substrate surface.[16] These constraints have limited the use of CAFM to specially-prepared metal substrates containing atomically-flat terraces. The hanging-drop Hg electrode[10,20] setup involves making direct macroscopic contact to a molecular assembly surface using a drop of Hg, as schematically illustrated in Figure 1.2. The very high surface tension of the liquid metal limits Hg penetration into pinhole defects, precluding electrical shorts.[10] As a result, the hanging-drop Hg setup reproducibly measures electrical response of molecular assemblies.[10] This technique has been successfully used to measure the electrical conduction of alkyl-based molecular assemblies on both metal and semiconductor substrates.[10,20-23]

In the second approach of 'wiring' the molecules, where a separate top contact is used, common techniques for top electrode deposition are described in Chapter 5 and include evaporation,[24-28] float-on,[29,30] and nano-transfer printing (nTP).[31] Regardless of the deposition technique, the pre-deposited top metal electrode is then contacted using a CAFM[18,19,32] tip or a macroscopic tungsten probe,[31,33-36] schematically illustrated in Figures 6.2a and b, respectively. Considering that CAFM measurements are very sensitive to the contact force of the tip and the surface topography,[19,37] this technique is difficult to implement on pre-deposited top electrodes. The use of macroscopic tungsten probes has been reported for the electrical studies of assembly-based GaAs—1,8-octanedithiol—Au junctions.[31,33-36] In this setup, a needle-like tungsten probe is brought in contact with the pre-deposited Au electrode manually. Generally, in all measurement techniques, besides single-molecule STM, the measured electrical response reflects the ensemble-average response of many molecules.

Having developed the ability to assemble QPDT, TPDT, and BPDT with control on both Au and GaAs substrates, we measured the electrical response of the conjugated assemblies using both of the routes to wire the molecules. In one case, we made electrical contact directly to the molecular assembly surfaces. In another case, we deposited top Au electrodes to make GaAs—molecule—Au junctions using nTP to minimize pinhole electrical shorts. We focused on GaAs as the substrate for our electrical studies because GaAs does not cold-weld with Au, thereby reducing the possibility of electrical shorts.[38]

Making reliable electrical contact to both the molecular assemblies and the GaAs—molecule—Au junctions was challenging because the roughness of our samples (0.3 nm and above) presented difficulties for STM and CAFM measurements. While the hanging-drop Hg setup is often used to make soft electrical contact to molecular assembly surfaces directly, it cannot be used to make contact with Au because Au tends to rapidly amalgamate with Hg.[39-41] As for the tungsten probes, we found it very difficult to achieve a well-controlled manual surface approach to avoid puncture.

To measure the electrical response of the n-phenyldithiol assemblies on GaAs, we developed an extension to the hanging-drop Hg setup (Figure 1.2). Specifically, we used galinstan instead of Hg as the soft contact material. Galinstan is a eutectic alloy of gallium, indium, and tin that is used increasingly in place of Hg in medical thermometers.[42] Galinstan does not pose any health hazards because of its negligible vapor pressure and is a superior electrical conductor featuring an electrical resistivity (435 nΩ m) that is roughly half of that of liquid Hg (≈980 nΩ m).[43] A recent report demonstrated galinstan to be a suitable alternative to Hg for voltammetric analysis in solution.[44] We constructed a simple in-house setup for making hanging galinstan drops reproducibly, described in detail in Chapter 2. Galinstan drops were formed using a syringe fitted with a goniometer needle with a diameter of 250 μm. This setup was wired to the probe station and bias was applied to the hanging galinstan drop as it was brought into contact with the target surface, as illustrated in Figure 2.11.

To examine the suitability of galinstan as a soft contact material for the characterization of charge transport across molecular assemblies, we reproduced reported studies of electrical conduction of a common alkylthiol assembly on GaAs.[10,20] Referring to studies of GaAs—1-hexadecanethiol—Hg junctions where mercury was used as the soft electrode material,[10,20] we used galinstan to make soft contact directly to 1-hexadecanethiol assembled on GaAs. We measured the thickness of the 1-hexadecanethiol molecular assembly on GaAs to be 20±1Å using ellipsometry. This thickness is consistent with an organized molecular assembly where the molecular backbones are oriented preferentially upright.[10] This thickness is also in close agreement with the reported thickness for 1-hexadecanethiol molecular assembly on GaAs (21Å),[10] suggesting that the final assemblies have comparable structures. We thus expected the electrical response of these assemblies to be similar to that reported by Nesher et. al.[10] The measured currents were normalized by the contact area of the galinstan droplet to obtain the current density, ***J***. To obtain the contact area, we imaged every soft contact during electrical data acquisition.

The absolute current density as a function of bias voltage applied to the galinstan drop measured by making direct soft contact to 1-hexadecanethiol molecular assemblies on GaAs are presented in Figure 6.3. The standard deviations (based on 23 separate measurements) are included. The general shape of the J-V curve is typical of that of alkylthiol junctions.[10,20] A higher absolute current density at positive bias (V>0) compared to that at negative bias (V<0) suggests that the flow of electrons from the n-type GaAs substrate through the molecular assembly to galinstan is easier than the reverse.[45] The current densities we measured for 1-hexadecanethiol assembled on GaAs at the lowest (-0.5 V) and the highest (0.5 V) bias applied to the galinstan drop are $1.1 \times 10^{-6} \pm 0.7 \times 10^{-6}$ (A/cm^2) and $5 \times 10^{-6} \pm 4 \times 10^{-6}$ (A/cm^2), respectively. These current densities are comparable to the reported values of ≈ $1x10^{-6}$ and ≈ $9x10^{-6}$ (A/cm^2) measured at -0.5 and 0.5 V, respectively, using the Hg setup.[10] The similarity in both the measured thickness of 1-hexadecanethiol molecular assembly and the resulting current densities using our galinstan setup and the reported Hg setup suggests galinstan to be a suitable soft electrode material.

Having verified that galinstan can make reproducible, soft electrical contact to molecular assembly surfaces directly, we used this setup to characterize charge transport across molecular assemblies of QPDT, TPDT, and BPDT on GaAs. Figure 6.4 contains the absolute current densities as a function of applied bias for assemblies of QPDT, TPDT, and BPDT. QPDT was assembled on GaAs from solutions with ethanol fraction (EF) of 0.75 without the addition of any NH_4OH (QPDT-0) and with 10 mM NH_4OH (QPDT-10). These processing conditions were selected to achieve two preferentially oriented QPDT assemblies with different molecular orientations. Specifically, as described in Chapter 4, QPDT assemblies on GaAs formed without the addition of NH_4OH (QPDT-0) are preferentially upright, with an ensemble-average backbone tilt of 29±3° away from the substrate normal, and are completely acetyl-terminated at the surface. QPDT assemblies on GaAs formed using 10 mM NH_4OH are more upright than QPDT-0, with an ensemble-average backbone tilt of 20±3° away from the substrate normal, and are partially acetyl-terminated at the surface. The shapes of the J-V curves exhibited by QPDT molecular assemblies are similar to that of 1-hexadecanethiol. The flow of electrons from the n-type GaAs substrate through the QPDT molecular assemblies to galinstan is therefore easier than the reverse, similar to that in 1-hexadecanethiol assemblies. The comparison of the current densities observed for QPDT-0 (blue circles) and QPDT-10 (red squares) in Figure 6.4 reveals that the current densities exhibited by QPDT-10 ($1.3 x10^{-4} \pm 0.6 x10^{-4}$ A/cm^2 at 0.5 V) are lower than those exhibited by QPDT-0 (7.3 $x10^{-4}$ ± 2.5 $x10^{-4}$ A/cm^2 at 0.5 V). We speculate that this difference stems from differences in the tunneling distance across which charge transport occurs. Theoretical calculations predict that the current densities through a molecular assembly are expected to decrease with increasing assembly thickness.[46,47] The lower current densities through the QPDT-10 molecular assembly than those through the QPDT-0 molecular assembly suggest that the QPDT-10 molecular assembly is thicker than QPDT-0. Indeed, we measured the thickness of QPDT-10 to be 23 ± 1Å using ellipsometry. The thickness of QPDT-0 was measured to be 21 ± 1Å. We attribute the decrease in thickness of QPDT-0 to a less upright molecular orientation compared to that of QPDT-10. The smaller tunneling distance across which charge transport occurs in the slightly thinner QPDT-0 compared to that of QPDT-10 is consistent with the higher current densities observed for QPDT-0. The observation of lower current densities through thicker molecular assemblies is also consistent with observations reported for other conjugated molecular assemblies.[7] For example, Ishida et. al.[7] reported higher current densities through the thicker molecular assemblies of 1-terphenylthiol on Au with a preferentially upright molecular orientation, compared to 1-terphenylthiol molecular assemblies in which molecules are generally ‘lying down’ on Au.[7]

TPDT assemblies on GaAs formed from EtOH using 1 mM NH_4OH (TPDT-1 in Figure 6.4) exhibit a preferentially upright structure similar to that of QPDT-0, with an ensemble-average backbone tilt of 27±3° away from the substrate normal, and are largely acetyl-terminated at the surface. Charge transport across the TPDT-1 assemblies (green triangles in Figure 6.4) is characterized by higher current densities of ($2.6x10^{-3} \pm 1.2x10^{-3}$ A/cm^2 at 0.5 V) than those observed for QPDT-10 and QPDT-0. We measured the thickness of the upright TPDT-1 molecular assembly on GaAs to be 17 ± 1Å. Considering that TPDT-1 is thinner than both QPDT-0 and QPDT-10, the higher current densities measured for TPDT-1 are consistent with the reduced tunneling distance across which charge transport must occur in this assembly.

BPDT assemblies on GaAs formed from EtOH using 1 mM NH_4OH (BPDT-1 in Figure 6.4) are disordered and are largely acetyl-terminated at the surface. BPDT-1 exhibits an ellipsometric thickness of 11 ± 1Å. Because the tunneling distance across BPDT-1 is significantly smaller than that across TPDT-1 (17 ± 1Å), the absolute current densities observed for BPDT-1 should be the highest. While BPDT-1 does indeed exhibit the highest current densities ($9x10^{-3} \pm 7x10^{-3}$ A/cm^2 at 0.5 V) amongst the samples examined at positive biases, the current densities measured near-zero and at negative voltages are comparable to those measured for TPDT-1. The shape of the J-V curve for BPDT is thus inherently different from those of TPDT or QPDT assemblies. The different shape of the J-V curve of BPDT-1 compared to that of the other samples examined suggests a different conduction mechanism and/or a different interface dominating the electrical response of this assembly. The characteristically different electrical response of BPDT assemblies may stem from the absence of order in these assemblies. For example, it has been reported that disorder in molecular assemblies affects their electrical properties.[7]

The electrical conduction of TPDT and QPDT molecular assemblies measured through direct soft contact with galinstan reveal that both the molecular orientation of the assemblies and the backbone length of the molecules affect the electrical response. Specifically, on the example of QPDT assemblies on GaAs, we demonstrated that the absolute current densities decrease with an increasingly upright molecular orientation. That the more upright QPDT assemblies result in the lower absolute current densities is attributed to increased tunneling distance across which charge transport must occur in these assemblies. Additionally, we found that the n-phenyldithiols with the longer backbones result in lower absolute current densities across GaAs-molecule-galinstan junctions. This trend can also be explained in terms of tunneling distance. Specifically, QPDT is longer than TPDT, resulting in a longer tunneling distance. The increase in the tunneling distance across which charge transport occurs in these assemblies results in reduction of absolute current densities.

Our preliminary measurements of the electrical response of n-phenyldithiol molecular assemblies on GaAs also illustrate the impact of backbone conjugation on charge transport across the assemblies. This impact is evident from comparing of the absolute current densities for the molecular assemblies of conjugated (Figure 6.4) and saturated molecules (Figure 6.3) that are of comparable thickness. For example, the conjugated QPDT-0 molecular assembly (21 ± 1Å) is comparable in thickness to the saturated 1-hexadecanethiol molecular assembly (20 ± 1Å). Despite similar tunneling distances, the absolute current densities observed for QPDT-0 ($7.3 \times 10^{-4} \pm 2.5 \times 10^{-4}$ A/cm^2 at 0.5 V) are roughly two orders of magnitude higher than those observed for 1-hexadecanethiol ($5 \times 10^{-6} \pm 4 \times 10^{-6}$ A/cm^2). Our observation that the absolute current densities are higher for the molecular assemblies of conjugated molecules than saturated molecules of comparable thickness is consistent with the idea that backbone conjugation aids charge transport. It has been reported that the currents measured through oligo(*para*-phenylenevinylene) molecules that are 14Å long are almost 4 orders of magnitude higher than those through shorter 1-octanethiol molecules that are less than 12Å in length.[3,7] Additionally, the current densities of benzenemethylthiol assemblies on Au were observed to be lower than those of terphenylthiol assemblies that are preferentially lying down on Au, although the two assemblies were of identical thickness.[7] This difference was attributed to the presence of the methyl group between the phenyl ring and the thiol group of benzenemethylthiol, effectively breaking the conjugation of the backbone and thus reducing the current flow.[7] Furthermore, the current densities observed for molecular assemblies of oligo(*para*-phenylenevinylene) were reported to be almost 2 orders of magnitude higher than those of the terphenylmethylthiol molecules of nearly identical thickness. This finding was attributed to improved backbone conjugation of the oligo(*para*-phenylenevinylene) systems compared to that of terphenylmethylthiol.[7]

Galinstan proved to be a suitable soft electrode material for directly measuring the electrical response of molecular assemblies. For comparison, we also measured the electrical response of our conjugated molecular assemblies after top Au electrodes have been deposited by nTP on the assembly surface. Specifically, we deposited top Au electrodes on the surfaces of QPDT-0 and QPDT-10 molecular assemblies on GaAs using nTP at ambient conditions. We also deposited top Au electrodes on the surfaces of QPDT-10 molecular assemblies on GaAs using 'wet' nTP in dichloroethane. The molecular assemblies of QPDT-10 are partially acetyl-terminated. According to our XPS studies, depositing Au on these assemblies via nTP in DCE results in reproducible formation of S-Au bonds at the molecule-Au contact interface. In contrast, depositing Au on QPDT-10 via nTP at ambient conditions results in reduced and irreproducible formation of S-Au bonds at the molecule-Au contact interface.

We first tested our galinstan setup by making soft electrical contact to freshly-evaporated Au. Figure 6.5 contains current-voltage (I-V) data obtained by contacting a freshly-evaporated Au substrate with a galinstan drop. The voltage was swept both forwards and backwards, and no hysteresis was observed. The I-V characteristics is linear, indicating that an ohmic contact was established between the galinstan drop and the Au surface. The presence of an ohmic contact between galinstan and Au ensures that the galinstan-Au contact does not limit the electrical response measured in GaAs—molecule—Au. We estimated the resistivity of the galinstan contact to be ≈100 nΩ m, assuming the length of the galinstan column in the needle to be 1 cm and using the area of the galinstan-Au contact. The estimated resistivity is of the same order of magnitude as that reported for pure galinstan (435 nΩ m).[48] Additionally, no amalgamation was observed between galinstan and Au over the course of several hours. This stability of the galinstan-Au contact is in sharp contrast to that of the Hg-Au contact.

We prepared GaAs—QPDT—Au junctions by first forming QPDT-0 and QPDT-10 assemblies on GaAs. Au electrodes 10-15 nm thick of varying areas were then transferred onto the assembly surfaces via nTP in DCE and at ambient conditions. We measured the currents through each device by bringing a galinstan drop into contact with the Au electrode. Normally, the current-voltage (I-V) characteristics from each device is normalized by the Au contact area to obtain absolute current densities (J-V) curve.[35] The current densities from all the devices are then averaged to provide relevant statistics. As expected, the currents measured for GaAs—QPDT-10—Au junctions where the Au electrodes were deposited by 'wet' nTP in DCE scale with the respective Au electrode areas thereby resulting in overlapping J-V curves. The fact that the measured currents scale with the Au electrode area suggests that the current densities in these junctions are distributed evenly across the entire Au electrode area. We were surprised to find, however, that such scaling did not apply to GaAs—QPDT—Au junctions where the Au electrodes were deposited by nTP at ambient conditions. Specifically, normalizing the measured currents by the respective Au electrode areas did not result in overlapping J-V curves. Instead, such normalization resulted in current density levels that differ by two orders of magnitude, as shown in Figure 6.6a. On the other hand, we found that the currents scale with the contact area of the galinstan drop, resulting in overlapping J-V curves, as shown in Figure 6.6b. The fact that the currents in GaAs—QPDT—Au junctions prepared via nTP at ambient conditions scale with the galinstan-Au contact area suggests that the charge transport across these junctions is concentrated in the region where the galinstan drop makes physical contact with the Au electrode, rather than across the entire Au electrode.

While we are uncertain about the origin of this disparity in the electrical behavior between the junctions formed by nTP in DCE and at ambient conditions, we suspect that it may stem from differences in the number of S-Au bonds at the molecule-Au interface. Specifically, when Au is deposited on QPDT-10 molecular assembly surfaces via nTP in DCE, our XPS studies indicate reproducible formation of S-Au bonds. On the other hand, when Au is deposited on QPDT-10 via nTP at ambient conditions, our XPS studies indicate that the formation of S-Au bonds is reduced and inconsistent. That the currents across these junctions scale with the galinstan contact area suggests that the electrical response is sensitive to the force applied. In fact, electrical responses that are force sensitive have been reported previously; this phenomenon was attributed to the absence of covalent bonds at the charge transfer interface. For example, Cui et. al.[3] reported that the currents in Au—1-octanethiol—Au junctions exhibited strong dependence on the compression force applied to the top Au electrode by the CAFM tip.[3] An increase in current of almost 2 orders of magnitude was reported to result when ≈2 nN per 10 nm^2 as compared to <0.5 nN per 10 nm^2 was applied.[3] In GaAs—QPDT—Au junctions prepared using nTP at ambient conditions, the absence of S-Au bonds at the molecule-Au interface likely provides a tunneling distance that is tunable; when force is applied to the Au electrode by the galinstan drop the tunneling distance decreases. On the other hand, in GaAs—QPDT—Au junctions prepared using nTP in DCE, the presence of S-Au bonds at the molecule-Au interface appears to fix the tunneling distance thereby resulting in currents that do not depend on the area of the galinstan-Au contact. This notion is consistent with the observation by Cui et. al.[3] that the currents in Au—1,8-

octanedithiol—Au junctions where S-Au bonds are present at the charge transfer interface are insensitive to the force applied to the top Au electrode by the CAFM tip.[3]

Provided we scale the currents of GaAs—QPDT-10—Au junctions formed using nTP in DCE and at ambient conditions with the appropriate contact areas, their absolute current densities are comparable, as shown in Figure 6.7. Also comparable are the current densities of GaAs—QPDT-10—Au and GaAs—QPDT-0—Au junctions formed using nTP at ambient conditions. These observations are surprising. First, the similarity between the current densities for GaAs—QPDT-10—Au junctions formed using nTP at ambient conditions and in DCE appears to suggest that the presence of S-Au bonds at the QPDT-Au interface does not impact the electrical response of the junctions. This observation is in contrast with studies that report that Au—1,8-octanedithiol—Au junctions are at least four orders of magnitude more conductive than Au—1-octanethiol—Au junctions.[3] Second, the similarity between the current densities for GaAs—QPDT-10—Au and GaAs—QPDT-0—Au junctions is in contrast with the trend observed previously when the QPDT assemblies were in direct contact with galinstan (Figure 6.4). In those cases, we observed a difference of almost an order of magnitude between the absolute current densities measured for QPDT-10 and QPDT-0. When these molecular assemblies are 'wired' by Au electrodes deposited by nTP at ambient conditions, however, we do not see a marked difference in current densities between QPDT-10 and QPDT-0.

We are currently uncertain about the origins of these discrepancies. We suspect, however, that they may stem from the quality of the Au electrode surface at which the Au-galinstan interface is subsequently formed. Specifically, nTP involves the evaporation of a Au layer on an elastomeric stamp. Following the transfer of Au from the stamp to the molecular assembly surface, the back surface of the Au electrode previously in direct contact with the elastomeric stamp becomes the surface onto which galinstan makes contact. The cleanness of the back Au surface formerly in contact with the elastomeric stamp is thus expected to be crucial for electrical studies. Felmet et. al.[49] discovered that the transferred Au surface is generally contaminated by residual oligomers via XPS. The researchers also reported that the residual oligomer contamination can be reduced by leaching the elastomeric stamps in boiling toluene for 2-3 days and drying them in the oven overnight prior to nTP.[49]

We thus examined the impact of the residual oligomeric contamination on the electrical characteristics of GaAs—1,8-octanedithiol—Au junctions.[49] We prepared the junctions by first forming 1,8-octanedithiol molecular assemblies on GaAs, followed by Au electrode deposition using nTP at ambient conditions. We used two types of elastomeric stamps during nTP: conventional unleached stamps (used for GaAs—QPDT—Au junction formation) and leached stamps. During electrical characterization, a soft contact was established between the galinstan drop and the Au electrode for each measurement. The current densities were obtained by normalizing the measured currents by the respective Au electrode areas. Figure 6.8 contains the absolute current densities as a function of applied bias to the galinstan drop for GaAs—1,8-octanedithiol—Au junctions prepared using unleached and leached elastomeric stamps. The absolute current densities for junctions prepared using unleached and leached elastomeric stamps reveal drastic differences. Specifically, the current densities measured for GaAs—1,8-octanedithiol—Au junctions prepared using unleached stamps are roughly two orders of magnitude lower than those of the junctions prepared using leached stamps. Given that the only difference in the fabrication of these junctions is the use of leached or unleached stamps, the difference in the current densities of these junctions must result from differences in the quality of the Au-galinstan interface. The greatly reduced current densities measured on the junctions whose Au electrodes were deposited with the unleached stamp are consistent with the presence of an insulating layer of residual oligomers at the Au-galinstan interface. The higher current densities measured on the junctions whose Au electrodes were deposited with the leached stamp are consistent with a cleaner, less insulating Au-galinstan interface. We therefore conclude that it is crucial to achieve a pristine Au-galinstan interface when working with Au electrodes deposited using nTP.

While leaching with toluene produces cleaner elastomeric stamps, it also makes these stamps less flexible and more 'sticky' toward the evaporated Au. While we were able to transfer 10-15 nm thick Au electrodes on the thiol-terminated 1,8-octanedithiol molecular assemblies, we were only able to transfer very thin ≈1.5 nm Au on acetyl-terminated QPDT-10 molecular assemblies (used for XPS studies in Chapter 5). We were not, however, able to transfer 10-15 nm thick Au electrodes on the acetyl-terminated QPDT-10 molecular assemblies to form junctions for electrical studies. For this reason, we were not able to evaluate the electrical response of GaAs—QPDT—Au junctions prepared using the cleaner leached stamps.

In this Chapter, we have developed an extension to the hanging-drop Hg setup using galinstan to make soft electrical contact to molecular assemblies. We have shown that galinstan is suitable for making soft contact to both molecular assembly surfaces directly and to pre-deposited Au electrodes. Galinstan does not pose health hazards, is easy to handle, and is very affordable. As a result, even a simple galinstan electrode setup constructed in-house allows for reliable electrical characterization of assembly-based molecular junctions. Using galinstan to make direct electrical contact to molecular assembly surfaces, we measured the electrical characteristics of QPDT, TPDT, and BPDT assemblies on GaAs. We found that both the molecular orientation of the assemblies and the backbone length of the molecules affect the electrical response of the conjugated assemblies. These conclusions emphasize that both the molecular orientation of molecular assemblies and the backbone structure of the comprising molecules govern electrical conduction across the molecular assemblies. This notion is important in light of published studies[50,51] presenting measurements of charge transport across molecular assemblies without any quantitative understanding of the assembly structure.

The examination of GaAs—QPDT—Au junctions prepared using nTP in DCE and at ambient conditions revealed characteristically different electrical behavior. Specifically, while the current densities are distributed evenly across the entire Au electrode area in junctions prepared using nTP in DCE, charge transport across junctions prepared nTP at ambient conditions is concentrated in the region where the galinstan drop makes physical contact with the Au electrode. We speculated this characteristic difference to stem from differences in the formation of S-Au bonds at the charge transfer interface. Additionally, the electrical response we measured for GaAs—QPDT—Au junctions was not affected by either the molecular orientation of the QPDT assemblies or the S-Au bond formation at the QPDT-Au interface. We suspect that this observation stems from the presence of oligomeric contamination on the Au electrode surface at which the electrical galinstan-Au contact is formed. Specifically, we demonstrated that the oligomeric contamination at the Au-galinstan interface resulting from the nTP process plays a role in the electrical response of the GaAs—1,8-octanedithiol—Au junctions. We were, however, unable to verify this hypothesis on GaAs—QPDT—Au junctions because we were not able to transfer cleaner Au electrodes using leached stamps onto QPDT assemblies. The impact of oligomeric contamination resulting from nTP on the electrical response of GaAs—1,8-octanedithiol—Au junctions we observed, however, underscores the importance of the galinstan-Au interface quality. The surface quality of the electrodes deposited on assembly surfaces using various techniques (nTP, float-on, evaporation) must therefore be carefully examined to avoid possible misinterpretation of the electrical junction characteristics due to contamination.

FIGURES

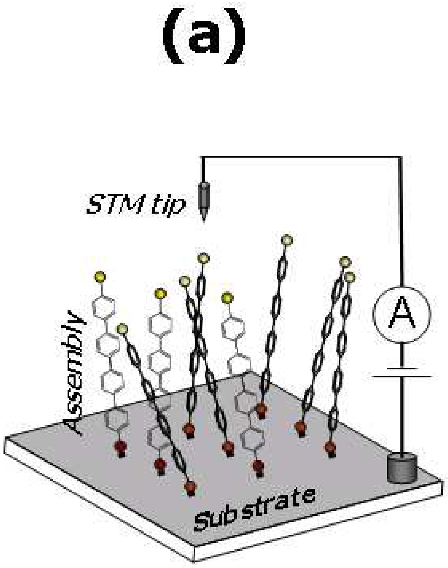

Figure 6.1. Schematic representations of the (a) STM setup and (b) CAFM setup for making electrical contact directly to molecular assembly surfaces.

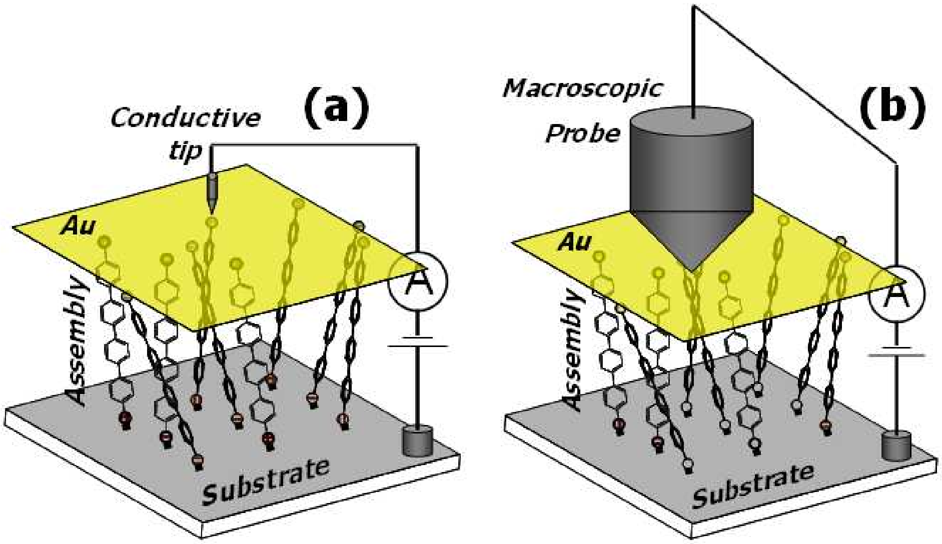

Figure 6.2. Schematic representations of (a) CAFM and (b) tungsten probe setups for making electrical contact to the top Au electrodes that had been pre-deposited on the molecular assembly surfaces.

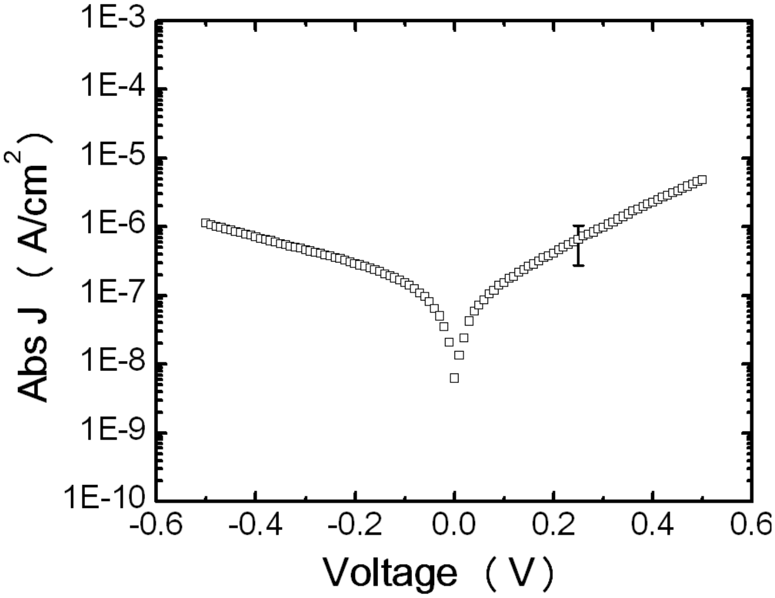

Figure 6.3. Absolute current density as a function of applied bias to the galinstan drop in contact with 1-hexadecanethiol molecular assembly on GaAs. Error bars reflect standard deviations based on 23 separate measurements on junctions of varying contact areas.

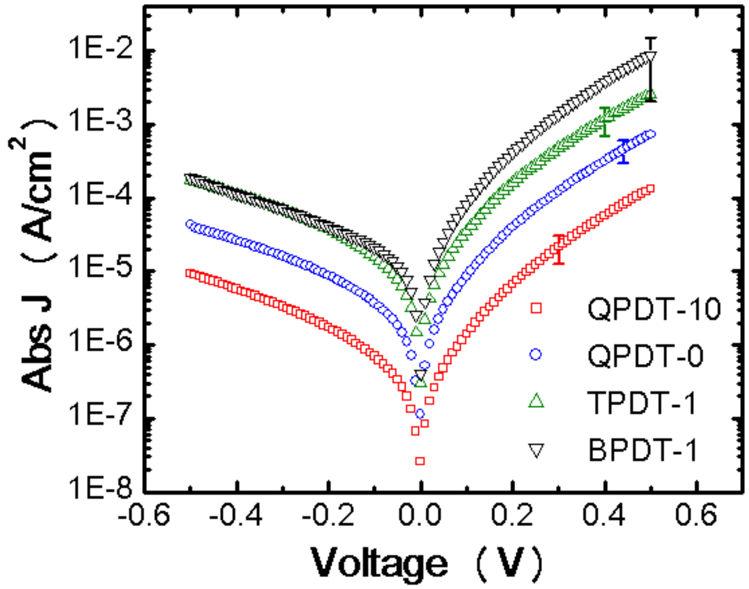

Figure 6.4. Absolute current density as a function of applied bias to the galinstan drop when galinstan is in contact with QPDT, TPDT, and BPDT assemblies on GaAs. The QPDT assemblies on GaAs were formed from solutions with EF = 0.75 using no NH_4OH (QPDT-0) and 10 mM NH_4OH (QPDT-10). The TPDT (TPDT-1) and BPDT (BPDT-1) assemblies on GaAs were formed from EtOH solutions using 1 mM NH_4OH. Error bars reflect standard deviations based on 20-25 separate measurements for BPDT-1 and TPDT-1 and on 40-50 separate measurements for QPDT-0 and QPDT-10 on junctions of varying contact areas.

.

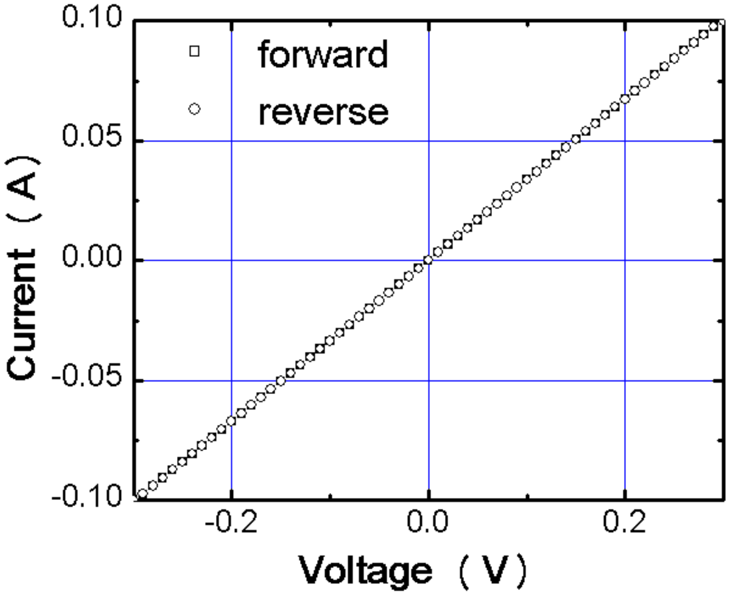

Figure 6.5. Current as a function of applied bias to the galinstan drop in contact with a freshly-evaporated Au substrate. The current was swept forwards and backwards and no hysteresis was observed. The linear I-V response indicates the formation of an ohmic contact between galinstan and the freshly-evaporated Au. We estimated the resistivity of galinstan to be ≈100 nΩ m.

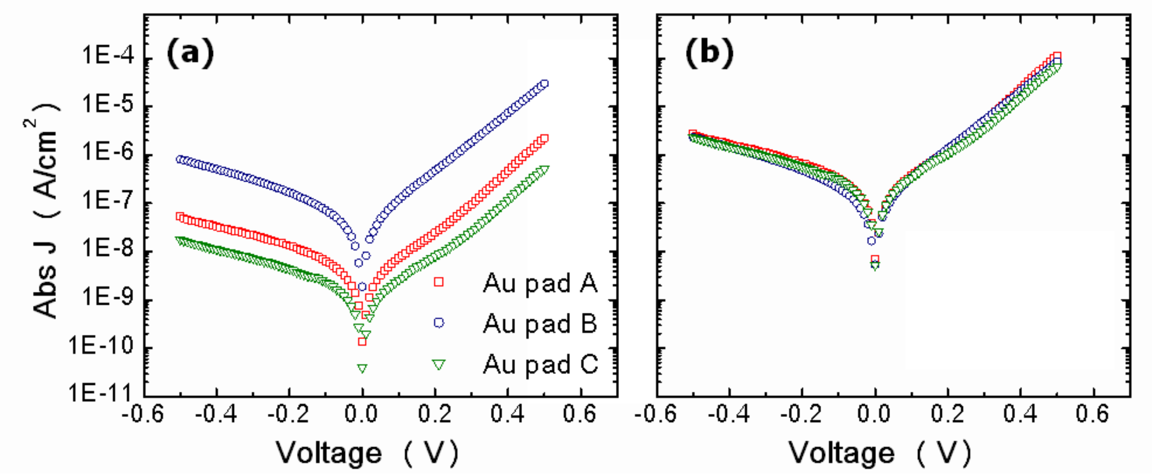

Figure 6.6. Absolute current densities of GaAs—QPDT-10—Au junctions where Au was transferred via nTP at ambient conditions as a function of applied bias to the galinstan drop. The J-V curves were obtained by normalizing the currents measured for the junctions (a) by Au electrode contact area and (b) by the contact area of the galinstan drop. The junctions were formed with Au electrode pads A, B, and C with areas of 3.1×10^{-2}, 2.0×10^{-3}, 2.5×10^{-1} cm^2, respectively. The areas of the contacts between the galinstan drop and the Au electrode pads A, B, and C were 6.2×10^{-4}, 6.9×10^{-4}, 1.9×10^{-3} cm^2, respectively.

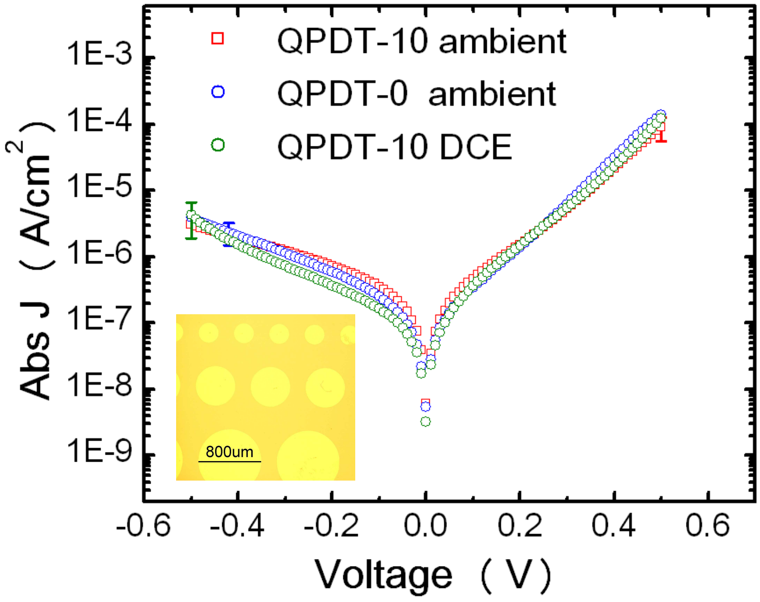

Figure 6.7. Absolute current density of GaAs—QPDT—Au junctions as a function applied bias to the galinstan drop. The QPDT assemblies on GaAs were formed from solutions with EF = 0.75 using no NH_4OH added (blue circles), and with 10 mM NH_4OH (red squares and green circles). Top Au electrodes were deposited by nTP at ambient conditions (QPDT-0 and QPDT-10 ambient) and in DCE (QPDT-10 DCE). To obtain the current densities, the currents were normalized by Au electrode areas for junctions prepared using nTP in DCE and by galinstan-Au contact areas for junctions prepared using nTP at ambient conditions. Error bars reflect standard deviations based on 50, 21, and 35 separate measurements for QPDT-10, QPDT-0, and QPDT-10 DCE, respectively, on junctions of varying contact areas. The inset shows a micrograph of Au electrodes deposited on a QPDT assembly surface using nTP at ambient conditions.

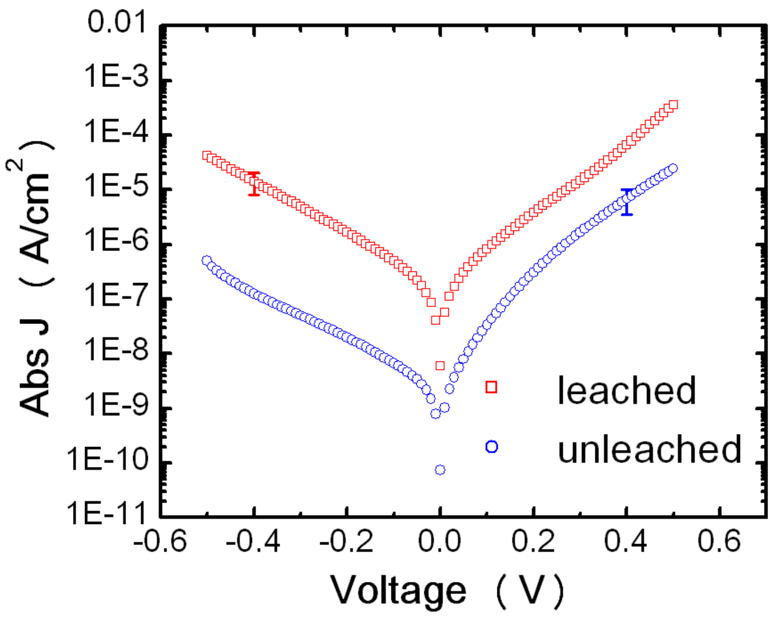

Figure 6.8. Absolute current density as a function of applied bias to the galinstan drop brought in contact with GaAs—1,8-octanedithiol—Au junctions. The top Au electrodes were deposited on the 1,8-octanedithiol molecular assemblies on GaAs by nTP using unleached (blue circles) and leached (red squares) elastomeric stamps at ambient conditions. Error bars reflect standard deviations based on 30 and 20 separate measurements for leached and unleached, respectively, on junctions of varying contact areas.

REFERENCES

1. Aviram, A.; Ratner, M. A. *Chemical Physics Letters* **1974,** *29*, 277.

2. Kwok, K. S.; Ellenbogen, J. C. *Materials Today* **2002,** *5*, 28.

3. Cui, X. D.; Primak, A.; Zarate, X.; Tomfohr, J.; Sankey, O. F.; Moore, A. L.; Moore, T. A.; Gust, D.; Harris, G.; Lindsay, S. M. *Science* **2001,** *294*, 571.

4. Hipps, K. W. *Science* **2001,** *294*, 536.

5. Akkerman Hylke, B.; Blom Paul, W. M.; de Leeuw Dago, M.; de Boer, B. *Nature* **2006,** *441*, 69.

6. Akkerman Hylke, B.; Naber Ronald, C. G.; Jongbloed, B.; van Hal Paul, A.; Blom Paul, W. M.; de Leeuw Dago, M.; de Boer, B. *Proceedings of the National Academy of Sciences of the United States of America* **2007,** *104*, 11161.

7. Ishida, T.; Mizutani, W.; Liang, T.-T.; Azehara, H.; Miyake, K.; Sasaki, S.; Tokumoto, H. *Annals of the New York Academy of Sciences* **2003,** *1006*, 164.

8. James, D. K.; Tour, J. M. *Chemistry of Materials* **2004,** *16*, 4423.

9. Attard, G.; Barnes, C., *Surfaces*. Oxford University Press Inc.: New York, 2004.

10. Nesher, G.; Vilan, A.; Cohen, H.; Cahen, D.; Amy, F.; Chan, C.; Hwang, J.; Kahn, A. *Journal of Physical Chemistry B* **2006,** *110*, 14363.

11. Cygan, M. T.; Dunbar, T. D.; Arnold, J. J.; Bumm, L. A.; Shedlock, N. F.; Burgin, T. P.; Jones, L., II; Allara, D. L.; Tour, J. M.; Weiss, P. S. *Journal of the American Chemical Society* **1998,** *120*, 2721.

12. Kobayashi, K.; Horiuchi, T.; Yamada, H.; Matsushige, K. *Thin Solid Films* **1998,** *331*, 210.

13. Yang, Y.-C.; Lee, Y.-L.; Yang, L.-Y. O.; Yau, S.-L. *Langmuir* **2006,** *22*, 5189.

14. Leung, T. Y. B.; Gerstenberg, M. C.; Lavrich, D. J.; Scoles, G.; Schreiber, F.; Poirier, G. E. *Langmuir* **2000,** *16*, 549.

15. Nicoara, N.; Cerrillo, I.; Xueming, D.; Garcia, J. M.; Garcia, B.; Gomez-Navarro, C.; Mendez, J.; Baro, A. M. *Nanotechnology* **2002,** *13*, 352.

16. Gosvami, N.; Lau, K. H. A.; Sinha, S. K.; O'Shea, S. J. *Applied Surface Science* **2006,** *252*, 3956.

17. Beebe, J. M.; Engelkes, V. B.; Miller, L. L.; Frisbie, C. D. *Journal of the American Chemical Society* **2002,** *124*, 11268.

18. Cui, X. D.; Primak, A.; Zarate, X.; Tomfohr, J.; Sankey, O. F.; Moore, A. L.; Moore, T. A.; Gust, D.; Nagahara, L. A.; Lindsay, S. M. *Journal of Physical Chemistry B* **2002,** *106*, 8609.

19. Cui, X. D.; Zarate, X.; Tomfohr, J.; Sankey, O. F.; Primak, A.; Moore, A. L.; Moore, T. A.; Gust, D.; Harris, G.; Lindsay, S. M. *Nanotechnology* **2002,** *13*, 5.

20. Nesher, G.; Shpaisman, H.; Cahen, D. *Journal of the American Chemical Society* **2007,** *129*, 734.

21. Salomon, A.; Boecking, T.; Gooding, J. J.; Cahen, D. *Nano Letters* **2006,** *6*, 2873.

22. Selzer, Y.; Salomon, A.; Cahen, D. *Journal of the American Chemical Society* **2002,** *124*, 2886.

23. Tran, E.; Rampi, M. A.; Whitesides, G. M. *Angewandte Chemie* **2004,** *43*, 3835.

24. Ohgi, T.; Sheng, H. Y.; Nejoh, H. *Applied Surface Science* **1998,** *130-132*, 919.

25. de Boer, B.; Frank, M. M.; Chabal, Y. J.; Jiang, W.; Garfunkel, E.; Bao, Z. *Langmuir* **2004,** *20*, 1539.

26. Guerin, D.; Merckling, C.; Lenfant, S.; Wallart, X.; Pleutin, S.; Vuillaume, D. *Journal of Physical Chemistry C* **2007,** *111*, 7947.

27. Walker, A. V.; Tighe, T. B.; Cabarcos, O. M.; Reinard, M. D.; Haynie, B. C.; Uppili, S.; Winograd, N.; Allara, D. L. *Journal of the American Chemical Society* **2004,** *126*, 3954.

28. Haick, H.; Ghabboun, J.; Niitsoo, O.; Cohen, H.; Cahen, D.; Vilan, A.; Hwang, J.; Wan, A.; Amy, F.; Kahn, A. *Journal of Physical Chemistry B* **2005,** *109*, 9622.

29. Vilan, A.; Cahen, D. *Advanced Functional Materials* **2002,** *12*, 795.

30. Shimizu, K. T.; Fabbri, J. D.; Jelincic, J. J.; Melosh, N. A. *Advanced Materials* **2006,** *18*, 1499.

31. Loo, Y.-L.; Willett, R. L.; Baldwin, K. W.; Rogers, J. A. *Applied Physics Letters* **2002,** *81*, 562.

32. Jiang, W.; Garfunkel, E.; Zhitenev, N.; Abusch-Magder, D.; Tennant, D.; Bao, Z. *Applied Physics Letters* **2006,** *89*, 113107/1.

33. Hsu, J. W. P.; Loo, Y. L.; Lang, D. V.; Rogers, J. A. *Journal of Vacuum Science & Technology B* **2003,** *21*, 1928.

34. Loo, Y.-L.; Hsu, J. W. P.; Willett, R. L.; Baldwin, K. W.; West, K. W.; Rogers, J. A. *Journal of Vacuum Science & Technology B* **2002,** *20*, 2853.

35. Loo, Y.-L.; Lang, D. V.; Rogers, J. A.; Hsu, J. W. P. *Nano Letters* **2003,** *3*, 913.

36. Loo, Y.-L.; Willett, R. L.; Baldwin, K. W.; Rogers, J. A. *Journal of the American Chemical Society* **2002,** *124*, 7654.

37. Morita, T.; Lindsay, S. *Journal of the American Chemical Society* **2007,** *129*, 7262.

38. Kim, C.; Burrows, P. E.; Forrest, S. R. *Science* **2000,** *288*, 831.

39. Levlin, M.; Niemi, H. E. M.; Hautojarvi, P.; Ikavalko, E. *Fresenius' Journal of Analytical Chemistry* **1996,** *355*, 2.

40. Butler, M. A.; Ricco, A. J.; Baughman, R. J. *Journal of Applied Physics* **1990,** *67*, 4320.

41. Thome, J.; Himmelhaus, M.; Zharnikov, M.; Grunze, M. *Langmuir* **1998,** *14*, 7435.

42. Smith Linda, S. *Journal of Gerontological Nursing* **2003,** *29*, 26.

43. See http://www.rgmd.com/msds/msds.pdf for MSDS of galinstan; see http://www.espimetals.com/tech/Tech-%20Mercury.htm for MSDS of Hg.

44. Surmann, P.; Zeyat, H. *Analytical and Bioanalytical Chemistry* **2005,** *383*, 1009.

45. Metzger, R. M.; Chen, B.; Hoepfner, U.; Lakshmikantham, M. V.; Vuillaume, D.; Kawai, T.; Wu, X.; Tachibana, H.; Hughes, T. V.; Sakurai, H.; Baldwin, J. W.; Hosch, C.; Cava, M. P.; Brehmer, L.; Ashwell, G. J. *Journal of the American Chemical Society* **1997,** *119*, 10455.

46. Magoga, M.; Joachim, C. *Physical Review B* **1999,** *59*, 16011.

47. Samanta, M. P.; Tian, W.; Datta, S.; Henderson, J. I.; Kubiak, C. P. *Physical Review B* **1996,** *53*, R7626.

48. See http://www.rgmd.com/msds/msds.pdf for MSDS of galinstan.

49. Felmet, K.; Loo, Y.-L.; Sun, Y. *Applied Physics Letters* **2004,** *85*, 3316.

50. Kushmerick, J. G.; Holt, D. B.; Yang, J. C.; Naciri, J.; Moore, M. H.; Shashidhar, R. *Physical Review Letters* **2002,** *89*, 086802/1.

51. Beebe, J. M.; Kushmerick, J. G. *Applied Physics Letters* **2007,** *90*, 083117/1.

Chapter 7: Conclusions and Future Work

CONCLUSIONS

In this work, we addressed the major aspects of forming the molecular assembly-based junctions. In particular, we addressed conjugated dithiol adsorption on two types of substrates – Au and GaAs. We also addressed the issues associated with making electrical contact to the surfaces of these molecular assemblies on GaAs. Finally, we measured the electrical response across some of these assemblies.

The research inquiries in the first part of our work allowed us to obtain a clear picture of how processing conditions affect the final structures of BPDT, TPDT, and QPDT assemblies. We found that BPDT molecular assemblies are largely disordered on both Au and GaAs when adsorbed from both EtOH and THF. In contrast to BPDT, TPDT and QPDT tend to adsorb on Au from both EtOH and THF an upright fashion.[1] Specifically, TPDT molecular assemblies exhibit ensemble-average backbone tilts of 30°±3° and 32°±3° away from the substrate normal when adsorbed on Au from EtOH and THF, respectively. QPDT molecular assemblies exhibit an ensemble-average backbone tilt of 28°±3° away from the substrate normal when adsorbed on Au from both EtOH-rich and THF solvents. We attributed the improvement in surface organization from BPDT to TPDT to QPDT to an increase in backbone rigidity and intermolecular interactions (Van der Waals and π-π) with increasing backbone length. The adsorption of TPDT and QPDT on GaAs is highly solvent sensitive. Specifically, TPDT and QPDT do not adsorb on GaAs from THF. The surface coverage and surface organization of the molecules improves with increasing EtOH fraction in the assembly solution. When the adsorption of TPDT and QPDT is carried out from EtOH and an EtOH-rich cosolvent, the molecular assemblies exhibit a preferentially upright orientation. Specifically, TPDT molecular assemblies on GaAs exhibit an ensemble-average backbone tilt of 33°±3° away from the substrate normal when adsorbed from EtOH. QPDT molecular assemblies on GaAs exhibit an ensemble-average backbone tilt of 27°±3° away from the substrate normal when adsorbed from a cosolvent with EF = 0.9. We concluded that assembly from EtOH-rich solvents results in better structural organization in n-phenyldithiols on GaAs.

These model conjugated systems are assembled from their acetyl-protected precursors, with the protecting acetyl groups cleaved *in-situ* using a deprotecting agent, NH_4OH. We discovered that the concentrations of both the deprotecting agent (NH_4OH) and the acetyl-protected precursors in the assembly solution affect the final assembly structures of n-phenyldithiols. Specifically, TPDT adsorbed from EtOH on Au at 1 mM NH_4OH exhibits an ensemble-average backbone tilt of 21°±3° away from the substrate normal. The assembly becomes less upright when formed at 160 mM NH_4OH, exhibiting an ensemble-average backbone tilt of 29°±3°. Similarly, TPDT adsorbed from EtOH on GaAs exhibits ensemble-average backbone tilts of 27°±3° and 34°±3° at 1 and 160 mM NH_4OH, respectively. We concluded that the final structure of TPDT assembled on GaAs from EtOH is upright at low NH_4OH concentrations and becomes less so with increasing NH_4OH concentrations. TPDT assemblies on GaAs carried out from THF are drastically different from those carried out from EtOH. Specifically, TPDT assemblies on GaAs carried out from THF at low NH_4OH concentrations exhibit negligible surface coverage. The surface coverage and structural organization of TPDT assemblies on GaAs carried out from THF improve with increasing NH_4OH concentrations, although these assemblies are never as upright as those achieved from EtOH at low NH_4OH

concentrations. We also investigated the effect of NH_4OH concentration on the final structure of QPDT assembled on GaAs from an EtOH-rich solvent (EF = 0.75). The final structures of these assemblies were found to also be NH_4OH concentration dependent. Specifically QPDT assembled on GaAs from EtOH-rich solutions is most upright at low NH_4OH concentrations of 1-10 mM, with an ensemble-average molecular tilt of 20°±3° away from the substrate normal. These assemblies are less upright at high NH_4OH concentrations of 160 mM, characterized by an ensemble-average molecular tilt of 38°±3° away from the substrate normal.

The molecular orientation of TPDT and QPDT assemblies is also sensitive to the concentrations of their acetyl-protected precursors. TPDT molecular assemblies on GaAs carried out from EtOH at 1 mM NH_4OH concentrations are nearly-disordered at low acetyl-protected TPDT precursor concentration of 50 μM. These assemblies are more upright at higher acetyl-protected TPDT precursor concentration of 250 μM. We found that the final structures of TPDT assemblies on GaAs carried out from THF are also acetyl-protected TPDT precursor concentration dependent. TPDT molecular assemblies adsorbed on GaAs from THF at 160 mM NH_4OH are disordered at low acetyl-protected TPDT precursor concentration of 80 μM. These assemblies are more upright at higher acetyl-protected TPDT precursor concentration of 500 μM. We found the final structures of QPDT assemblies on GaAs from THF at 160 mM NH_4OH to also be acetyl-precursor concentration dependent similar to TPDT.

Considering the variety of final assembly structures that can result from varying the NH_4OH and the acetyl-protected precursor concentrations, it is important to realize that these molecular assemblies are compositionally different. Specifically, low NH_4OH and high acetyl-protected precursor concentrations lead to low fractions of thiolates in solution at the point of substrate immersion. The assembly formation process in these cases is often dominated by the adsorption of thioacetyl-terminated molecules. Accordingly, the surfaces of these assemblies are often acetyl-terminated. On the other hand, high NH_4OH and low acetyl-protected precursor concentrations lead to increased fractions of thiolates in solution at the point of substrate immersion. Here, the assembly formation process is dominated by the adsorption of thiolate-terminated molecules. The surfaces of these assemblies are therefore acetyl-free. Better final assembly structures result when the adsorption of thioacetyl-terminated molecules dominates.

Our findings demonstrate that the processing-structure relationships of conjugated dithiols are non-trivial, and the assembly of these molecules requires the consideration of multiple conditions. The conditions we investigated, including the types of substrate used, the solvent quality, NH_4OH and acetyl-protected precursor concentrations, provide examples of parameters that can be used to control the surface coverage and molecular orientation of the model conjugated dithiols. The processing-structure relationships we observed helped identify pitfalls in some of the common assembly practices. For instance, the assembly of conjugated systems on Au has been commonly carried out from THF at high NH_4OH concentrations.[2-4] Our findings revealed that, at these conditions, the molecular assemblies n-phenyldithiols on Au are the least ordered.

We also addressed the deposition of top Au electrodes directly on the assembly surface using nTP. Specifically, we have shown that the conditions under which the top Au electrode is deposited affect the nature of dithiol-Au interactions. The deposition of Au electrodes on largely acetyl-terminated QPDT assemblies on GaAs via ‘wet’ nTP that is carried out in dichloroethane results in reproducible formation of S-Au bonds between the functional groups at the assembly surface and the printed Au. On the other hand, nTP that is carried out at ambient conditions on the same QPDT assemblies results in reduced and irreproducible formation of S-Au bonds, as quantified by XPS measurements.

Finally, we measured the electrical response of model conjugated molecular assemblies on GaAs. To this end, we showed that the electrical response of the molecular assemblies is sensitive to both the molecular orientation and the backbone length of the molecules comprising the assembly. We found that QPDT assemblies on GaAs with more upright molecular orientation exhibit lower current densities than QPDT assemblies on GaAs with less upright molecular orientation. Specifically, QPDT assemblies with an ensemble-average backbone tilt of 20±3° away from the substrate normal and a thickness of 23±1Å exhibit an absolute current density of 1.3 $x10^{-4}$ ± 0.6 $x10^{-4}$ A/cm^2 at 0.5 V applied bias. On the other hand, the less upright QPDT assemblies with an ensemble-average backbone tilt of 29±3° away from the substrate normal and a thickness of 21±1Å exhibit an absolute current density of 7.3 $x10^{-4}$ ± 2.5 $x10^{-4}$ A/cm^2 at 0.5 V applied bias. We also found that assemblies of n-phenyldithiols on GaAs exhibiting comparable molecular orientation but comprised of molecules with more aromatic rings in the backbone exhibit lower current densities. QPDT assemblies on GaAs with an ensemble-average backbone tilt of 29±3° away from the substrate normal and a thickness of 21±1Å exhibit an absolute current density of 7.3 $x10^{-4}$ ± 2.5 $x10^{-4}$ A/cm^2 at 0.5 V applied bias. On the other hand, TPDT assemblies on GaAs with an ensemble-average backbone tilt of 27±3° away from the substrate normal and a thickness of 17±1Å are characterized by an absolute current density $2.6x10^{-3}$ ± $1.2x10^{-3}$ A/cm^2 at 0.5 V applied bias. Our findings emphasize that the electrical response of molecular assemblies is governed not only by the details of the backbone structure, but also the details of how the molecules are organized on the surface. Thus, any comparisons of electrical responses of various molecular assemblies must be coupled with an understanding of the final assembly structures from which they were measured. Although we were able to measure the electrical response of molecular assemblies on GaAs by making direct electrical contact to their surfaces, we found the electrical studies of GaAs—dithiol—Au junctions prepared by nTP to be technically challenging. Specifically, the oligomeric contamination left on the top Au electrode surface by the unleached elastomeric stamp during nTP significantly impacts the measured electrical response. The current densities measured from GaAs—1,8-octanedithiol—Au junctions where the Au electrodes were deposited using unleached elastomeric stamps are nearly two orders of magnitude lower compared to those of junctions prepared using leached elastomeric stamps. The measured electrical response of the GaAs—QPDT—Au junctions where the Au electrodes were deposited by nTP using unleached stamps do not exhibit substantial dependence on either the molecular orientation of QPDT or whether significant amount of S-Au bonds is present at the charge transfer interface. The similarity in the electrical response of these junctions likely stems from the presence of oligomeric contamination on the Au electrodes. Although using leached elastomeric stamps resulted in cleaner top Au electrodes, we found that the reduced flexibility and increased brittleness of the leached elastomeric stamps make transferring Au on assembly surfaces that are not thiol-terminated challenging. We were thus not able to transfer Au electrodes using leached elastomeric stamps onto the surfaces of QPDT assemblies on GaAs which are largely acetyl-terminated.

During the course of experimentation, we also developed a number of spectroscopic approaches to elucidate the organization of molecules on GaAs. First, we developed off-normal s-polarized transmission IR spectroscopy for the in-house characterization of these molecular assemblies. This technique provided chemical identification and the average molecular orientation of the molecular assemblies of conjugated dithiols on GaAs. In addition, this transmission IR approach permitted the direct evaluation of terminal groups at the assembly surface. The off-normal s-polarized transmission IR is applicable for a wide range of conjugated adsorbates, including n-phenyl,[5] n-phenyldimethyl,[6] and oligo (phenylene ethynylene),[7] because the dipole selection rules for these systems are analogous. We thus expect this approach to be a valuable addition to the suite of characterization techniques available to the molecular electronics community.

Second, we demonstrated the use of grazing-incidence x-ray photoelectron spectroscopy (XPS) for examining the nature of top molecule-metal interfaces in substrate—molecule—metal architectures. The idea of acquiring XPS signal though thin Au deposited by nTP allowed us to examine the molecule-Au interface and directly verify the presence of S-Au bonds between the function groups at the dithiol assembly surfaces and the Au deposited by nTP.

Finally, we extended the hanging-drop mercury electrode setup by using galinstan as the soft electrode contact material to measure electrical conduction of molecular assemblies. The use of galinstan to make soft electrical contact proved valuable in measuring charge transport across our molecular assemblies. We demonstrated that galinstan is a suitable alternative to mercury[8,9] for use as a soft electrode. Unlike mercury which rapidly amalgamates with Au, galinstan can also be used to make soft electrical contact to Au electrodes because the galinstan-Au contact remains stable for several hours. Additionally, galinstan does not pose any health hazards, is easy to handle, and is very affordable. We expect the hanging-drop galinstan setup to be a useful addition to the list of test-beds available for measuring the electrical conduction of molecular assemblies.

In summary, the fabrication and testing of molecular assembly-based electrical junctions presents serious challenges from the standpoints of both controlling the final assembly structures and measuring their electrical conduction. Careful attention must be paid to each aspect of molecular assembly-based junction formation and analysis. We also presented a number of technical approaches to help address both the structural details of the molecular assemblies and their electrical response.

FUTURE WORK

We elucidated the ensemble-average structural details of n-phenyldithiol assemblies on GaAs. We also demonstrated macroscopic electrical characterization of charge transport across these assemblies. Our ensemble-average studies can be complemented by understanding the structure and charge transport characteristics at the individual molecule level. The understanding of the local structure and electrical characteristics would help shed light on the fundamental properties of the single molecules comprising the assembly structure. The comparison of single-molecule characteristics to the ensemble-average characteristics of molecular assemblies will help determine whether differences between the two exist. The structural and charge transport details at the molecular scale are commonly examined using scanning tunneling microscopy (STM). Etched GaAs surfaces like those we used for molecular assembly formation, however, are not smooth enough for STM characterization. Instead, atomically-flat topographies are required. We propose that work should be carried out to form molecular assemblies on cleaved, rather than etched GaAs surfaces. Cleaved GaAs surfaces are known to contain atomically-flat regions.[10,11] If cleaved *in-situ* in the assembly solution, the GaAs surface should remain oxide-free and allow the formation of molecular assemblies. The local details of molecular surface organization on GaAs and charge transport through such assemblies should then be accessible via STM characterization.

We also propose that additional work should be carried out on the electrical characterization of GaAs—molecule—Au in which the top Au electrodes are deposited using nTP. We demonstrated that the cleanness of the transferred Au impacts the quality of the Au-galinstan electrical contact and is important for measuring the electrical response of the molecular assemblies. Using leached elastomeric stamps to transfer Au electrodes resulted in a cleaner Au-galinstan interface in the GaAs—molecule—Au junctions. Leached stamps, however, are mechanically less flexible and more ‘sticky’ to Au, preventing Au transfer on molecular assembly surfaces that are not thiol-terminated. Further work should be done to allow the formation of cleaner Au-galinstan interfaces in the GaAs-molecule-Au junctions. One way to potentially achieve cleaner Au-galinstan interfaces involves modifying the printing process. For instance, it has been demonstrated that that by carefully controlling the speed at which the stamp is removed during nTP, metal films can be transferred even onto relatively ‘non-stick’ target surfaces, such as glass treated with (tridecafluoro-1,1,2,2-tetrahydrooctyl) trichlorosilane.[12] The implementation of a mechanical setup allowing stamp removal at controlled speeds may aid in transferring Au electrodes on acetyl-terminated assemblies or even assemblies without a reactive surface functionality with leached stamps. Having a pristine Au-galinstan interface would allow for high quality electrical contact to GaAs-molecule-Au junctions and enable reliable characterization of charge transfer across the molecular assemblies.

Having developed the ability to control the structure of the molecular assembly and to measure the electrical response of the molecular assemblies of simple n-phenyldithiols, we propose extending the studies to more complex conjugated chemistries relevant to the molecular electronics community. For example, asymmetric conjugated molecules, including thiophene-, pyrole-, and oligo(phenylene ethynylene)-based systems have been reported to exhibit conductance switching.[13,14] The development of conjugated molecules capable of useful electrical response and their implementation in functional junction architectures would help realize the potential of molecular electronics originally envisioned by Aviram and Ratner[15] three decades ago.

Finally, we propose the simultaneous spectroscopic and electrical characterization of GaAs-molecule-Au junctions. Provided that the continuity and cleanness of thin Au layers deposited on assembly surfaces can be improved, setups combining spectroscopic structural characterization through the metal overlayer with electrical characterization can be envisioned. For example, the fluorescence yield (FY) capability of near-edge absorption fine structure (NEXAFS) spectroscopy[16,17] can be used for spectroscopic characterization of buried interfaces. Specifically, in the FY mode, fluorescent radiation that results from radiative core hole annihilation is detected.[17] Fluorescent radiation is more penetrating (≈50 nm)[17] than electrons (≈5 nm),[17] extending the depth of detection. FY NEXAFS can therefore be used for characterizing molecular assemblies buried under top Au electrodes. In fact, preliminary experiments have shown that we are indeed able to observe a single layer of molecules constrained between a GaAs substrate and 5 nm thick Au deposited by nTP. Figure 7.1 contains C 1s pre- and post-edge normalized FY NEXAFS spectra of QPDT molecular assemblies on GaAs before (bottom) and after (top) depositing 5 nm thick Au by nTP. As illustrated by the presence of π^* and σ^* resonances characteristic of the molecular assembly in the spectrum of the GaAs—QPDT—Au junction, we are able to observe the QPDT molecular assembly through the Au. Given that sufficiently continuous and clean Au can be deposited on the molecular assembly surfaces to form GaAs—molecule—Au junctions, and an electrical stage can be constructed within the NEXAFS chamber so bias can be applied to these junctions *in-*

situ, both the structure and the electrical behavior of the molecular assembly can be characterized simultaneously.

FIGURES

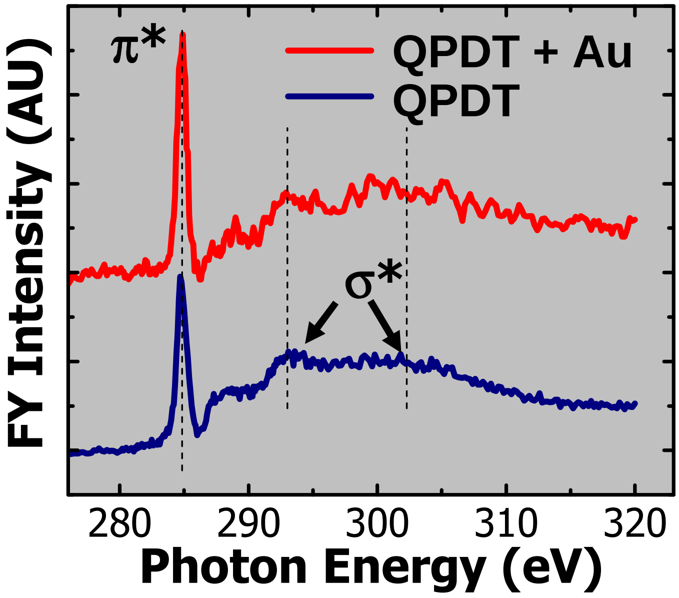

Figure 7.1. C 1s pre- and post-edge normalized FY NEXAFS spectra of QPDT assembled on GaAs before (bottom) and after (top) depositing 5 nm thick Au by nTP. The spectra were acquired near the magic angle, at an x-ray incident angle of 50°.

REFERENCES

1. Krapchetov, D. A.; Ma, H.; Jen, A. K. Y.; Fischer, D. A.; Loo, Y.-L. *Langmuir* **2005,** *21*, 5887.

2. Cai, L.; Yao, Y.; Yang, J.; Price, D. W., Jr.; Tour, J. M. *Chemistry of Materials* **2002,** *14*, 2905.

3. de Boer, B.; Meng, H.; Perepichka, D. F.; Zheng, J.; Frank, M. M.; Chabal, Y. J.; Bao, Z. *Langmuir* **2003,** *19*, 4272.

4. Jiang, W.; Zhitenev, N.; Bao, Z.; Meng, H.; Abusch-Magder, D.; Tennant, D.; Garfunkel, E. *Langmuir* **2005,** *21*, 8751.

5. Krapchetov, D. A.; Ma, H.; Jen, A. K. Y.; Fischer, D. A.; Loo, Y.-L. *Langmuir* **2006,** *22*, 9491.

6. Tai, Y.; Shaporenko, A.; Rong, H. T.; Buck, M.; Eck, W.; Grunze, M.; Zharnikov, M. *Journal of Physical Chemistry B* **2004,** *108*, 16806.

7. Richter, L. J.; Yang, C. S. C.; Wilson, P. T.; Hacker, C. A.; Van Zee, R. D.; Stapleton, J. J.; Allara, D. L.; Yao, Y.; Tour, J. M. *Journal of Physical Chemistry B* **2004,** *108*, 12547.

8. Akkerman Hylke, B.; Naber Ronald, C. G.; Jongbloed, B.; van Hal Paul, A.; Blom Paul, W. M.; de Leeuw Dago, M.; de Boer, B. *Proceedings of the National Academy of Sciences of the United States of America* **2007,** *104*, 11161.

9. Nesher, G.; Vilan, A.; Cohen, H.; Cahen, D.; Amy, F.; Chan, C.; Hwang, J.; Kahn, A. *Journal of Physical Chemistry B* **2006,** *110*, 14363.

10. Jiang, C.-S.; Nakayama, T.; Aono, M. *Applied Surface Science* **1998,** *130-132*, 425.

11. Ruppalt, L. B.; Albrecht, P. M.; Lyding, J. W. *Fourth IEEE Conference on Nanotechnology, Muenchen, Germany* **2004**, 7.

12. Feng, X.; Meitl, M. A.; Bowen, A. M.; Huang, Y.; Nuzzo, R. G.; Rogers, J. A. *Langmuir* **2007,** *23*, 12555.

13. Beebe, J. M.; Kushmerick, J. G. *Applied Physics Letters* **2007,** *90*, 083117/1.

14. Whalley, A. C.; Steigerwald, M. L.; Guo, X.; Nuckolls, C. *Journal of the American Chemical Society* **2007,** *129*, 12590.

15. Aviram, A.; Ratner, M. A. *Chemical Physics Letters* **1974,** *29*, 277.

16. Fischer, D.; Marti, A.; Hahner, G. *Journal of Vacuum Science & Technology A* **1997,** *15*, 2173.

17. Stohr, J., *NEXAFS Spectroscopy*. Springer: Berlin, 1992.

REFERENCES

1. Ulman, A. *Chemical Reviews* **1996,** *96*, 1533.

2. Lim, H.; Carraro, C.; Maboudian, R.; Pruessner, M. W.; Ghodssi, R. *Langmuir* **2004,** *20*, 743.

3. Baum, T.; Ye, S.; Uosaki, K. *Langmuir* **1999,** *15*, 8577.

4. Cox, J. D.; Curry, M. S.; Skirboll, S. K.; Gourley, P. L.; Sasaki, D. Y. *Biomaterials* **2001,** *23*, 929.

5. Ostuni, E.; Chapman, R. G.; Liang, M. N.; Meluleni, G.; Pier, G.; Ingber, D. E.; Whitesides, G. M. *Langmuir* **2001,** *17*, 6336.

6. Sung, I.-H.; Kim, D.-E. *Applied Surface Science* **2005,** *239*, 209.

7. Tiberio, R. C.; Craighead, H. G.; Lercel, M.; Lau, T.; Sheen, C. W.; Allara, D. L. *Applied Physics Letters* **1993,** *62*, 476.

8. Ahn, H.-S.; Cuong, P. D.; Park, S.; Kim, Y.-W.; Lim, J.-C. *Wear* **2003,** *255*, 819.

9. Perry, S. S.; Lee, S.; Shon, Y.-S.; Colorado, R., Jr.; Lee, T. R. *Tribology Letters* **2001,** *10*, 81.

10. Maboudian, R.; Carraro, C. *Annual Review of Physical Chemistry* **2004,** *55*, 35.

11. Maboudian, R.; Carraro, C. *Journal of Adhesion Science and Technology* **2003,** *17*, 583.

12. Hang, Q.; Wang, F.; Carpenter, P. D.; Zemlyanov, D.; Zakharov, D.; Stach, E. A.; Buhro, W. E.; Janes, D. B. *Nano Letters* **2008,** *8*, 49.

13. Aviram, A.; Ratner, M. A. *Chemical Physics Letters* **1974,** *29*, 277.

14. Hipps, K. W. *Science* **2001,** *294*, 536.

15. Nesher, G.; Shpaisman, H.; Cahen, D. *Journal of the American Chemical Society* **2007,** *129*, 734.

16. Nesher, G.; Vilan, A.; Cohen, H.; Cahen, D.; Amy, F.; Chan, C.; Hwang, J.; Kahn, A. *Journal of Physical Chemistry B* **2006,** *110*, 14363.

17. Loo, Y.-L.; Willett, R. L.; Baldwin, K. W.; Rogers, J. A. *Applied Physics Letters* **2002,** *81*, 562.

18. Hsu, J. W. P.; Loo, Y. L.; Lang, D. V.; Rogers, J. A. *Journal of Vacuum Science & Technology B* **2003,** *21*, 1928.

19. Loo, Y.-L.; Lang, D. V.; Rogers, J. A.; Hsu, J. W. P. *Nano Letters* **2003,** *3*, 913.

20. Loo, Y.-L.; Hsu, J. W. P.; Willett, R. L.; Baldwin, K. W.; West, K. W.; Rogers, J. A. *Journal of Vacuum Science & Technology B* **2002,** *20*, 2853.

21. Loo, Y.-L.; Willett, R. L.; Baldwin, K. W.; Rogers, J. A. *Journal of the American Chemical Society* **2002,** *124*, 7654.

22. Kushmerick, J. G. *Materials Today* **2005,** *8*, 26.

23. Smith Linda, S. *Journal of Gerontological Nursing* **2003,** *29*, 26.

24. Krapchetov, D. A.; Ma, H.; Jen, A. K. Y.; Fischer, D. A.; Loo, Y.-L. *Langmuir* **2005,** *21*, 5887.

25. Jun, Y.; Zhu, X. Y.; Hsu, J. W. P. *Langmuir* **2006,** *22*, 3627.

26. Nicoara, N.; Cerrillo, I.; Xueming, D.; Garcia, J. M.; Garcia, B.; Gomez-Navarro, C.; Mendez, J.; Baro, A. M. *Nanotechnology* **2002,** *13*, 352.

27. de Boer, B.; Meng, H.; Perepichka, D. F.; Zheng, J.; Frank, M. M.; Chabal, Y. J.; Bao, Z. *Langmuir* **2003,** *19*, 4272.

28. Camillone, N.; Khan, K. A.; Osgood, R. M. *Surface Science* **2000,** *453*, 83.

29. Kim, C.; Burrows, P. E.; Forrest, S. R. *Science* **2000,** *288*, 831.

30. Dubois, L. H.; Nuzzo, R. G. *Annual Review of Physical Chemistry* **1992,** *43*, 437.

31. Dubois, L. H.; Zegarski, B. R.; Nuzzo, R. G. *Journal of Chemical Physics* **1993,** *98*, 678.

32. Ye, S.; Li, G.; Noda, H.; Uosaki, K.; Osawa, M. *Surface Science* **2003,** *529*, 163.

33. Karpovich, D. S.; Blanchard, G. J. *Langmuir* **1994,** *10*, 3315.

34. Fischer, D.; Marti, A.; Hahner, G. *Journal of Vacuum Science & Technology A* **1997,** *15*, 2173.

35. Laibinis, P. E.; Whitesides, G. M.; Allara, D. L.; Tao, Y. T.; Parikh, A. N.; Nuzzo, R. G. *Journal of the American Chemical Society* **1991,** *113*, 7152.

36. Kondoh, H.; Nambu, A.; Ehara, Y.; Matsui, F.; Yokoyama, T.; Ohta, T. *Journal of Physical Chemistry B* **2004,** *108*, 12946.

37. Tamam, L.; Kraack, H.; Sloutskin, E.; Ocko, B. M.; Pershan, P. S.; Ulman, A.; Deutsch, M. *Journal of Physical Chemistry B* **2005,** *109*, 12534.

38. McGuiness, C. L.; Shaporenko, A.; Mars, C. K.; Uppili, S.; Zharnikov, M.; Allara, D. L. *Journal of the American Chemical Society* **2006,** *128*, 5231.

39. Dannenberger, O.; Buck, M.; Grunze, M. *Journal of Physical Chemistry B* **1999,** *103*, 2202.

40. Bain, C. D.; Troughton, E. B.; Tao, Y. T.; Evall, J.; Whitesides, G. M.; Nuzzo, R. G. *Journal of the American Chemical Society* **1989,** *111*, 321.

41. Asadi, K.; Gholamrezaie, F.; Smits, E. C. P.; Blom, P. W. M.; de Boer, B. *Journal of Materials Chemistry* **2007,** *17*, 1947.

42. Castner, D. G.; Hinds, K.; Grainger, D. W. *Langmuir* **1996,** *12*, 5083.

43. Shaporenko, A.; Adlkofer, K.; Johansson, L. S. O.; Ulman, A.; Grunze, M.; Tanaka, M.; Zharnikov, M. *Journal of Physical Chemistry B* **2004,** *108*, 17964.

44. Shaporenko, A.; Elbing, M.; Blaszczyk, A.; Von Haenisch, C.; Mayor, M.; Zharnikov, M. *Journal of Physical Chemistry B* **2006,** *110*, 4307.

45. Cai, L.; Yao, Y.; Yang, J.; Price, D. W., Jr.; Tour, J. M. *Chemistry of Materials* **2002,** *14*, 2905.

46. Hutchison, J. E.; Postlethwaite, T. A.; Murray, R. W. *Langmuir* **1993,** *9*, 3277.

47. Collier, C. P.; Wong, E. W.; Belohradsky, M.; Raymo, F. M.; Stoddart, J. F.; Kuekes, P. J.; Williams, R. S.; Heath, J. R. *Science* **1999,** *285*, 391.

48. Kang, J. F.; Ulman, A.; Liao, S.; Jordan, R.; Yang, G.; Liu, G.-Y. *Langmuir* **2001,** *17*, 95.

49. Zharnikov, M.; Grunze, M. *Journal of Physics: Condensed Matter* **2001,** *13*, 11333.

50. Frey, S.; Stadler, V.; Heister, K.; Eck, W.; Zharnikov, M.; Grunze, M.; Zeysing, B.; Terfort, A. *Langmuir* **2001,** *17*, 2408.

51. Himmel, H.-J.; Terfort, A.; Woell, C. *Journal of the American Chemical Society* **1998,** *120*, 12069.

52. Tour, J. M.; Jones, L.; Pearson, D. L.; Lamba, J. J. S.; Burgin, T. P.; Whitesides, G. M.; Allara, D. L.; Parikh, A. N.; Atre, S. *Journal of the American Chemical Society* **1995,** *117*, 9529.

53. Weckenmann, U.; Mittler, S.; Naumann, K.; Fischer, R. A. *Langmuir* **2002,** *18*, 5479.

54. Tour, J. M.; II, L. J.; Pearson, D. L.; Lamba, J. J. S.; Burgin, T. P.; Whitesides, G. M.; Allara, D. L.; Parikh, A. N.; Atre, S. V. *Journal of American Chemical Society* **1995,** *117*, 9529.

55. Krapchetov, D. A.; Ma, H.; Jen, A. K. Y.; Fischer, D. A.; Loo, Y.-L. *Langmuir* **2008,** *24*, 851.

56. Azzam, W.; Wehner, B. I.; Fischer, R. A.; Terfort, A.; Woell, C. *Langmuir* **2002,** *18*, 7766.

57. Jiang, W.; Zhitenev, N.; Bao, Z.; Meng, H.; Abusch-Magder, D.; Tennant, D.; Garfunkel, E. *Langmuir* **2005,** *21*, 8751.

58. de Boer, B.; Frank, M. M.; Chabal, Y. J.; Jiang, W.; Garfunkel, E.; Bao, Z. *Langmuir* **2004,** *20*, 1539.

59. Kushmerick, J. G.; Holt, D. B.; Yang, J. C.; Naciri, J.; Moore, M. H.; Shashidhar, R. *Physical Review Letters* **2002,** *89*, 086802/1.

60. Mann, B.; Kuhn, H. *Journal of Applied Physics* **1971,** *42*, 4398.

61. Akkerman Hylke, B.; Naber Ronald, C. G.; Jongbloed, B.; van Hal Paul, A.; Blom Paul, W. M.; de Leeuw Dago, M.; de Boer, B. *Proceedings of the National Academy of Sciences of the United States of America* **2007,** *104*, 11161.

62. Cui, X. D.; Primak, A.; Zarate, X.; Tomfohr, J.; Sankey, O. F.; Moore, A. L.; Moore, T. A.; Gust, D.; Harris, G.; Lindsay, S. M. *Science* **2001,** *294*, 571.

63. Engelkes, V. B.; Beebe, J. M.; Frisbie, C. D. *Journal of the American Chemical Society* **2004,** *126*, 14287.

64. Milani, F.; Grave, C.; Ferri, V.; Samori, P.; Rampi, M. A. *ChemPhysChem* **2007,** *8*, 515.

65. Kim, T.-W.; Wang, G.; Lee, H.; Lee, T. *Nanotechnology* **2007,** *18*, 315204/1.

66. Ishida, T.; Mizutani, W.; Liang, T.-T.; Azehara, H.; Miyake, K.; Sasaki, S.; Tokumoto, H. *Annals of the New York Academy of Sciences* **2003,** *1006*, 164.

67. Lummerstorfer, T.; Sohar, C.; Friedbacher, G.; Hoffmann, H. *Langmuir* **2006,** *22*, 18.

68. Richter, C. A.; Hacker, C. A.; Richter, L. J. *Journal of Physical Chemistry B* **2005,** *109*, 21836.

69. Haick, H.; Ghabboun, J.; Niitsoo, O.; Cohen, H.; Cahen, D.; Vilan, A.; Hwang, J.; Wan, A.; Amy, F.; Kahn, A. *Journal of Physical Chemistry B* **2005,** *109*, 9622.

70. Walker, A. V.; Tighe, T. B.; Cabarcos, O. M.; Reinard, M. D.; Haynie, B. C.; Uppili, S.; Winograd, N.; Allara, D. L. *Journal of the American Chemical Society* **2004,** *126*, 3954.

71. Qu, D.; Uosaki, K. *Journal of Physical Chemistry B* **2006,** *110*, 17570.

72. Salomon, A.; Boecking, T.; Gooding, J. J.; Cahen, D. *Nano Letters* **2006,** *6*, 2873.

73. Pinchart, A.; Dallaire, C.; Van Bierbeek, A.; Gingras, M. *Tetrahedron Letters* **1999,** *40*, 5479.

74. Pearson, D. L.; Tour, J. M. *Journal of Organic Chemistry* **1997,** *62*, 1376.

75. Xia, Y.; Whitesides, G. M. *Angewandte Chemie* **1998,** *37*, 550.

76. Kumar, A.; Whitesides, G. M. *Applied Physics Letters* **1993,** *63*, 2002.

77. Xia, Y.; Rogers, J. A.; Paul, K. E.; Whitesides, G. M. *Chemical Reviews* **1999,** *99*, 1823.

78. Felmet, K.; Loo, Y.-L.; Sun, Y. *Applied Physics Letters* **2004,** *85*, 3316.

79. Shimizu, K. T.; Fabbri, J. D.; Jelincic, J. J.; Melosh, N. A. *Advanced Materials* **2006,** *18*, 1499.

80. Vilan, A.; Cahen, D. *Advanced Functional Materials* **2002,** *12*, 795.

81. Lide, D. R., *CRC Handbook of Chemistry and Physics*. CRC Press: Boca Raton, FL, 1994.

82. Stohr, J.; Outka, D. A. *Physical Review B* **1987,** *36*, 7891.

83. Detailed information on the NIST/Dow Soft X-Ray Materials Characterization Facility at NSLS BNL see: http://www.nsls.bnl.gov/newsroom/publications/newsletters/1996/96-nov.pdf

84. Genzer, J.; Kramer, E. J.; Fischer, D. A. *Journal of Applied Physics* **2002,** *92*, 7070.

85. Genzer, J.; Sivaniah, E.; Kramer, E. J.; Wang, J.; Koerner, H.; Char, K.; Ober, C. K.; DeKoven, B. M.; Bubeck, R. A.; Fischer, D. A.; Sambasivan, S. *Langmuir* **2000,** *16*, 1993.

86. Fischer, D. A.; Efimenko, K.; Bhat, R. R.; Sambasivan, S.; Genzer, J. *Macromolecular Rapid Communications* **2004,** *25*, 141.

87. Stohr, J., *NEXAFS Spectroscopy*. Springer: Berlin, 1992.

88. Banerjee, S.; Hemraj-Benny, T.; Sambasivan, S.; Fischer, D. A.; Misewich, J. A.; Wong, S. S. *Journal of Physical Chemistry B* **2005,** *109*, 8489.

89. Kinzler, M.; Schertel, A.; Haehner, G.; Woell, C.; Grunze, M.; Albrecht, H.; Holzhueter, G.; Gerber, T. *Journal of Chemical Physics* **1994,** *100*, 7722.

90. Outka, D. A.; Stoehr, J.; Rabe, J. P.; Swalen, J. D. *Journal of Chemical Physics* **1988,** *88*, 4076.

91. Trotter, J. *Acta Crystallographica* **1961,** *14*, 1135.

92. Shaporenko, A.; Adlkofer, K.; Johansson, L. S. O.; Tanaka, M.; Zharnikov, M. *Langmuir* **2003,** *19*, 4992.

93. Corish, J.; Morton-Blake, D. A.; O'Donoghue, F.; Baudour, J. L.; Beniere, F.; Toudic, B. *Theochem* **1995,** *358*, 29.

94. Cailleau, H.; Baudour, J. L.; Zeyen, C. M. E. *Acta Crystallographica* **1979,** *B35*, 426.

95. Baudour, J. L.; Delugeard, Y.; Rivet, P. *Acta Crystallographica* **1978,** *B34*, 625.

96. Stapleton, J. J.; Harder, P.; Daniel, T. A.; Reinard, M. D.; Yao, Y.; Price, D. W.; Tour, J. M.; Allara, D. L. *Langmuir* **2003,** *19*, 8245.

97. Hacker, C. A.; Batteas, J. D.; Garno, J. C.; Marquez, M.; Richter, C. A.; Richter, L. J.; Van Zee, R. D.; Zangmeister, C. D. *Langmuir* **2004,** *20*, 6195.

98. Nuzzo, R. G.; Dubois, L. H.; Allara, D. L. *Journal of the American Chemical Society* **1990,** *112*, 558.

99. Niklewski, A.; Azzam, W.; Strunskus, T.; Fischer, R. A.; Woell, C. *Langmuir* **2004,** *20*, 8620.

100. Krapchetov, D. A.; Ma, H.; Jen, A. K. Y.; Fischer, D. A.; Loo, Y.-L. *Langmuir* **2006,** *22*, 9491.

101. Tolstoy, V. P.; Chernyshova, I. V.; Skryshevsky, V. A., *Handbook of Infrared Spectroscopy of Ultrathin Films*. John Wiley & Sons, Inc.: 2003.

102. Lebedev, M. V.; Mayer, T.; Jaegermann, W. *Surface Science* **2003,** *547*, 171.

103. Cranstoun Stephen, D.; Ombao Hernando, C.; von Sachs, R.; Guo, W.; Litt, B. *IEEE Transactions on Bio-Medical Engineering* **2002,** *49*, 988.

104. Maoz, R.; Sagiv, J.; Degenhardt, D.; Moehwald, H.; Quint, P. *Supramolecular Science* **1995,** *2*, 9.

105. Sheen, C. W.; Shi, J. X.; Maartensson, J.; Parikh, A. N.; Allara, D. L. *Journal of the American Chemical Society* **1992,** *114*, 1514.

106. Collins, R. W.; Kim, Y. T. *Analytical Chemistry* **1990,** *62*, 887A.

107. Shi, J.; Hong, B.; Parikh, A. N.; Collins, R. W.; Allara, D. L. *Chemical Physics Letters* **1995,** *246*, 90.

108. Heister, K.; Zharnikov, M.; Grunze, M.; Johansson, L. S. O. *Journal of Physical Chemistry B* **2001,** *105*, 4058.

109. Chaki, N. K.; Vijayamohanan, K. *Biosensors & Bioelectronics* **2002,** *17*, 1.

110. Tai, Y.; Shaporenko, A.; Rong, H. T.; Buck, M.; Eck, W.; Grunze, M.; Zharnikov, M. *Journal of Physical Chemistry B* **2004,** *108*, 16806.

111. Moulder, J. F.; Stickle, W. E.; Sobol, P. E.; Bomben, K. D., *Handbook of X-ray Photoelectron Spectroscopy*. Perkin-Elmer Corp.: Eden Prairie, MN: 1992.

112. Shirley, D. A. *Physical Review B* **1972,** *[3]5*, 4709.

113. Aronniemi, M.; Sainio, J.; Lahtinen, J. *Surface Science* **2005,** *578*, 108.

114. Surmann, P.; Zeyat, H. *Analytical and Bioanalytical Chemistry* **2005,** *383*, 1009.

115. Poirier, G. E.; Pylant, E. D. *Science* **1996,** *272*, 1145.

116. Leung, T. Y. B.; Gerstenberg, M. C.; Lavrich, D. J.; Scoles, G.; Schreiber, F.; Poirier, G. E. *Langmuir* **2000,** *16*, 549.

117. Kobayashi, K.; Horiuchi, T.; Yamada, H.; Matsushige, K. *Thin Solid Films* **1998,** *331*, 210.

118. Ishida, T.; Mizutani, W.; Azehara, H.; Sato, F.; Choi, N.; Akiba, U.; Fujihira, M.; Tokumoto, H. *Langmuir* **2001,** *17*, 7459.

119. Fuxen, C.; Azzam, W.; Arnold, R.; Witte, G.; Terfort, A.; Woell, C. *Langmuir* **2001,** *17*, 3689.

120. Mekhalif, Z.; Laffineur, F.; Couturier, N.; Delhalle, J. *Langmuir* **2003,** *19,* 637.

121. Schlenoff, J. B.; Li, M.; Ly, H. *Journal of the American Chemical Society* **1995,** *117,* 12528.

122. Lavrich, D. J.; Wetterer, S. M.; Bernasek, S. L.; Scoles, G. *Journal of Physical Chemistry B* **1998,** *102,* 3456.

123. Pollack, S. K.; Naciri, J.; Mastrangelo, J.; Patterson, C. H.; Torres, J.; Moore, M.; Shashidhar, R.; Kushmerick, J. G. *Langmuir* **2004,** *20*, 1838.

124. Donhauser, Z. J.; Mantooth, B. A.; Kelly, K. F.; Bumm, L. A.; Monnell, J. D.; Stapleton, J. J.; Price Jr, D. W.; Rawlett, A. M.; Allara, D. L.; Tour, J. M.; Weiss, P. S. *Science* **2001,** *292,* 2303.

125. Cai, L.; Bahr, J. L.; Yao, Y.; Tour, J. M. *Chemistry of Materials* **2002,** *14,* 4235.

126. Ke, Y.; Milano, S.; Wang, X. W.; Tao, N.; Darici, Y. *Surface Science* **1998,** *415,* 29.

127. Liao, S.; Shnidman, Y.; Ulman, A. *Journal of the American Chemical Society* **2000,** *122*, 3688.

128. L.G. Wade, J., *Organic Chemistry*. Prentice-Hall, Inc.: Upper Saddle River, New Jersey, 1999.

129. Lau, K. H. A.; Huang, C.; Yakovlev, N.; Chen, Z. K.; O'Shea, S. J. *Langmuir* **2006,** *22*, 2968.

130. Akkerman Hylke, B.; Blom Paul, W. M.; de Leeuw Dago, M.; de Boer, B. *Nature* **2006,** *441*, 69.

131. Ohgi, T.; Sheng, H. Y.; Nejoh, H. *Applied Surface Science* **1998,** *130-132*, 919.

132. Guerin, D.; Merckling, C.; Lenfant, S.; Wallart, X.; Pleutin, S.; Vuillaume, D. *Journal of Physical Chemistry C* **2007,** *111*, 7947.

133. Ohgi, T.; Sheng, H. Y.; Dong, Z. C.; Nejoh, H.; Fujita, D. *Applied Physics Letters* **2001,** *79,* 2453.

134. Haick, H.; Ambrico, M.; Ghabboun, J.; Ligonzo, T.; Cahen, D. *Physical Chemistry Chemical Physics* **2004,** *6,* 4538.

135. Haick, H.; Ghabboun, J.; Cahen, D. *Applied Physics Letters* **2005,** *86*, 042113/1.

136. Zhou, C.; Deshpande, M. R.; Reed, M. A.; Jones, K., II; Tour, J. M. *Applied Physics Letters* **1997,** *71*, 611.

137. Schumm, J. S.; Pearson, D. L.; Jones, L., II; Hara, R.; Tour, J. M. *Nanotechnology* **1996,** *7*, 430.

138. McGuiness, C. L.; Shaporenko, A.; Zharnikov, M.; Walker, A. V.; Allara, D. L. *Journal of Physical Chemistry C* **2007,** *111*, 4226.

139. Esplandiu, M. J.; Noeske, P. L. M. *Applied Surface Science* **2002,** *199*, 166.

140. Deng, W.; Yang, L.; Fujita, D.; Nejoh, H.; Bai, C. *Applied Physics A* **2000,** *71*, 639.

141. Rieley, H.; Kendall, G. K.; Zemicael, F. W.; Smith, T. L.; Yang, S. *Langmuir* **1998,** *14*, 5147.

142. Xu, L.; Liao, J.; Huang, L.; Gu, N.; Zhang, H.; Liu, J. *Applied Surface Science* **2003,** *211*, 184.

143. Shaporenko, A.; Roessler, K.; Lang, H.; Zharnikov, M. *Journal of Physical Chemistry B* **2006,** *110*, 24621.

144. Bensebaa, F.; Voicu, R.; Huron, L.; Ellis, T. H.; Kruus, E. *Langmuir* **1997,** *13*, 5335.

145. Feng, X.; Meitl, M. A.; Bowen, A. M.; Huang, Y.; Nuzzo, R. G.; Rogers, J. A. *Langmuir* **2007,** *23*, 12555.

146. Hur, S.-H.; Khang, D.-Y.; Kocabas, C.; Rogers, J. A. *Applied Physics Letters* **2004,** *85*, 5730.

147. Kwok, K. S.; Ellenbogen, J. C. *Materials Today* **2002,** *5*, 28.

148. James, D. K.; Tour, J. M. *Chemistry of Materials* **2004,** *16*, 4423.

149. Attard, G.; Barnes, C., *Surfaces*. Oxford University Press Inc.: New York, 2004.

150. Cygan, M. T.; Dunbar, T. D.; Arnold, J. J.; Bumm, L. A.; Shedlock, N. F.; Burgin, T. P.; Jones, L., II; Allara, D. L.; Tour, J. M.; Weiss, P. S. *Journal of the American Chemical Society* **1998,** *120*, 2721.

151. Yang, Y.-C.; Lee, Y.-L.; Yang, L.-Y. O.; Yau, S.-L. *Langmuir* **2006,** *22*, 5189.

152. Gosvami, N.; Lau, K. H. A.; Sinha, S. K.; O'Shea, S. J. *Applied Surface Science* **2006,** *252*, 3956.

153. Beebe, J. M.; Engelkes, V. B.; Miller, L. L.; Frisbie, C. D. *Journal of the American Chemical Society* **2002,** *124*, 11268.

154. Cui, X. D.; Primak, A.; Zarate, X.; Tomfohr, J.; Sankey, O. F.; Moore, A. L.; Moore, T. A.; Gust, D.; Nagahara, L. A.; Lindsay, S. M. *Journal of Physical Chemistry B* **2002,** *106*, 8609.

155. Cui, X. D.; Zarate, X.; Tomfohr, J.; Sankey, O. F.; Primak, A.; Moore, A. L.; Moore, T. A.; Gust, D.; Harris, G.; Lindsay, S. M. *Nanotechnology* **2002,** *13*, 5.

156. Selzer, Y.; Salomon, A.; Cahen, D. *Journal of the American Chemical Society* **2002,** *124*, 2886.

157. Tran, E.; Rampi, M. A.; Whitesides, G. M. *Angewandte Chemie* **2004,** *43*, 3835.

158. Jiang, W.; Garfunkel, E.; Zhitenev, N.; Abusch-Magder, D.; Tennant, D.; Bao, Z. *Applied Physics Letters* **2006,** *89*, 113107/1.

159. Morita, T.; Lindsay, S. *Journal of the American Chemical Society* **2007,** *129*, 7262.

160. Levlin, M.; Niemi, H. E. M.; Hautojarvi, P.; Ikavalko, E. *Fresenius' Journal of Analytical Chemistry* **1996,** *355*, 2.

161. Butler, M. A.; Ricco, A. J.; Baughman, R. J. *Journal of Applied Physics* **1990,** *67*, 4320.

162. Thome, J.; Himmelhaus, M.; Zharnikov, M.; Grunze, M. *Langmuir* **1998,** *14*, 7435.

163. See http://www.rgmd.com/msds/msds.pdf for MSDS of galinstan; see http://www.espimetals.com/tech/Tech-%20Mercury.htm for MSDS of Hg.

164. Metzger, R. M.; Chen, B.; Hoepfner, U.; Lakshmikantham, M. V.; Vuillaume, D.; Kawai, T.; Wu, X.; Tachibana, H.; Hughes, T. V.; Sakurai, H.; Baldwin, J. W.; Hosch, C.; Cava, M. P.; Brehmer, L.; Ashwell, G. J. *Journal of the American Chemical Society* **1997,** *119*, 10455.

165. Magoga, M.; Joachim, C. *Physical Review B* **1999,** *59*, 16011.

166. Samanta, M. P.; Tian, W.; Datta, S.; Henderson, J. I.; Kubiak, C. P. *Physical Review B* **1996,** *53*, R7626.

167. See http://www.rgmd.com/msds/msds.pdf for MSDS of galinstan.

168. Beebe, J. M.; Kushmerick, J. G. *Applied Physics Letters* **2007,** *90*, 083117/1.

169. Richter, L. J.; Yang, C. S. C.; Wilson, P. T.; Hacker, C. A.; Van Zee, R. D.; Stapleton, J. J.; Allara, D. L.; Yao, Y.; Tour, J. M. *Journal of Physical Chemistry B* **2004,** *108*, 12547.

170. Jiang, C.-S.; Nakayama, T.; Aono, M. *Applied Surface Science* **1998,** *130-132*, 425.

171. Ruppalt, L. B.; Albrecht, P. M.; Lyding, J. W. *Fourth IEEE Conference on Nanotechnology, Muenchen, Germany, Aug. 16-19* **2004**, 7.

172. Whalley, A. C.; Steigerwald, M. L.; Guo, X.; Nuckolls, C. *Journal of the American Chemical Society* **2007,** *129*, 12590.

Vita

Dmitri Alexandrovich Kraptchetov was born on February 10, 1982, in Azov, Russia, the son of Svetlana Stepanovna Krapchetova and Alexander Vasilyevich Krapchetov. He graduated from Kamensk High School in 1998 in Kamensk, Russia and spent an additional year as an exchange student in Clear Lake High School in Houston, the United States. In 1999, he entered Blinn Community College in Bryan, TX, from where he transferred to Texas A&M University in College Station, TX in 2000. Dmitri earned his Bachelor of Science degree in Chemical Engineering from Texas A&M University in 2003. Immediately after the completion of his studies at Texas A&M University, he entered the Ph.D. program in Chemical Engineering at the University of Texas at Austin under the supervision of Professor Yueh-Lin Loo. Upon completion of his doctorate degree, Dmitri will begin work with Rohm and Haas Company in Spring House, PA.

Permanent address: Rostov Region, 78756 Kamensk-Shahtinski, Voroshilova 5-A, 24

This dissertation was typed by Dmitri A. Kraptchetov.